# Effects of Partial Sarcoplasmic Reticulum Calcium Depletion on Calcium Release in Frog Cut Muscle Fibers Equilibrated with 20 mM EGTA

Paul C. Pape, De-Shien Jong, and W. Knox Chandler

From the Department of Cellular and Molecular Physiology, Yale University School of Medicine, New Haven, Connecticut 06510-8026

ABSTRACT Resting sarcoplasmic reticulum (SR) Ca content ($[Ca_{SR}]_R$) was varied in cut fibers equilibrated with an internal solution that contained 20 mM EGTA and 0–1.76 mM Ca. SR Ca release and $[Ca_{SR}]_R$ were measured with the EGTA–phenol red method (Pape et al. 1995. *J. Gen. Physiol.* 106:259–336). After an action potential, the fractional amount of Ca released from the SR increased from 0.17 to 0.50 when $[Ca_{SR}]_R$ was reduced from 1,200 to 140 μM. This increase was associated with a prolongation of release (final time constant, from 1–2 to 10–15 ms) and of the action potential (by 1–2 ms). Similar changes in release were observed with brief stimulations to −20 mV in voltage-clamped fibers, in which charge movement ($Q_{cm}$) could be measured. The peak values of $Q_{cm}$ and the fractional rate of SR Ca release, as well as their ON time courses, were little affected by reducing $[Ca_{SR}]_R$ from 1,200 to 140 μM. After repolarization, however, the OFF time courses of $Q_{cm}$ and the rate of SR Ca release were slowed by factors of 1.5–1.7 and 6.5, respectively. These and other results suggest that, after action potential stimulation of fibers in normal physiological condition, the increase in myoplasmic free [Ca] that accompanies SR Ca release exerts three negative feedback effects that tend to reduce additional release: (*a*) the action potential is shortened by current through Ca-activated potassium channels in the surface and/or tubular membranes; (*b*) the OFF kinetics of $Q_{cm}$ is accelerated; and (*c*) Ca inactivation of Ca release is increased. Some of these effects of Ca on an SR Ca channel or its voltage sensor appear to be regulated by the value of [Ca] within 22 nm of the mouth of the channel.

KEY WORDS: calcium-activated potassium channel • charge movement • excitation–contraction coupling

## INTRODUCTION

Pape et al. (1995) described a method for the direct measurement of sarcoplasmic reticulum (SR)[1] Ca release and $[Ca_{SR}]_R$ in frog cut muscle fibers equilibrated with an internal solution that contains 20 mM EGTA and phenol red. With 1.76 mM Ca in the internal solution, the value of $[Ca_{SR}]_R$ varied threefold, between 1,391 and 4,367 μM, whereas that of the fractional amount of $[Ca_{SR}]_R$ released from the SR by a single action potential ($f_1$) remained relatively constant, between 0.13 and 0.17. During the course of those experiments, some of the fibers were partially depleted of Ca by decreasing the concentration of Ca in the internal solution and by repetitive stimulation. After the value of $[Ca_{SR}]_R$ fell below 1,000–1,200 μM, the value of $f_1$ began to increase and, with $[Ca_{SR}]_R$ = 150 μM, it was 0.5. This increase in $f_1$ helped stabilize the amount of Ca released from the SR. Since such stabilization may be important in helping to maintain normal contractile activation, experiments were undertaken to determine the factors involved in the regulation of $f_1$ by $[Ca_{SR}]_R$.

This article describes our results. They show that three factors participate in this regulation: (*a*) Ca-activated potassium channels in the surface and/or tubular membranes that, when opened, can shorten the duration of the action potential; (*b*) the OFF kinetics of $Q_{cm}$ that determines the rate of removal of voltage-dependent activation during the repolarization phase of an action potential; and (*c*) inhibition of SR Ca release

Dr. Pape's current address is Département de Physiologie et Biophysique, Faculté de Médecine, Université de Sherbrooke, Sherbrooke, Québec J1H5N4, Canada. Dr. Jong's current address is Department of Animal Science, National Taiwan University, Taipei 106, Taiwan, R.O.C

Portions of this work were previously published in abstract form (Pape, P.C., D.-S. Jong, and W.K. Chandler. 1997. *Biophys. J.* 72:*A*120).

Address correspondence to Dr. W.K. Chandler, Department of Cellular and Molecular Physiology, Yale University School of Medicine, 333 Cedar Street, New Haven, Connecticut 06510-8026. Fax: 203-785-4951; E-mail: knox.chandler@yale.edu

[1]*Abbreviations used in this paper:* EGTA, ethyleneglycol-bis-(β-aminoethyl ether)-*N*,*N*′-tetraacetic acid; MOPS, 3-[*N*-Morpholino]-propanesulfonic acid; $pH_R$, resting value of myoplasmic pH; SR, sarcoplasmic reticulum; $[Ca]_R$, resting concentration of myoplasmic free Ca; $[Ca_{SR}]$, readily releasable SR Ca content, expressed in terms of myoplasmic concentration; $[Ca_{SR}]_R$, resting value of $[Ca_{SR}]$; $\Delta[Ca_T]$, the amount of Ca released from the SR; $f_1$, the fractional amount of $[Ca_{SR}]_R$ released from the SR by a single action potential; $Q_{cm}$, intramembranous charge movement; $I_{cm}$, current from intramembranous charge movement.

caused by an elevation of myoplasmic free [Ca] (called Ca inactivation of Ca release).

The DISCUSSION presents a comparison of the effects on SR Ca release produced by the addition of high affinity Ca buffers to the myoplasm and by a reduction of SR Ca content (which is expected to reduce the single-channel Ca flux). APPENDIXES B and C give derivations of steady state and transient solutions of $\Delta$[Ca] near a point source in the presence of different kinds of Ca buffers. With these derivations, APPENDIX A shows that some of the effects of Ca on release appear to be controlled by the concentration of Ca ions within a region $\leq$22 nm from the mouth of the channel. Such effects of Ca could be mediated by a receptor or receptors located on the SR Ca channel (including the foot structure) and/or its voltage sensor. The appendixes also show that, in the absence of extrinsic Ca buffers, the concentration of Ca ions near the mouth of a channel can contain a large contribution from Ca ions that are released from neighboring channels and that this contribution is markedly decreased by the addition of 0.5–1.0 mM fura-2 or 20 mM EGTA to the myoplasm. The general features of this theoretical analysis may apply to other nonmuscle cells.

## MATERIALS AND METHODS

Action potential and voltage-clamp experiments were carried out on frog cut muscle fibers mounted in a double Vaseline-gap chamber and equilibrated with an internal solution that contained 20 mM EGTA and phenol red. The theoretical and experimental basis for the measurement of SR Ca release with EGTA–phenol red is described in Pape et al. (1995). After stimulation by an action potential, EGTA is expected to capture almost all ($\sim$96%) of the Ca released from the SR, to capture it rapidly ($<$0.1 ms), and to exchange it for protons with a 1:2 stoichiometry. $\Delta[Ca_T]$ is calculated from the associated decrease in myoplasmic pH (which is monitored with phenol red) and the value of myoplasmic buffering power (which was determined in a separate set of experiments with EGTA, phenol red, and fura-2). This method for the measurement of SR Ca release has the advantage that it is direct and little influenced by the presence of intrinsic myoplasmic Ca buffers. Indeed, for reasons that are not completely clear, the amount of Ca that appears to be complexed by the Ca-regulatory sites on troponin after an action potential is negligibly small and not statistically significant, 2.9 $\mu$M (SEM, 3.8 $\mu$M) out of a total site concentration of 240 $\mu$M (column 8 in Table III in Pape et al., 1995). The expectation that the EGTA–phenol red method gives an accurate measurement of the amplitude and time course of SR Ca release is validated by the finding that values of the peak rate of release and time to half-peak measured with this method are not significantly different from those estimated from Ca transients measured with low affinity Ca indicators (antipyrylazo III, tetramethylmurexide, and purpurate-3,3′diacetic acid [PDAA]) in cut fibers with only 0.1 mM EGTA (Pape et al., 1995). On the other hand, the half-width of the rate of SR Ca release measured with EGTA–phenol red is 0.7–0.9 ms longer than that estimated with 0.1 mM EGTA, an increase likely caused by the ability of 20 mM EGTA to reduce Ca inactivation of Ca release (Pape et al., 1995). Another feature of the EGTA–phenol red method is that $[Ca_{SR}]_R$ can be monitored routinely by the measurement of $\Delta[Ca_T]$ after a train of action potentials or after a long lasting step depolarization that releases essentially all of the readily releasable Ca from the SR. Additional information about the EGTA–phenol red method is given in Pape et al. (1995).

The methods used for the determination of $Q_{cm}$ are described in Chandler and Hui (1990), Hui and Chandler (1990, 1991), and Jong et al. (1995*b*). For the estimation of $I_{cm}$ associated with a brief depolarization (see Fig. 8 *A*), the final level of the OFF $I_{TEST}$–$I_{CONTROL}$ was used for the template of the OFF ionic current, and the template of the ON ionic current was adjusted to make the amplitudes of ON and OFF charge equal.

In the action potential experiments, a K-glutamate internal solution was used in the end pools. It contained (mM): 45 K-glutamate, 20 EGTA as a combination of K and Ca salts, 6.8 $MgSO_4$, 5.5 $Na_2$-ATP, 20 $K_2$-creatine phosphate, 5 $K_3$-phospho(enol)pyruvate, and 5 MOPS, with pH adjusted to 7.0 by the addition of KOH. The concentration of Ca-complexed EGTA was 0, 0.44, or 1.76 mM; at pH 7.0, the calculated concentration of free Ca was 0, 0.008, or 0.036 $\mu$M, respectively, and the calculated concentration of free Mg was 1 mM. A NaCl Ringer's solution was used in the central pool in the action potential experiments (see Table I of Irving et al., 1987).

In the voltage-clamp experiments, a Cs-glutamate internal solution was used in the end pools. It was similar to the K-glutamate internal solution except that Cs replaced K and Na. The composition of the external solution used in the central pool was 110 mM tetraethylammonium-gluconate, 10 mM $MgSO_4$, 10 mM MOPS, and 1 $\mu$M tetrodotoxin; it was nominally Ca-free and had a pH of 7.1.

In the experiments, the sarcomere length of the fibers was 3.3–3.7 $\mu$m, the holding potential was $-$90 mV, and the temperature was 14–15°C. The difference between the mean values of two sets of results was assessed with Student's two-tailed *t* test and considered to be significant if $P < 0.05$.

## RESULTS

### *Effect of a Reduction of $[Ca_{SR}]_R$ on SR Ca Release During a Train of Action Potentials*

Fig. 1 *A* shows traces from a fiber that was initially equilibrated with an end-pool solution that contained 20 mM EGTA and 1.76 mM Ca. The top traces show superimposed voltage records taken during four trials in which the fiber was stimulated to give a train of action potentials with different amounts of Ca inside the SR. The other four traces show the associated $\Delta[Ca_T]$ signals.

The first $\Delta[Ca_T]$ signal (Fig. 1 *A*, *a*) was obtained 125 min after saponin treatment. The first action potential elicited an abrupt increase in $\Delta[Ca_T]$ of 445 $\mu$M. This amount of release is similar to that obtained from other fibers equilibrated with the same internal solution and having a similar value of $[Ca_{SR}]_R$ (Pape et al., 1995). On the other hand, it may be somewhat larger than that obtained in fibers not equilibrated with EGTA because of a reduction of Ca inactivation of Ca release caused by the ability of EGTA to reduce myoplasmic free [Ca]. Ca inactivation of Ca release represents an inhibition of Ca flux through SR Ca channels that is produced by an increase in myoplasmic free [Ca] (Baylor et al., 1983; Simon et al., 1985, 1991; Schneider and Simon,

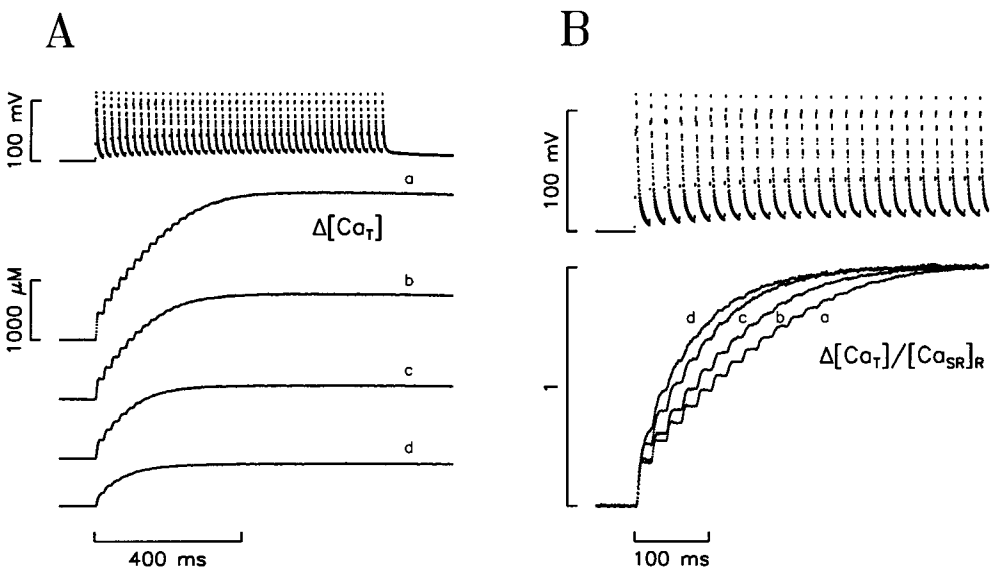


FIGURE 1. Effect of $[Ca_{SR}]_R$ on the time course of Ca release during a train of action potentials. (*A*) The top trace shows four superimposed records of 40 action potentials at 50 Hz. The next four traces show the associated $\Delta[Ca_T]$ signals arranged in chronological order, with $[Ca_{SR}]_R$ = 2,452 μM in *a*, 1,760 μM in *b*, 1,224 μM in *c*, and 708 μM in *d*. (*B*) The top superimposed traces show the first 24 action potentials from the traces in *A*, plotted with expanded vertical and horizontal gains. The four superimposed traces at the bottom were obtained by dividing each of the $\Delta[Ca_T]$ traces in *A* by the corresponding value of $[Ca_{SR}]_R$ to give a final amplitude of unity. Fiber reference, 425911; time after saponin treatment, 125 min in *a*, 143 min in *b*, 153 min in *c*, and 173 min in *d*. First-to-last measurements: fiber diameter, 86–82 μm; holding current, −40 to −52 nA; amplitude of the first action potential in each trial (measured on a digital oscilloscope), 118 mV throughout; concentration of phenol red at the optical site, 0.974–1.644 mM; estimated $pH_R$, 6.882–6.804. Estimated $[Ca]_R$, 0.062 μM in *a* and unknown in *b*–*d* (because the values of resting [CaEGTA] and [EGTA] at the optical site were uncertain after the removal of Ca from the end-pool solutions); interval of time between data points, 0.48 ms. The K-glutamate solution used in the end pools contained 1.76 mM Ca during the first 129 min after saponin treatment and 0 mM Ca thereafter. In this and subsequent figures, the left tick on the time calibration bar marks the onset of the first stimulation.

1988). According to Schneider and Simon (1988) (see also Jong et al., 1995*a*), its properties can be described by a model in which Ca equilibrates rapidly with a receptor on the release channel, after which the Ca receptor–channel complex is able to undergo a slower transition to an inactivated state.

The amplitude of the $\Delta[Ca_T]$ signal elicited by the second action potential in Fig. 1 *A*, *a*, was only half that elicited by the first action potential. Part of the reduction can be attributed to a decrease in $[Ca_{SR}]$ after the first response. Most of the reduction, however, is probably caused by Ca inactivation of Ca release produced by the first response, even though the internal solution contained 20 mM EGTA (Jong et al., 1995*a*). The responses elicited by the third and subsequent action potentials progressively decreased, and, after 20–30 action potentials, $\Delta[Ca_T]$ had reached a maximal value of 2,452 μM, which is taken for the value of $[Ca_{SR}]_R$.

4 min after Fig. 1 *A*, *a*, was taken, Ca was removed from the end-pool solution. *b*–*d* were obtained after the SR Ca content had been reduced by repeated stimulation with a train of action potentials, delivered first every 5 min and then every 2 min. During this period, the value of $[Ca_{SR}]_R$ decreased from 2,452 μM in *a* to 1,760 μM in *b*, 1,224 μM in *c*, and 708 μM in *d*.

Fig. 1 *B* shows voltage and $\Delta[Ca_T]$ during the first 24 action potentials in *A*; the $\Delta[Ca_T]$ signals have been normalized by $[Ca_{SR}]_R$ to give a maximal value of unity and have been plotted on expanded horizontal and vertical gains. $f_1$ was 0.181 in *a* and 0.194 in *b*. These values are slightly larger than the mean value of 0.144 (SEM, 0.004) found by Pape et al. (1995) in 12 fibers with $[Ca_{SR}]_R$ = 1,391–4,367 μM. The normalized increase in $\Delta[Ca_T]$ produced by the first few action potentials became progressively larger from *a* to *d*, indicating a more rapid fractional depletion of Ca from the SR. In addition, the stepwise appearance of the $\Delta[Ca_T]$ signal after each action potential became progressively more rounded from *a* to *d*. The experiments described below were undertaken to study possible causes of these changes, such as a reduction of Ca inactivation of Ca release associated with partial SR Ca depletion.

### *Changes in the Action Potential when $[Ca_{SR}]_R$ Is Varied between 150 and 1,200 μM*

The purpose of the experiment described in Figs. 2–4 was to reduce $[Ca_{SR}]_R$ to values smaller than those used in Fig. 1 and to study the effect on the action potential, as described in this section, and on SR Ca release, as described in the following section. The value of $[Ca_{SR}]_R$ was varied reversibly between 140 and 1,154 μM by the use of 0.44 mM Ca in the end-pool solution and by variation of the recovery period between successive trials between 0.5 and 10 min.

Fig. 2 *A*, *top*, shows superimposed voltage records from four trials. A single action potential was followed by a 150-ms recovery period. Then, a train of action

potentials was used to deplete the SR of its readily releasable Ca so that the value of $[Ca_{SR}]_R$ could be determined. During the first part of each trace, the interval of time between data points was 0.12 ms, which is sufficiently brief to resolve the time courses of the first action potential and of the associated rate of SR Ca release. After the recovery period, the interval of time between data points was increased to 0.6 ms, which allowed resolution of the relatively slow changes in $\Delta[Ca_T]$, but not the time courses of the individual action potentials in the train.

Fig. 2 *A, a–d,* show the $\Delta[Ca_T]$ signals associated with the four trials. The value of $[Ca_{SR}]_R$ was decreased from 512 μM in *a* to 296 μM in *b* to 146 μM in *c* by the use of progressively shorter recovery periods between trials (see legend). The recovery period was increased after *c,* and, when *d* was taken, the value of $[Ca_{SR}]_R$ was 876 μM. More information about the $\Delta[Ca_T]$ signals is given in the legend of Fig. 2 and in the following section.

In Fig. 2 *B, top,* superimposed traces show the first action potential of each trial, plotted on expanded vertical and horizontal gains. Action potentials *a* and *d* are similar to each other and have a shorter duration than *b,* which has a shorter duration than *c.*

The difference between action potentials is seen more clearly in Fig. 2 *C, c* and *d,* where the time scale has been expanded. The top pair of traces shows that, during the first 2 ms after stimulation, the two action potentials were virtually identical. During the next millisecond, the traces started to diverge as the slope of *d* became more negative than that of *c.*

For a membrane action potential in an axon with

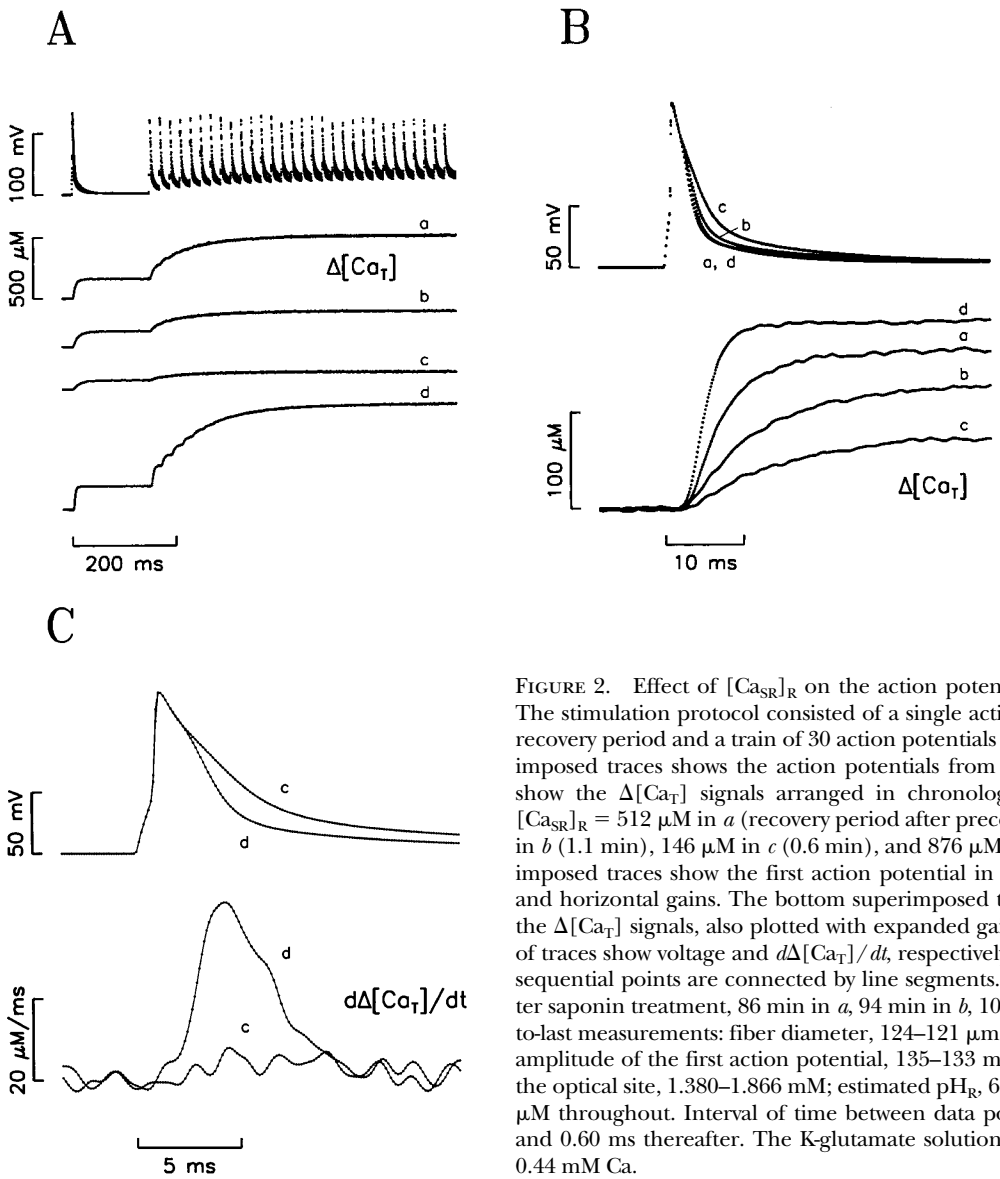


FIGURE 2. Effect of $[Ca_{SR}]_R$ on the action potential and associated SR Ca release. The stimulation protocol consisted of a single action potential followed by a 150-ms recovery period and a train of 30 action potentials at 50 Hz. (*A*) The top set of superimposed traces shows the action potentials from four trials. The other four traces show the $\Delta[Ca_T]$ signals arranged in chronological order from top to bottom; $[Ca_{SR}]_R$ = 512 μM in *a* (recovery period after preceding stimulation, 2 min), 296 μM in *b* (1.1 min), 146 μM in *c* (0.6 min), and 876 μM in *d* (10 min). (*B*) The top superimposed traces show the first action potential in *A*, plotted with expanded vertical and horizontal gains. The bottom superimposed traces show the initial segments of the $\Delta[Ca_T]$ signals, also plotted with expanded gains. (*C*) The top and bottom pairs of traces show voltage and $d\Delta[Ca_T]/dt$, respectively, from *c* and *d* in *B*; in each trace, sequential points are connected by line segments. Fiber reference, O03911; time after saponin treatment, 86 min in *a*, 94 min in *b*, 101 min in *c*, and 136 min in *d*. First-to-last measurements: fiber diameter, 124–121 μm; holding current, −59 to −69 nA; amplitude of the first action potential, 135–133 mV; concentration of phenol red at the optical site, 1.380–1.866 mM; estimated $pH_R$, 6.964–6.962; estimated $[Ca]_R$, 0.009 μM throughout. Interval of time between data points, 0.12 ms for the first 180 ms and 0.60 ms thereafter. The K-glutamate solution used in the end pools contained 0.44 mM Ca.

constant surface capacitance ($C$), a more negative slope would be expected to have been caused by an increase in outward ionic current equal to $-CdV/dt$ (Hodgkin and Huxley, 1952). In a muscle fiber, however, the situation is complicated by the presence of the transverse tubular system. As a consequence, if $C$ represents the capacitance of the surface membrane of the fiber, $-CdV/dt$ would equal the sum of the ionic current through the surface membrane and the current from the mouths of the transverse tubules where they invaginate from the surface membrane. Another complication of the muscle fiber experiment is that the ideal of a membrane action potential is only approximately realized in a fiber mounted in a double Vaseline-gap chamber. In spite of these complications, however, the idea that the more negative slope of $d$ is caused by an increase in outward ionic current across the surface and/or tubular membranes is still expected to apply. During the period when $c$ and $d$ diverged, the maximal value of the difference between the derivatives of the traces (not shown) occurred 3.2 ms after stimulation and was 17 mV/ms. This indicates that the outward ionic current at this time was larger in $d$ than in $c$ by $\sim$17 mV/ms = 17 $\mu$A/$\mu$F. With the internal and external solutions used in this experiment, such an outward ionic current could have been carried by potassium ions leaving the fiber or chloride ions entering the fiber.

At about the time that action potentials $c$ and $d$ in Fig. 2 started to diverge, the associated $d\Delta[Ca_T]/dt$ signals became noticeably different; $d\Delta[Ca_T]/dt$ represents the estimated rate of SR Ca release. A possible explanation for the extra outward ionic current in action potential $d$ is that SR Ca release produced an increase in myoplasmic free [Ca], which is expected to be approximately proportional to the rate of SR Ca release (Pape et al., 1995), and that this, in turn, activated ionic channels permeable to potassium or chloride. A comparison (not shown) of the differences between the two $dV/dt$ signals and the two $d\Delta[Ca_T]/dt$ signals in Fig. 2 $C$ indicates that such channel activation by Ca must have been rapid, with a delay no greater than 1–2 ms.

Fig. 3 shows the amplitude of the first action potential of a stimulation ($A$) and its half-width ($B$) plotted as a function of $[Ca_{SR}]_R$, from the experiment in Fig. 2. The half-width is taken to be the interval between the times to half-peak on the rising and falling phases of the signal. In this figure, filled circles (which include $a$–$c$) denote values obtained during the first part of the experiment, when the value of $[Ca_{SR}]_R$ was decreased from 1,154 to 146 $\mu$M by a progressive decrease in the recovery period between successive trials from 5 to 0.5–0.6 min. Open circles (including $d$) denote values obtained thereafter, when the recovery period was progressively increased to 10 min, decreased to 0.5 min, and finally increased again to 10 min.

In Fig. 3 $A$, the first stimulation occurred when $[Ca_{SR}]_R$ = 1,154 $\mu$M and the amplitude of the first action potential was 135.0 mV (● at extreme right). The amplitude showed little change during the experiment, with a small progressive decrease, $\leq$3 mV, that can be reasonably attributed to fiber run down.

In contrast, Fig. 3 $B$ shows that the half-width of the action potential was increased when the value of $[Ca_{SR}]_R$ was decreased from its initial value of 1,154 to 146 $\mu$M (Fig. 3 $B$, ●). The increase in half-width was most pronounced for $[Ca_{SR}]_R \leq 500$ $\mu$M. Most of this increase in half-width was reversed when the value of $[Ca_{SR}]_R$ was allowed to increase (○).

The tentative conclusions of this section are that ($a$) an increase in the value of $[Ca_{SR}]_R$ from 150 to 800 $\mu$M

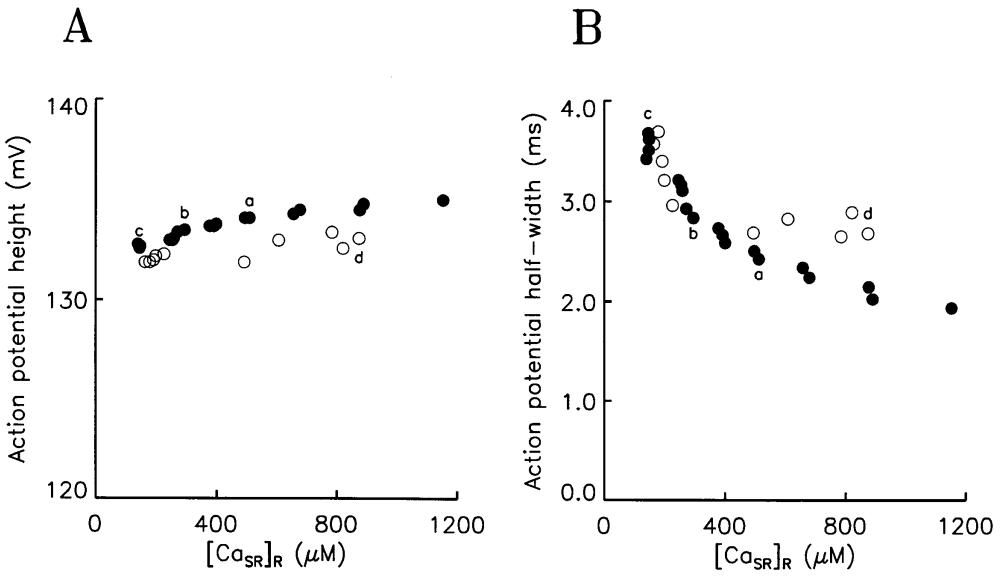


FIGURE 3. Amplitude ($A$) and half-width ($B$) of the first action potential in each trial in the experiment illustrated in Fig. 2, plotted as a function of $[Ca_{SR}]_R$. In this and the following figure, filled and open circles denote values from the first and second set of measurements made 63–101 min and 106–161 min, respectively, after saponin treatment. The letters $a$–$d$ are placed at the horizontal locations of $[Ca_{SR}]_R$ from the traces in Fig. 2; measurement $c$ was made 101 min after saponin treatment. Additional information is given in the text.

produces a reversible 1–2-ms decrease in the half-width of the action potential, (*b*) the outward ionic current responsible for this decrease flows through Ca-activated potassium or chloride channels, and (*c*) the activation of these channels by Ca is normally rapid, developing within 1–2 ms after SR Ca release begins.

### *Changes in SR Ca Release Elicited by a Single Action Potential when $[Ca_{SR}]_R$ Is Varied between 150 and 1,200 μM*

Fig. 2 *A, a–d*, shows four $\Delta[Ca_T]$ signals obtained with $[Ca_{SR}]_R$ = 146–876 μM. The value of $[Ca_{SR}]_R$ and the amplitude of the $\Delta[Ca_T]$ signal after the first action potential progressively decreased from *a* to *b* to *c*, and then increased in *d* to values larger than those in *a*. The initial segments of the $\Delta[Ca_T]$ traces are shown in Fig. 2 *B*, plotted on expanded horizontal and vertical gains. These signals show that, as the value of $[Ca_{SR}]_R$ was decreased, the $\Delta[Ca_T]$ signal became more rounded, indicating a longer period of SR Ca release.

Fig. 4 *A* shows the value of $\Delta[Ca_T]$ after the first action potential in each trial, plotted as a function of $[Ca_{SR}]_R$. The concave curvature of the relation between $\Delta[Ca_T]$ and $[Ca_{SR}]_R$ indicates that the reduction in $\Delta[Ca_T]$ was less marked than that in $[Ca_{SR}]_R$. For example, a threefold decrease in $[Ca_{SR}]_R$ from 1,200 to 400 μM resulted in a reduction of $\Delta[Ca_T]$ of only 30%. Thus, under these conditions, the amount of Ca released by an action potential is relatively insensitive to SR Ca content. On the other hand, a steeper dependence was observed for values of $[Ca_{SR}]_R < 400$ μM. The open and filled circles track the same relation between $\Delta[Ca_T]$ and $[Ca_{SR}]_R$, showing that the effect of $[Ca_{SR}]_R$ on $\Delta[Ca_T]$ was reversible.

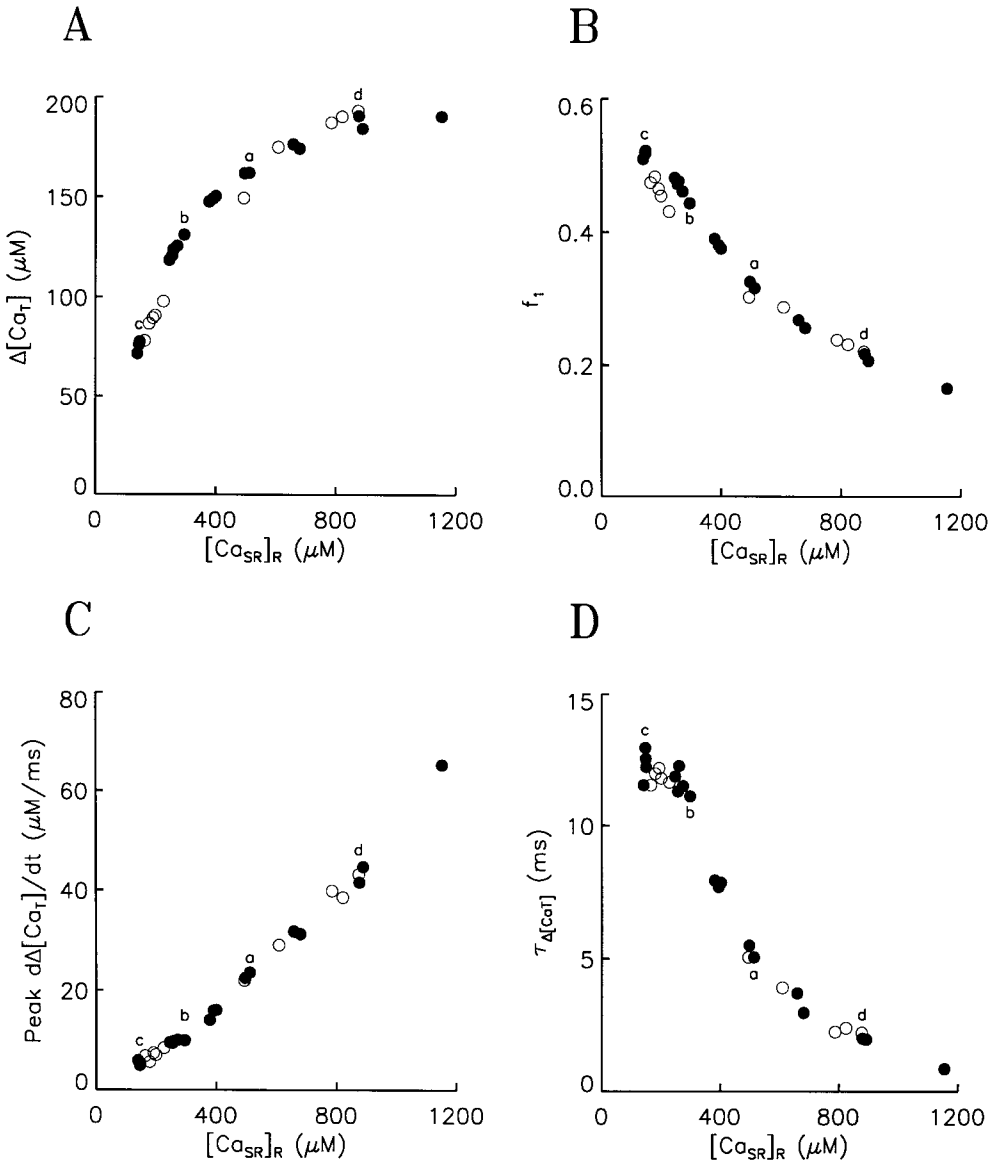


FIGURE 4. Parameters associated with SR Ca release after the first action potential in each trial in the experiment illustrated in Fig. 2, plotted as a function of $[Ca_{SR}]_R$. (*A*) $\Delta[Ca_T]$. (*B*) $f_1$. (*C*) Peak values of $d\Delta[Ca_T]/dt$. (*D*) Final time constant of $\Delta[Ca_T]$ ($\tau_{\Delta[CaT]}$); this was determined from a least-squares fit of a single exponential function plus a constant to $\Delta[Ca_T]$ in the interval between the time to half steady value and 100 ms after stimulation. Additional information is given in the text.

Fig. 4 *B* shows the corresponding dependence of $f_1$ on $[Ca_{SR}]_R$. The value of $f_1$ increased threefold from 0.165 at $[Ca_{SR}]_R$ = 1,154 μM to 0.51–0.52 at $[Ca_{SR}]_R$ = 140–150 μM. Remarkably, at the smallest values of $[Ca_{SR}]_R$ obtained in this experiment, 140–150 μM, slightly more than half of the readily releasable Ca inside the SR was released by the first action potential.

Fig. 4 *C* shows the peak value of $d\Delta[Ca_T]/dt$ plotted as a function of $[Ca_{SR}]_R$. The relation is slightly convex, indicating that the increase in $f_1$ associated with decreasing $[Ca_{SR}]_R$ (Fig. 4 *B*) is not caused by an increase in the fractional rate of SR Ca release; rather, it occurs in spite of a small decrease in the peak fractional rate of release.

Since the $d\Delta[Ca_T]/dt$ signals are noisier than the $\Delta[Ca_T]$ signals (compare, for example, Fig. 2, *B* and *C*), the data in Fig. 4 *C* have more fractional scatter than those in Fig. 4 *A*, especially at small values of $[Ca_{SR}]_R$. Noise reduces the reliability of estimates of the half-width of $d\Delta[Ca_T]/dt$ and its final time constant when the value of $[Ca_{SR}]_R$ is small (Fig. 2 *C*; but see Fig. 7, *C* and *D*). In this situation, the time constant associated with the final half of the $\Delta[Ca_T]$ signal ($\tau_{\Delta[CaT]}$) can be used as an estimate of the duration of SR Ca release. Fig. 4 *D* shows $\tau_{\Delta[CaT]}$ plotted as a function of $[Ca_{SR}]_R$. From $[Ca_{SR}]_R$ = 1,154 to 140–150 μM, the value of $\tau_{\Delta[CaT]}$ increased by an order of magnitude, from 0.9 to 11–13 ms.

The value 11–13 ms is similar to the time constant expected for Ca dissociation from the Ca-regulatory sites on troponin, estimated to be 8.7 ms (column 5 in Table I, model 2, in Baylor et al., 1983). This similarity raises the possibility that, with $[Ca_{SR}]_R$ = 140–150 μM, the Ca complexed by EGTA (which determines $\Delta[Ca_T]$) came from Ca that had just dissociated from troponin rather than from Ca that had just left the SR. This seems unlikely for the following reason. In fibers with $[Ca_{SR}]_R \geq$ 1,391 μM, the increase in [CaEGTA] that accompanies Ca dissociation from troponin after an action potential appears to be negligibly small and not statistically significant, 2.9 μM (SEM, 3.8 μM) (Table III in Pape et al., 1995). Since a decrease in $[Ca_{SR}]_R$ would be expected to produce a decrease, not an increase, in the amount of Ca complexed by troponin, it seems unlikely that Ca that dissociated from troponin made a significant contribution to the Ca that was complexed by EGTA during the 140–150 μM $\Delta[Ca_T]$ signals that had the 11–13-ms time constant.

These results show that, when the SR is partially depleted of Ca, the amount of Ca released by a single action potential does not decrease in proportion to the value of $[Ca_{SR}]_R$ (Fig. 4 *A*). Rather, its value is partially stabilized by an increase in $f_1$ (Fig. 4 *B*) that is caused by a prolongation of Ca release (increase in $\tau_{\Delta[CaT]}$, Fig. 4 *D*). This prolongation of Ca release may be due, at least in part, to the accompanying prolongation of the action potential (Figs. 2 *C* and 3 *B*). The order-of-magnitude increase in $\tau_{\Delta[CaT]}$, however, suggests that some other effect may also be involved (next section).

### *The Effect of Partial SR Ca Depletion on Action Potential–stimulated SR Ca Release Can Be Mimicked by a Brief Voltage-Clamp Depolarization*

To study further the effect of $[Ca_{SR}]$ on the rate of turnoff of SR Ca release, experiments were carried out on voltage-clamped fibers. One advantage of this method is that, unlike experiments with action potential stimulation, the voltage waveform is constant and does not depend on the value of $[Ca_{SR}]_R$; thus, any changes in release that are observed cannot be attributed to changes in voltage. Another advantage is that measurements can be made of intramembranous charge movement ($Q_{cm}$), which is thought to arise from movement of the voltage sensors for SR Ca release. Such information might help determine whether changes in the turnoff of SR Ca release are caused by changes in the voltage sensor. Before describing the effects of $[Ca_{SR}]$ on $Q_{cm}$, however, it is important to establish that the effect of SR Ca depletion on Ca release is similar with voltage-clamp and action potential stimulation.

Fig. 5 shows the results of a voltage-clamp experiment that was designed to mimic the action potential experiment illustrated in Fig. 2. For this purpose, the same concentration of Ca, 0.44 mM, was used in the end-pool solution. A 10-ms pulse to −20 mV was used to release a small fraction of the readily releasable Ca from the SR, similar to that released by the first action potential in a trial in Fig. 2. This pulse was followed by a 200-ms repolarization to −90 mV, and then a 420-ms depolarization to −40 mV to deplete the SR of its remaining Ca so that the value of $[Ca_{SR}]_R$ could be determined.

Fig. 5 *A, a,* shows the $\Delta[Ca_T]$ signal that was obtained 78 min after saponin treatment. After the first depolarization, $\Delta[Ca_T]$ reached a value of 229 μM. By the end of the second depolarization, $\Delta[Ca_T]$ had increased to a quasi-steady value of 1,152 μM, which is taken for the value of $[Ca_{SR}]_R$. Thus, the first depolarization released 229/1,152 = 0.199 of the readily releasable Ca from the SR, similar to the fraction $f_1$ released by the first action potential in Fig. 2 *d* (0.221 with $[Ca_{SR}]_R$ = 876 μM). Fig. 5 *A, b* and *c,* were obtained later in the experiment after the value of $[Ca_{SR}]_R$ had decreased to 430 and 213 μM, respectively. The $\Delta[Ca_T]$ traces in Fig. 5, *A* and *B,* are similar to those in Fig. 2, *A* and *B.*

Fig. 6 shows the effect of $[Ca_{SR}]_R$ on $\Delta[Ca_T]$ (*A*), $f_1$ (*B*), peak $d\Delta[Ca_T]/dt$ (*C*), and $\tau_{\Delta[CaT]}$ (*D*), from the experiment illustrated in Fig. 5. It is plotted with the same format used in Fig. 4. Filled circles represent measurements made when the recovery period between successive trials was progressively decreased from 5 to 1 min.

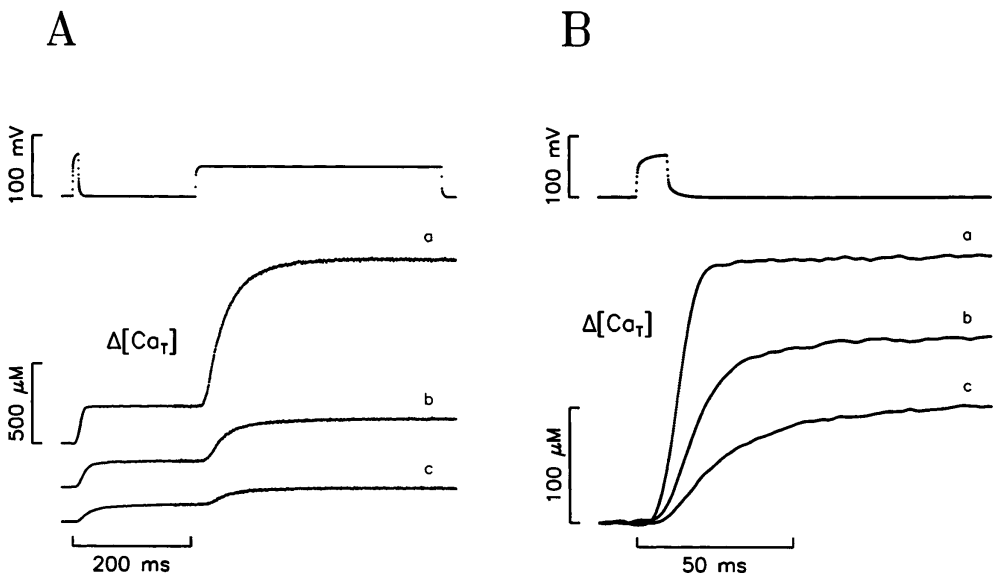


FIGURE 5. Effect of $[Ca_{SR}]_R$ on Ca release elicited by a brief voltage-clamp depolarization, plotted with the same format used for Fig. 2, *A* and *B*. $[Ca_{SR}]_R$ = 1,152 μM in *a* (recovery period after preceding stimulation, 5 min), 430 μM in *b* (3 min), and 213 μM in *c* (1.5 min). Fiber reference, O08911; time after saponin treatment, 78 min in *a*, 103 min in *b*, and 113 min in *c*. First-to-last measurements: fiber diameter, 134–135 μm; holding current, −34 to −36 nA; concentration of phenol red at the optical site, 1.142–1.530 mM; estimated $pH_R$, 6.824–6.797; estimated $[Ca]_R$, 0.017–0.019 μM. Interval of time between data points, 0.12 ms for the first 204 ms and 0.60 ms thereafter. The Cs-glutamate solution used in the end pools contained 0.44 mM Ca.

After the value of $[Ca_{SR}]_R$ had decreased to 141 μM by three successive stimulations with recovery periods of 1 min (three ● at extreme left in each panel), the recovery period was increased to 10 min for two trials (○), and then, 35 min later in the experiment, to 5 min for two trials (□). The relations between release parameters and $[Ca_{SR}]_R$ in Fig. 6 are similar to those in Fig. 4.

In the experiment in Fig. 6, after the value of $[Ca_{SR}]_R$ had been decreased to 141 μM, its value was increased to only 205–212 μM by increasing the recovery period to 10 min (○). A similar small increase in $[Ca_{SR}]_R$, from 148 μM after two 1-min recovery periods to 174 μM after a 10-min recovery period, was observed in the other voltage-clamp experiment in which 0.44 mM Ca was used in the end-pool solution (fiber O08912). This small recovery of $[Ca_{SR}]_R$ is unlike the large recovery observed in the action potential experiment in Fig. 2, from 146 μM in *c* to 876 μM in *d*. Although the reason for this difference is unknown, an important factor may be the presence of 1.8 mM Ca in the external solution in the action potential experiments and the absence of external Ca in the voltage-clamp experiments. Whatever the reason, the poor recovery of $[Ca_{SR}]_R$ in the voltage-clamp experiments makes it difficult to study the reversibility of the effect of $[Ca_{SR}]_R$ on SR Ca release in these experiments, as was done in the action potential experiments (Fig. 2).

Experiments similar to the one in Figs. 5 and 6 were carried out on three other voltage-clamped fibers in which a 10–12-ms pulse to −20 mV was used for the first stimulation. In one of the experiments (O08912), 0.44 mM Ca was used in the end-pool solution, and the value of $[Ca_{SR}]_R$ was reduced by progressively decreasing the recovery period between successive trials from 5 to 1 min, as was done in the experiment in Figs. 5 and 6. In the other two experiments (N14911 and N15911), the fibers were first equilibrated with an end-pool solution that contained 1.76 mM Ca. Then, Ca was removed from the end-pool solution and the value of $[Ca_{SR}]_R$ was reduced by successive stimulations every 1.5 min. The results of all four experiments were similar; the mean value of $f_1$ was 0.147 (SEM, 0.022) with $[Ca_{SR}]_R$ = 1,000–1,200 μM and 0.267 (SEM, 0.082) with $[Ca_{SR}]_R$ = 140–300 μM; the mean value of the ratio $f_1([Ca_{SR}]_R = 140–300\ \mu M)/f_1([Ca_{SR}]_R = 1{,}000–1{,}200\ \mu M)$ was 1.71 (SEM, 0.33), which is not significantly different from unity. The mean value of $\tau_{\Delta[CaT]}$ was 3.63 ms (SEM, 0.54 ms) with $[Ca_{SR}]_R$ = 1,000–1,200 μM and 16.9 ms (SEM, 4.0 ms) with $[Ca_{SR}]_R$ = 140–300 μM; the mean value of the ratio $\tau_{\Delta[CaT]}([Ca_{SR}]_R = 140–300\ \mu M)/\tau_{\Delta[CaT]}([Ca_{SR}]_R = 1{,}000–1{,}200\ \mu M)$ was 4.51 (SEM, 0.59), which is significantly different from unity.

The results in Fig. 6 and those described in the preceding paragraph are qualitatively similar to those in Fig. 4. This suggests that the effect of $[Ca_{SR}]_R$ on $\Delta[Ca_T]$ signals elicited by action potential stimulation cannot be explained primarily by the effect of $[Ca_{SR}]_R$ on the duration of the action potential.

### *The Effect of Partial SR Ca Depletion on $d\Delta[Ca_T]/dt$*

Further analysis of the $\Delta[Ca_T]$ signals in Fig. 5 is shown in Fig. 7. Fig. 7 *A, middle*, shows $d\Delta[Ca_T]/dt$ expressed in units of micromolar per millisecond. As the value of

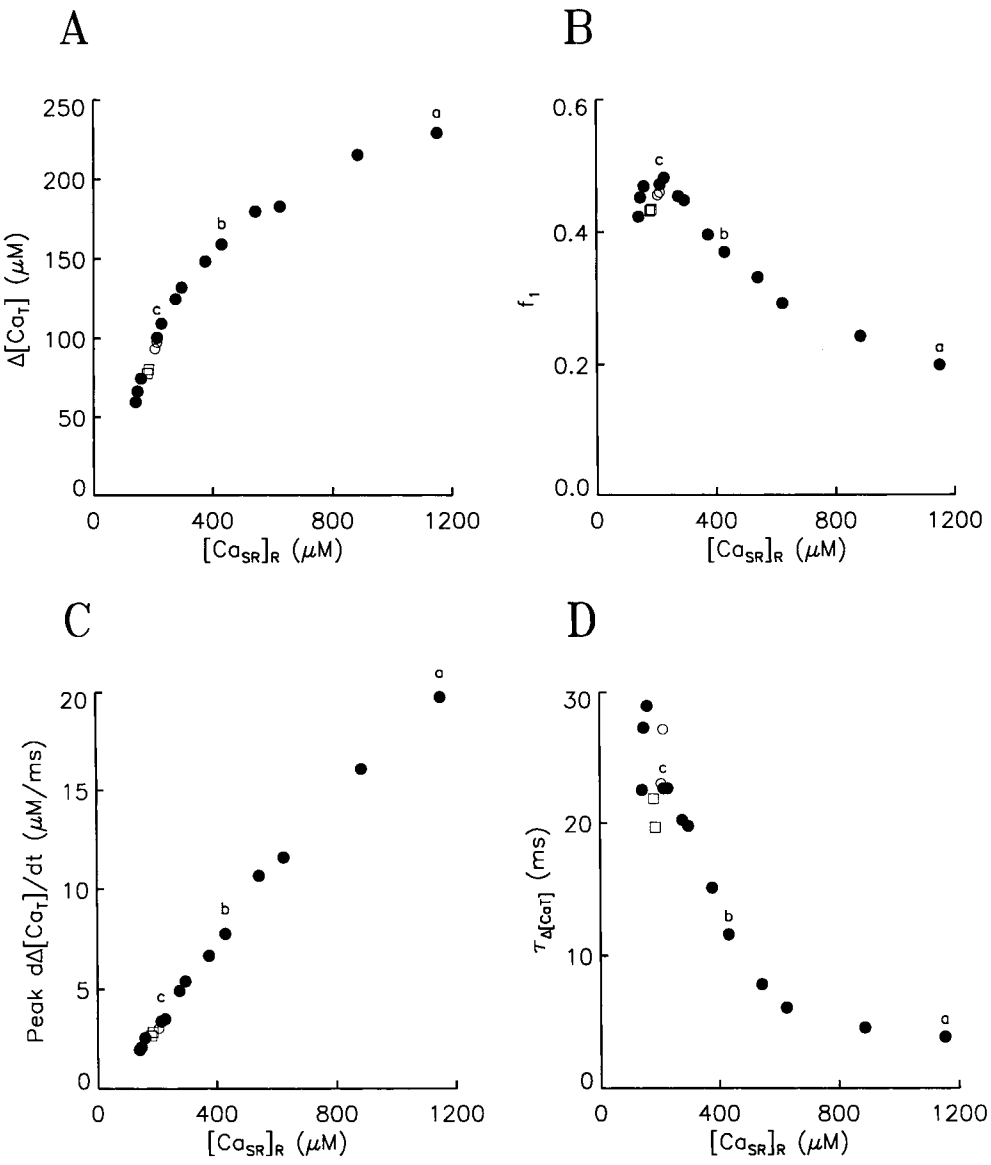


FIGURE 6. Parameters associated with SR Ca release after a brief voltage pulse plotted as a function of $[Ca_{SR}]_R$, from the experiment illustrated in Fig. 5. Same format as Fig. 4. Filled circles denote measurements made 78–116 min after saponin treatment. Open symbols denote measurements made when the recovery period was either 10 min (126–136 min after saponin treatment, *circles*) or 5 min (171–181 min after saponin treatment, *squares*). The letters *a–c* are placed at the horizontal locations of $[Ca_{SR}]_R$ from the traces in Fig. 5. Additional information is given in the text.

$[Ca_{SR}]_R$ decreased from 1,152 (*a*) to 430 (*b*) to 213 (*c*) μM (only *a* and *c* are labeled), the amplitude of $d\Delta[Ca_T]/dt$ was decreased and its duration was increased.

Fig. 7 *A, bottom*, shows $d\Delta[Ca_T]/dt$ corrected for SR Ca depletion. At each moment in time, the value of $d\Delta[Ca_T]/dt$ in units of micromolar per millisecond was divided by $[Ca_{SR}]_R - \Delta[Ca_T]$ and multiplied by 100 to give units in percent per millisecond (Jacquemond et al., 1991). Because of the division by $[Ca_{SR}]_R - \Delta[Ca_T]$, each trace becomes progressively noisier with time, and the noise increases from *a* to *b* to *c*. Within the noise of the signals, the initial time courses are similar. After the peak value was reached, however, the duration became progressively longer from *a* to *b* to *c*.

Fig. 7 *B* shows the peak amplitude of $d\Delta[Ca_T]/dt$ in units of percent per millisecond, plotted as a function of $[Ca_{SR}]_R$. The values increased slightly from $[Ca_{SR}]_R$ = 1,152 to 300–400 μM, and then decreased as the value of $[Ca_{SR}]_R$ became smaller than 300 μM. In 25 measurements of $d\Delta[Ca_T]/dt$ in four fibers, the mean peak value of $d\Delta[Ca_T]/dt$ with $[Ca_{SR}]_R$ = 140–300 μM was 0.861 (SEM, 0.016) times that measured in the same fiber with $[Ca_{SR}]_R$ = 600–1,200 μM; the value 0.861 is significantly different from unity.

Fig. 7 *C* shows the half-width of $d\Delta[Ca_T]/dt$ (●, ○, and □) and its time to half-peak (■), plotted as a function of $[Ca_{SR}]_R$. Fig. 7 *D* shows the final time constant of $d\Delta[Ca_T]/dt$ ($\tau_{d\Delta[CaT]/dt}$). As the value of $[Ca_{SR}]_R$ decreased from 1,152 to 141 μM, the half-width of $d\Delta[Ca_T]/dt$ (*C*) and the value of $\tau_{d\Delta[CaT]/dt}$ (*D*) progressively increased; in both panels, the open symbols and filled circles superimpose within the scatter of the points. On the other hand, the relative constancy of Fig. 7 *C*, ■, shows that the rising phase of $d\Delta[Ca_T]/dt$ was little affected by $[Ca_{SR}]_R$.

It is clear from Fig. 7 *A, bottom*, that the $d\Delta[Ca_T]/dt$

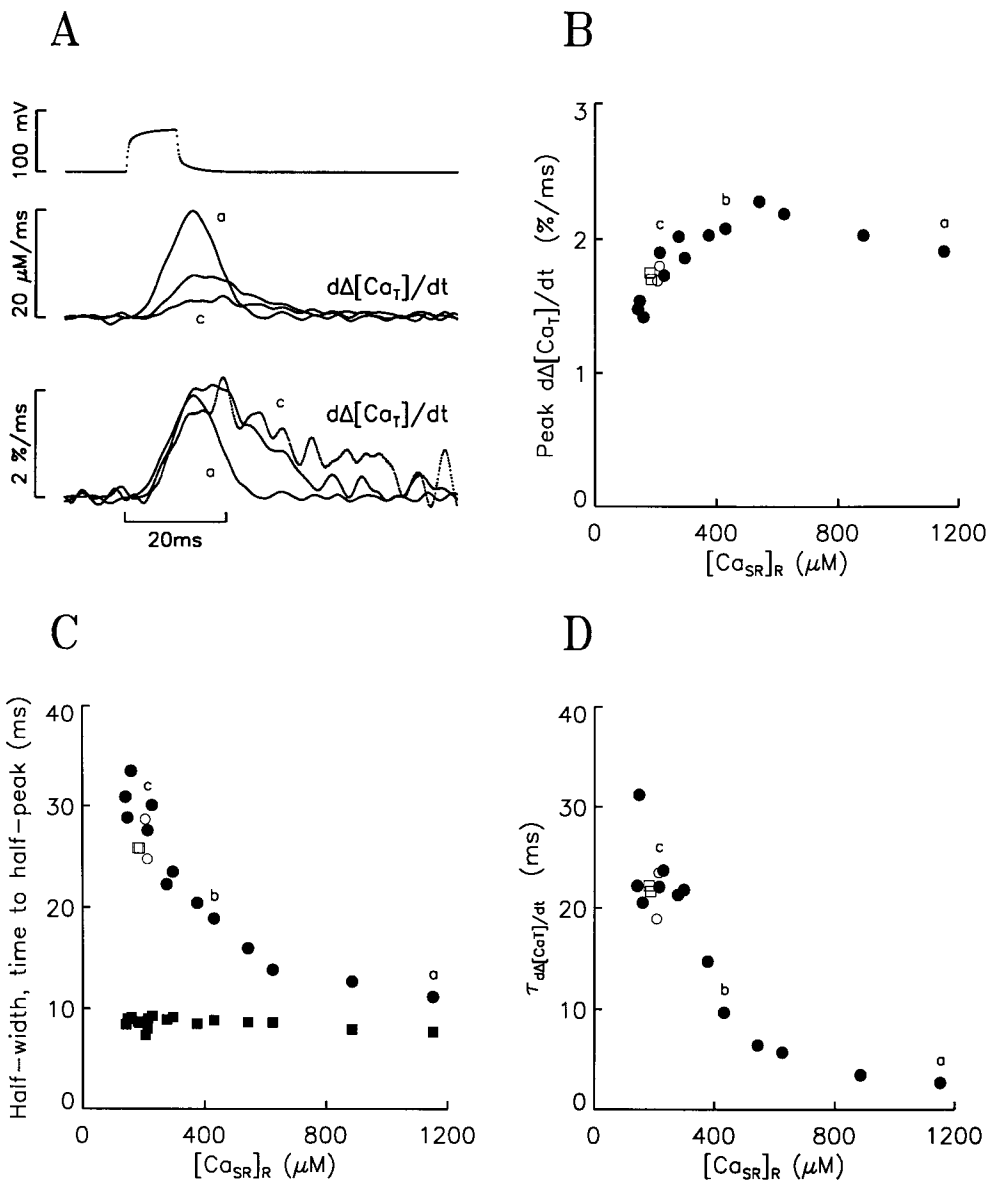


FIGURE 7. Properties of $d\Delta[Ca_T]/dt$ elicited by a brief voltage pulse, from the experiment illustrated in Fig. 5. (*A*) Three superimposed traces of $V$ (*top*), $d\Delta[Ca_T]/dt$ expressed in units of μM/ms (*middle*), and $d\Delta[Ca_T]/dt$ expressed in units of %/ms (*bottom*) from the same trials used for Fig. 5; only traces *a* and *c* are labeled. (*B*) Peak $d\Delta[Ca_T]/dt$ (%/ms) plotted as a function of $[Ca_{SR}]_R$, with filled and open symbols as described in Fig. 6. (*C*) Half-width of $d\Delta[Ca_T]/dt$ (%/ms) (*filled circles and open symbols*) and time to half-peak (*filled squares*). (*D*) Final time constant of $d\Delta[Ca_T]/dt$ (%/ms) ($\tau_{d\Delta[CaT]/dt}$).

signal became noisier as the value of $[Ca_{SR}]_R$ became smaller, making the determinations of the half-width of $d\Delta[Ca_T]/dt$ (Fig. 7 *C*) and of the value of $\tau_{d\Delta[CaT]/dt}$ (Fig. 7 *D*) more difficult. For this reason, the filled circles at the left-hand side of Fig. 7, *C* and *D*, with small values of $[Ca_{SR}]_R$, show considerable scatter. In spite of this, the relation between $\tau_{d\Delta[CaT]/dt}$ and $[Ca_{SR}]_R$ in Fig. 7 *D* is similar to that between $\tau_{\Delta[CaT]}$ and $[Ca_{SR}]_R$ in Fig. 6 *D*, which suggests that the relation in Fig. 7 *D* is reliable within the noise of the $d\Delta[Ca_T]/dt$ signals. This being the case, it seems likely that the relation between the half-width of $d\Delta[Ca_T]/dt$ and $[Ca_{SR}]_R$ in Fig. 7 *C* is also reliable.

In four fibers, the mean value of $\tau_{d\Delta[CaT]/dt}$ was 2.48 ms (SEM, 0.53 ms) with $[Ca_{SR}]_R$ = 1,000–1,200 μM and 16.2 ms (SEM, 4.0 ms) with $[Ca_{SR}]_R$ = 140–300 μM; the mean value of the ratio $\tau_{d\Delta[CaT]/dt}$ ($[Ca_{SR}]_R$ = 140–300 μM)/$\tau_{d\Delta[CaT]/dt}$($[Ca_{SR}]_R$ = 1,000–1,200 μM) was 6.47 (SEM, 0.76), which is significantly different from unity.

The results in this section, obtained from voltage-clamped fibers, confirm those obtained with action potential stimulation (Fig. 4). In particular, when the value of $[Ca_{SR}]_R$ is decreased from 1,000–1,200 to 140–300 μM, the observed increase in $f_1$ (Fig. 6 *B*) is caused by a prolongation of SR Ca release (Fig. 7, *C* and *D*), and not by an increase in the fractional rate of release (Fig. 7 *B*).

### *The Effect of Partial SR Ca Depletion on $Q_{cm}$*

The next question to consider is whether partial SR Ca depletion affects the voltage sensor for SR Ca release. Fig. 8 *A, middle*, shows the currents from intramembranous charge movement ($I_{cm}$) associated with Fig. 5, *a–c* (only *a* and *c* are labeled). The ON waveforms of *a* and

*b* superimpose, with an amplitude that is slightly larger than that of *c*, owing to a small decrease in the amount of charge in *c* (see below). On the other hand, the OFF waveforms of $I_{cm}$ are clearly different. From *a* to *b* to *c*, as the value of $[Ca_{SR}]_R$ decreased from 1,152 to 430 to 213 μM, the amplitude of the OFF response became smaller and its duration became longer.

Fig. 8 *A*, *bottom*, shows $Q_{cm}$, the running integral of $I_{cm}$, which is expected to be more closely related than $I_{cm}$ to the state of activation of the SR Ca channels. Except for a small reduction in the amplitude of *c*, the initial time courses of the three traces are similar until the time to peak; thereafter, the return to baseline became progressively slower from *a* to *b* to *c*.

Fig. 8 *B*, ●, shows the peak value of $Q_{cm}$ plotted as a function of $[Ca_{SR}]_R$. As expected from Fig. 8 *A*, *bottom*, the peak value of $Q_{cm}$ was similar in *a* and *b* and was slightly smaller in *c*. The 10–15% decrease in $Q_{cm}$ that was associated with the decrease in $[Ca_{SR}]_R$ from 600 to 141 μM may have been caused by a direct effect of the reduction in $[Ca_{SR}]_R$ or by the decrease in the recovery period between successive trials that was used to reduce $[Ca_{SR}]_R$ from 4 to 1 min. Since the decrease in $Q_{cm}$ was reversed by increasing the recovery period to 5 or 10 min (□ and ○, respectively), which increased $[Ca_{SR}]_R$ only slightly, the decrease in recovery period is the more likely explanation. Such a decrease in $Q_{cm}$ could have been caused by slow inactivation of charge movement (Chandler et al., 1976). According to this idea, a small amount of slow inactivation would develop during the 10-ms pulse to −20 mV and the subsequent 420-ms pulse to −40 mV. This inactivation would then

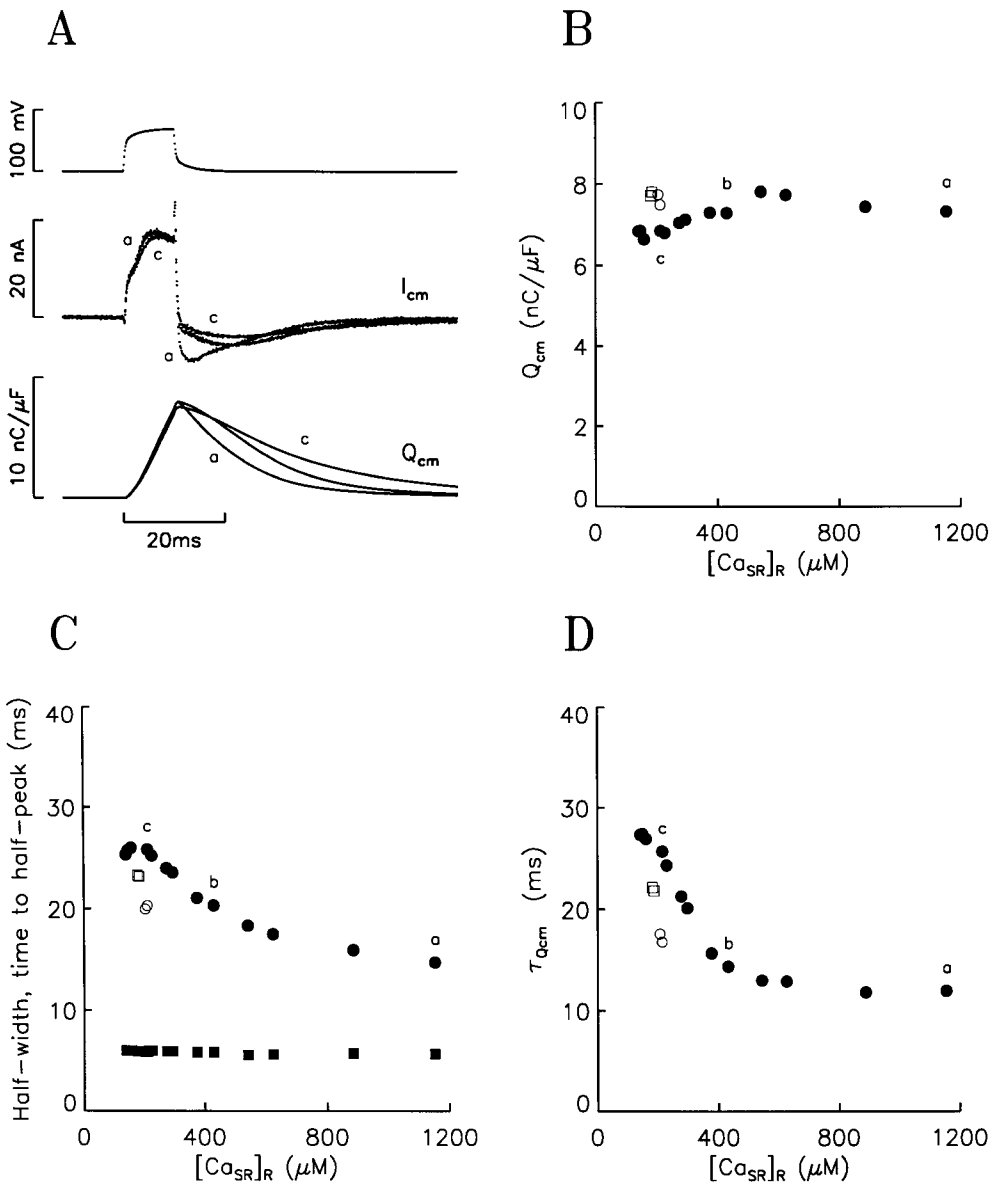


FIGURE 8. Properties of $Q_{cm}$ elicited by a brief voltage pulse, from the experiment illustrated in Fig. 5. (*A*) Three superimposed traces of V (*top*), $I_{cm}$ (*middle*), and $Q_{cm}$ (*bottom*, obtained by integration of $I_{cm}$), from the same trials used for Fig. 5. (*B*) Peak value of $Q_{cm}$ plotted as a function of $[Ca_{SR}]_R$, with filled and open symbols as described in Fig. 6. (*C*) Half-width of $Q_{cm}$ (*filled circles and open symbols*) and time to half-peak (*filled squares*). (*D*) Final time constant of $Q_{cm}$ ($\tau_{Qcm}$).

be removed during the recovery period at −90 mV, and removal would be more complete with a 3–4-min recovery period than with a 1-min period.

Fig. 8 *C* shows the half-width of $Q_{cm}$ (●, ○, and □) and the time to half-peak of $Q_{cm}$ (■) plotted as a function of $[Ca_{SR}]_R$. The filled circles show that the half-width progressively increased when the value of $[Ca_{SR}]_R$ was decreased from 1,152 to 141 μM (○ and □ are discussed in the following section). The increase in half-width is caused by a prolongation of the falling phase of the signal since the time to half-peak of the rising phase of the signal was constant (■).

The falling phase of $Q_{cm}$ was analyzed by fitting an exponential function to the final half of the signal, starting at the time from half-peak and ending 164 ms after repolarization (not shown). Fig. 8 *D*, ●, shows the values of the time constant of the exponential function that were obtained in this manner ($\tau_{Qcm}$). The value of $\tau_{Qcm}$ increased from 12 to 27 ms as the value of $[Ca_{SR}]_R$ was decreased from 1,152 to 141 μM.

Results similar to those shown in Fig. 8, ●, were obtained in four fibers in which the value of $[Ca_{SR}]_R$ was progressively decreased from 1,000–1,200 to 140 μM. In the two fibers with 0.44 mM Ca in the end-pool solution (O08911 and O08912), this depletion was accomplished by decreasing the recovery period between trials from 5 to 1 min. In the two fibers with 0 mM Ca in the end-pool solution (N14911 and N15911), the recovery period was 1.5 min throughout. The mean value of $\tau_{Qcm}$ was 10.0 ms (SEM, 1.1 ms) with $[Ca_{SR}]_R$ = 1,000–1,200 μM and 17.7 ms (SEM, 3.7 ms) with $[Ca_{SR}]_R$ = 140–300 μM; the mean value of the ratio $\tau_{Qcm}([Ca_{SR}]_R$ = 140–300 μM)/$\tau_{Qcm}([Ca_{SR}]_R$ = 1,000–1,200 μM) was 1.71 (SEM, 0.20), which is significantly different from unity.

### *The Effect of the Duration of the Recovery Period on OFF $Q_{cm}$*

Fig. 8, *B–D*, ●, denotes measurements made when the value of $[Ca_{SR}]_R$ was decreased by reducing the duration of the recovery period between successive trials. With the shortest recovery period used, 1 min, the value of $[Ca_{SR}]_R$ was 141–159 μM (three left-most ● in each panel). When the recovery period was then increased to 5 or 10 min, the value of $[Ca_{SR}]_R$ was increased to 180–185 μM (□) or 205–212 (○), respectively. The associated values of the half-width of $Q_{cm}$ (Fig. 8 *C*) and of the value of $\tau_{Qcm}$ (*D*) were reduced by the longer recovery periods so that the open symbols lie below the relation defined by the filled circles; the reduction was larger with a 10-min recovery period (○) than with a 5-min period (□). Recovery periods >10 min were not studied.

In two fibers, a 10-min recovery period was used after the value of $[Ca_{SR}]_R$ had decreased to 141 (O08911) or 148 (O08912) μM. The mean value of $\tau_{Qcm}$ was 11.9 ms (SEM, 0.1 ms) with $[Ca_{SR}]_R$ = 1,000–1,200 μM and 17.4 ms (SEM, 0.2 ms) with a 10-min recovery period and $[Ca_{SR}]_R$ = 140–300 μM; the mean value of the ratio $\tau_{Qcm}([Ca_{SR}]_R$ = 140–300 μM)/$\tau_{Qcm}([Ca_{SR}]_R$ = 1,000–1,200 μM) was 1.47 (SEM, 0.03), which is significantly different from unity.

This dependence of the half-width of $Q_{cm}$ and of the value of $\tau_{Qcm}$ on recovery period was not observed in fibers with $[Ca_{SR}]_R$ > 1,200 μM. (In two experiments, not shown, fibers N14911 and N15911 were first equilibrated with an end-pool solution that contained 1.76 mM Ca and had initial values of $[Ca_{SR}]_R$ that were >2,000 μM. Later in the experiment, Ca was removed from the end-pool solution and intramembranous charge movement and SR Ca release were monitored with 10-ms pulses to −20 mV, as was used in Fig. 5. In fiber N14911, the values of $Q_{cm}$ half-width and $\tau_{Qcm}$ were 9.66 and 7.37 ms, respectively, after a 6.9-min recovery period ($[Ca_{SR}]_R$ = 2,442 μM) and were 9.94 and 7.12 ms after a 1.57-min recovery period ($[Ca_{SR}]_R$ = 1,729 μM). In fiber N15911, the values of $Q_{cm}$ half-width and $\tau_{Qcm}$ were 10.02 and 6.64 ms, respectively, after a 13-min recovery period ($[Ca_{SR}]_R$ = 2,268 μM) and were 10.88 and 8.01 ms after a 1.5-min recovery period ($[Ca_{SR}]_R$ = 1,289 μM). These small changes in $Q_{cm}$ half-width and $\tau_{Qcm}$ are probably within the error of measurement.)

The results described above suggest that, as the value of $[Ca_{SR}]_R$ is reduced from 1,200 to 140–210 μM, the OFF kinetics of $Q_{cm}$ is slowed in a use-dependent manner. With $[Ca_{SR}]_R$ >1,200 μM, either the slowing effect does not occur or, if it does, it is removed by a 1.5-min recovery period. Unfortunately, recovery periods <1 min could not be studied with our voltage-clamp method owing to the time required to take and process data during the CONTROL and TEST pulses of each trial.

The main conclusion from this and the preceding section is that a reduction in $[Ca_{SR}]_R$ from 1,000–1,200 to 140–300 μM is able to prolong the duration of OFF $Q_{cm}$ after a brief depolarization in a use-dependent manner with little, if any, effect on ON $Q_{cm}$. In four fibers in which a recovery period as brief as 1–1.5 min was used to determine $\tau_{Qcm}$ with $[Ca_{SR}]_R$ = 140–300 μM, the final time constant of OFF $Q_{cm}$ was increased by the factor 1.71 (SEM, 0.33) (see preceding section). In the two fibers in which a 10-min recovery period was also used, the factor was 1.47 (SEM, 0.03) (this section). As mentioned above, recovery periods >10 min were not studied.

### *A Comparison of the Effect of Partial SR Ca Depletion on the Time Courses of $Q_{cm}$ and $d\Delta[Ca_T]/dt$*

Fig. 9 *A* shows three pairs of $Q_{cm}$ and $d\Delta[Ca_T]/dt$ traces, replotted from Figs. 8 *A* and 7 *A*, *bottom*, respectively; the same calibration factors, 4 nC/μF and 1%/ms, apply, respectively, to all the $Q_{cm}$ and $d\Delta[Ca_T]/dt$ traces. Within each pair of traces, the rising phase of the nois-

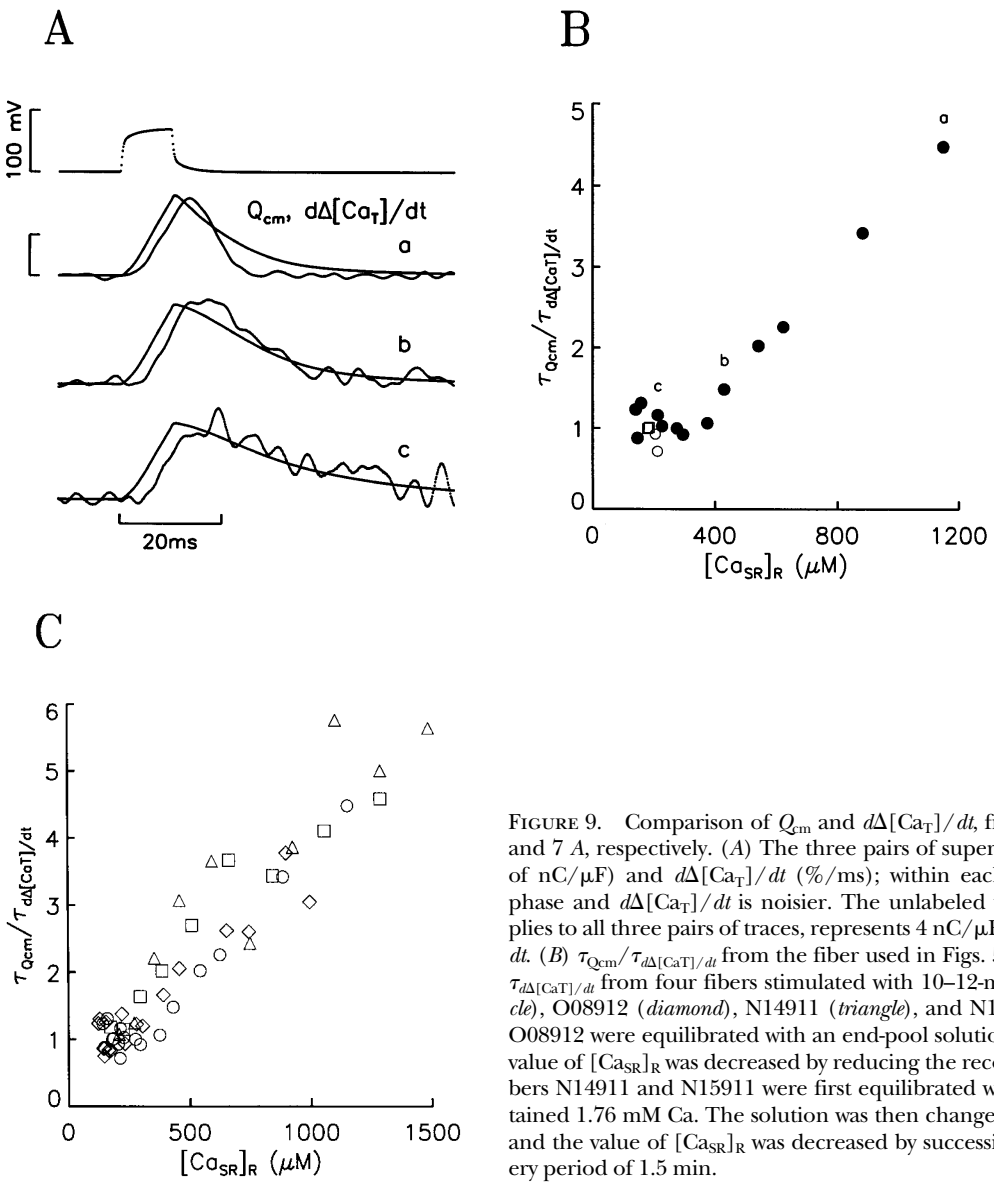


FIGURE 9. Comparison of $Q_{cm}$ and $d\Delta[Ca_T]/dt$, from the bottom traces in Figs. 8 *A* and 7 *A*, respectively. (*A*) The three pairs of superimposed traces show $Q_{cm}$ (in units of nC/μF) and $d\Delta[Ca_T]/dt$ (%/ms); within each pair, $Q_{cm}$ has the earlier rising phase and $d\Delta[Ca_T]/dt$ is noisier. The unlabeled vertical calibration bar, which applies to all three pairs of traces, represents 4 nC/μF for $Q_{cm}$ and 1%/ms for $d\Delta[Ca_T]/dt$. (*B*) $\tau_{Qcm}/\tau_{d\Delta[CaT]/dt}$ from the fiber used in Figs. 5–8 and *A* of this figure. (*C*) $\tau_{Qcm}/\tau_{d\Delta[CaT]/dt}$ from four fibers stimulated with 10–12-ms pulses to −20 mV: O08911 (*circle*), O08912 (*diamond*), N14911 (*triangle*), and N15911 (*square*). Fibers O08911 and O08912 were equilibrated with an end-pool solution that contained 0.44 mM Ca; the value of $[Ca_{SR}]_R$ was decreased by reducing the recovery period (see Figs. 5 and 6). Fibers N14911 and N15911 were first equilibrated with an end-pool solution that contained 1.76 mM Ca. The solution was then changed to one that contained 0 mM Ca, and the value of $[Ca_{SR}]_R$ was decreased by successive stimulations with a fixed recovery period of 1.5 min.

ier $d\Delta[Ca_T]/dt$ signal lagged that of the $Q_{cm}$ signal by 2–3 ms so that its peak value was reached after that of $Q_{cm}$.

Simon and Hill (1992) measured the time course of charge movement and SR Ca release during and after 100-ms depolarizations to potentials between −60 and 20 mV. A depolarizing prepulse was used to produce Ca inactivation of Ca release so that the time course of $d\Delta[Ca_T]/dt$ would, according to them, correspond to the time course of voltage activation of the noninactivating component of $d\Delta[Ca_T]/dt$. They found that the time course of $d\Delta[Ca_T]/dt$ matched that of $Q_{cm}^4$. Based on this result, they proposed that four identical voltage sensors, which move independently, act in concert to gate the SR Ca release channel. In our experiments, with 10-15 ms depolarizations, the time courses of $Q_{cm}^4$ and of $d\Delta[Ca_T]/dt$ were clearly different (not shown). For example, the peak value of $d\Delta[Ca_T]/dt$ occurred after that of $Q_{cm}^4$ or, for that matter, $Q_{cm}$ raised to any positive power (see Fig. 9 *A*). Moreover, the later time to peak of $d\Delta[Ca_T]/dt$ cannot be attributed to the development of Ca inactivation of Ca release since this would be expected to decrease, not increase, the time to peak of $d\Delta[Ca_T]/dt$. Thus, if four voltage sensors act in concert to gate the SR Ca channel, as proposed by Simon and Hill (1992), the opening of the channel does not occur immediately with the movement of the voltage sensors, but after a 2–3-ms delay.

After the peak values of $d\Delta[Ca_T]/dt$ in Fig. 9 *A* were reached, both $Q_{cm}$ and $d\Delta[Ca_T]/dt$ returned to zero with rates that progressively decreased from *a* to *b* to *c*. In *a*, the final return of $d\Delta[Ca_T]/dt$ to zero was more rapid than that of $Q_{cm}$. The relative difference in the final time courses of $Q_{cm}$ and $d\Delta[Ca_T]/dt$ was less marked in *b*. In *c*, the final time courses of the two signals were

similar, with the $Q_{cm}$ trace lying within the noise of the $d\Delta[Ca_T]/dt$ trace.

Since, with small values of $[Ca_{SR}]_R$, the value of $\tau_{Qcm}$ with a 1.5-min recovery period was larger than that with a 10-min recovery period (Fig. 8 *D*, ● *c* and ○), whereas the corresponding values of $\tau_{d\Delta[CaT]/dt}$ were within the scatter of the points (Fig. 7 *D*), it was of interest to compare $Q_{cm}$ and $d\Delta[Ca_T]/dt$ signals with a 10-min recovery period. Within the noise of the $\Delta[Ca_T]/dt$ signal, the final time courses of the two signals were similar (not shown).

Fig. 9 *B* shows the ratio $\tau_{Qcm}/\tau_{d\Delta[CaT]/dt}$ plotted as a function of $[Ca_{SR}]_R$. Its value decreased from 4.5 with $[Ca_{SR}]_R$ = 1,152 μM (*a*) to values that fluctuated around unity with values of $[Ca_{SR}]_R < 400$ μM. With $[Ca_{SR}]_R < 400$ μM, the mean value of $\tau_{Qcm}/\tau_{d\Delta[CaT]/dt}$ was 1.07 (SEM, 0.05) for the filled circles and 0.91 (SEM, 0.07) for the open symbols; these two values are not significantly different from each other or from unity. The comparisons described in this and the preceding paragraph show that, with $[Ca_{SR}]_R < 400$ μM, the noise in the $d\Delta[Ca_T]/dt$ signals makes it difficult to assess quantitatively the effect of increasing the recovery period from 1–2 to 10 min on the relation between $Q_{cm}$ and $d\Delta[Ca_T]/dt$.

Results similar to those in Fig. 9 *B* were obtained in three other fibers, and the combined data are shown in Fig. 9 *C*. The mean value of $\tau_{Qcm}/\tau_{d\Delta[CaT]/dt}$ with $[Ca_{SR}]_R$ = 1,000–1,500 μM was 4.66 (SEM, 0.35) and, with $[Ca_{SR}]_R$ = 140–300 μM, was 1.06 (SEM, 0.04). The first, but not the second, value is significantly different from unity.

Jong et al. (1995*a*) also measured $Q_{cm}$ and $d\Delta[Ca_T]/dt$ after brief depolarizations (10–15 ms to −20 mV) in fibers equilibrated with an end-pool solution similar to that used here with 1.76 mM Ca. In five fibers in which $[Ca_{SR}]_R$ = 2,003–2,759 μM, the mean values of $\tau_{Qcm}$ and $\tau_{d\Delta[CaT]/dt}$ were 8.45 ms (SEM, 1.76 ms) and 1.64 ms (SEM, 0.17 ms), respectively; the mean value of $\tau_{Qcm}/\tau_{d\Delta[CaT]/dt}$, 4.96 (SEM, 0.61), is significantly different from unity. These values with $[Ca_{SR}]_R$ = 2,003–2,759 μM are generally consistent with the results in Figs. 7 *D*, 8 *D*, and 9 *C*.

The main conclusion of this section is that, after a brief depolarization, (*a*) with $[Ca_{SR}]_R$ = 1,000–1,500 μM, $d\Delta[Ca_T]/dt$ returns to its resting state several times more rapidly than $Q_{cm}$; and (*b*) with $[Ca_{SR}]_R$ = 140–300 μM and the associated increase in noise of the $d\Delta[Ca_T]/dt$ signal, the final time courses of $Q_{cm}$ and $d\Delta[Ca_T]/dt$, appropriately scaled, are indistinguishable from each other.

## DISCUSSION

This article describes the effects of partial SR Ca depletion on SR Ca release in cut muscle fibers that have been equilibrated with an internal solution that contains 20 mM EGTA. One of the most interesting of these effects is that the fractional amount of SR Ca released by a single action potential is increased when the value of $[Ca_{SR}]_R$ is decreased. In the experiment in Fig. 4, for example, when the value of $[Ca_{SR}]_R$ was reduced from 1,154 to 140–150 μM, the value of $f_l$ was increased threefold, from 0.165 to 0.51–0.52. Three factors appear to contribute to this marked effect: a prolongation of the action potential, a slowing of the OFF kinetics of $Q_{cm}$, and a decrease in Ca inactivation of Ca release. Because some or all of these factors may be caused by alterations in the increase in myoplasmic free [Ca] that occurs during release, it is instructive to compare the two methods that have been used by others and by us to attenuate myoplasmic free Ca transients: the addition of high affinity Ca buffers to the myoplasm and a reduction of SR Ca content. As shown below, such information can be used to estimate an upper limit for the distance between a putative regulatory Ca receptor and the mouth of the SR Ca channel.

### *Comparison of the Use of High Affinity Ca Buffers and Partial SR Ca Depletion to Decrease Myoplasmic Free [Ca] during SR Ca Release*

One way to reduce the increase in myoplasmic free [Ca] that accompanies SR Ca release is with high affinity Ca buffers such as fura-2, the Ca indicator developed by Grynkiewicz et al. (1985) (Baylor and Hollingworth, 1988; Jacquemond et al., 1991; Hollingworth et al., 1992; Csernoch et al., 1993; Jong et al., 1993; Pape et al., 1993). Another way is with partial SR Ca depletion, which is expected to reduce single-channel Ca flux (this article). These two methods are expected to reduce [Ca] in spatially different ways. This can be illustrated by the theoretical example of a single SR Ca channel that behaves as a point source of Ca immersed in an infinite medium of myoplasm that is isotropic and isopotential. In the absence of freely diffusible Ca buffers, the steady-state increase in myoplasmic free [Ca] at a distance $r$ from the mouth of the channel ($\Delta[Ca]_{ps}$) satisfies the well-known relation

$$\Delta[Ca]_{ps} = \frac{\phi_{point}}{4\pi D_{Ca} r}. \quad (1)$$

$\phi_{point}$ represents the flux of Ca ions through the point source or channel, and $D_{Ca}$ represents the diffusion coefficient of Ca in myoplasm. The subscript "ps" refers to a single point source.

In the presence of a large concentration of a freely diffusible Ca buffer such as EGTA or fura-2, Eq. 1 can be replaced by

$$\Delta[Ca]_{ps} = \frac{\phi_{point}}{4\pi D_{Ca} r} \cdot \exp(-r/\lambda_{Ca}) \quad (2)$$

if the fractional change in concentration of Ca-free buffer is small (Neher, 1986; Stern, 1992; Appendix B

in Pape et al., 1995) and $D_{Ca}/[B]_R << D_B/([Ca]_R + K_d)$ (Appendix B in Pape et al., 1995). $D_B$ represents the diffusion coefficient of the Ca buffer in myoplasm (which is assumed to be independent of the state of Ca complexation), $K_d$ represents the Ca buffer's dissociation constant, and $[B]_R$ represents the resting concentration of Ca-free buffer. The value of $\lambda_{Ca}$, which determines the distance that Ca diffuses before capture by the buffer, is given by

$$\lambda_{Ca} = \sqrt{\frac{D_{Ca}}{k_1 [B]_R}}, \quad (3)$$

where $k_1$ is the forward rate constant for Ca binding to the Ca buffer. The steady-state value of $\Delta[Ca]_{ps}$ given by either Eq. 1 or 2 is unaffected by the presence of immobile Ca buffers such as troponin.

In fibers equilibrated with 20 mM EGTA and 1.76 mM Ca, the value of $\lambda_{Ca}$ is estimated to be 81 nm (Pape et al., 1995). Although the exact value of $\phi_{point}$ for an SR Ca channel inside a muscle fiber is unknown, measurements on canine cardiac SR Ca channels incorporated into lipid bilayers indicate that, under physiological conditions, the single-channel current is ≤0.5 pA (Mejia-Alvarez et al., 1998), which gives $\phi_{point} \leq 1.5 \times 10^6$ ions $s^{-1}$. In this case, for $r > 400$ nm, the value of $\Delta[Ca]_{ps}$ calculated from Eq. 2 with $\lambda_{Ca} = 81$ nm is expected to be negligible, ≤0.01 μM. Thus, in fibers equilibrated with 20 mM EGTA and 1.76 mM Ca, the spread of $\Delta[Ca]_{ps}$ from an open SR Ca channel is expected to be confined to a region that is no farther than 400 nm from the mouth of the channel. Since the value of $\lambda_{Ca}$ is decreased if the amount of Ca added to the EGTA is decreased, this condition holds for 20 mM EGTA and 0–1.76 mM Ca.

Fura-2 complexes Ca much more rapidly than EGTA. According to Jong et al. (1995*a*), the myoplasmic value of $k_1$ for fura-2 is 28 times that for EGTA. Consequently, 0.65 mM Ca-free fura-2 is expected to be equivalent to 18.24 mM Ca-free EGTA (the concentration of Ca-free EGTA in an internal solution containing 20 mM EGTA and 1.76 mM Ca) in its ability to decrease $\Delta[Ca]_{ps}$. With 0.65, 2, 4, 6, and 8 mM Ca-free fura-2, the estimated values of $\lambda_{Ca}$ are 81, 46, 33, 27, and 23 nm, respectively.

Comparison of Eqs. 1 and 2 shows that the fractional reduction of $\Delta[Ca]_{ps}$ produced by high affinity Ca buffers depends on distance from the mouth of a channel according to the factor $\exp(-r/\lambda_{Ca})$. In contrast, with partial SR Ca depletion, the fractional reduction of $\Delta[Ca]_{ps}$ is independent of $r$ and is given by the fractional reduction of $\phi_{point}$. As a result, high affinity Ca buffers would be expected to be more effective than SR Ca depletion in reducing $\Delta[Ca]_{ps}$ at large distances from the mouth of an open SR Ca channel, whereas partial SR Ca depletion would be expected to be more effective near the mouth of the channel.

Although the spatial profile of $\Delta[Ca]_{ps}$ near an open SR Ca channel is not expected to be as simple as that described by Eq. 1 or 2, these equations may help evaluate, at least qualitatively, the differences between reducing $\Delta[Ca]_{ps}$ by high affinity Ca buffers and by SR Ca depletion. To apply these equations to our results, a relation between $\phi_{point}$ and $[Ca_{SR}]$ must be specified. In principle, this requires knowledge of (*a*) the relation between $\phi_{point}$ and free [Ca] inside the SR, which depends on the properties of the SR Ca channel, and (*b*) the relation between free [Ca] and $[Ca_{SR}]$, which depends on the amount and properties of luminal Ca buffers such as calsequestrin. Since these relations inside a muscle fiber are unknown, a direct proportionality between $\phi_{point}$ and $[Ca_{SR}]$ has been assumed in the discussion below. This assumption is consistent with the finding that the peak fractional rate of SR Ca release is relatively independent of the value of $[Ca_{SR}]_R$ between 140 and 1,200 μM (Figs. 4 *C*, 6 *C*, and 7 *B*).

In addition to the $\Delta[Ca]_{ps}$ signal produced by Ca flux through a particular channel of interest, an increase in free [Ca] can also be produced by Ca flux through other open channels. The total increase in free [Ca] ($\Delta[Ca]$) is given by

$$\Delta[Ca] = \Delta[Ca]_{ps} + \Delta[Ca]_{os}. \quad (4)$$

$\Delta[Ca]_{os}$ represents the sum of the contributions from all other open channels, with the contribution from each channel described by an equation similar to Eq. 1 or 2; the subscript "os" refers to other sources. The principle of superposition applies to cases in which Ca buffers are either absent or, as is the case with EGTA in the experiments reported here, present in a sufficiently large concentration to ensure that, after an action potential or brief voltage pulse, the fractional change in concentration of Ca-free buffer is small. Estimates of $\Delta[Ca]_{ps}$ and $\Delta[Ca]_{os}$ with various Ca buffers are given in APPENDIX A. These show that the contribution of $\Delta[Ca]_{os}$ to $\Delta[Ca]$ can be substantial, especially in the absence of high affinity Ca buffers such as EGTA or, during the early part of a transient, in the absence of troponin (an immobile Ca buffer that makes no contribution to $\Delta[Ca]$ in the steady state).

### *Effect of SR Ca Depletion on the Time Course of the Action Potential*

One of the effects of partial SR Ca depletion is a prolongation of the action potential (Fig. 2 *C*), which is caused by a decrease in net outward ionic current during repolarization. The ion whose current is decreased could be either potassium or chloride since the internal solution contained potassium as the predominant cation and the external solution contained chloride as the predominant anion. Because the affected current depends on SR Ca release and develops soon after re-

lease begins, it seems likely that it is carried by ions that move through channels in the surface and/or tubular membranes that are activated rapidly, within 1–2 ms, by the increase in myoplasmic free [Ca] that accompanies release. With the large concentration of EGTA used in these experiments, the increase in free [Ca] is expected to be confined to a region ≤400 nm from the SR Ca channels (preceding section). Thus, any Ca-activated channels that are opened would be expected to be located in the transverse tubular membrane or in the surface membrane within 400 nm of the Z line.

The surface and/or tubular membranes of skeletal muscle contain both Ca-activated potassium channels (Pallotta et al., 1981) and Ca-activated chloride channels (Hui and Chen, 1994). In cut fibers equilibrated with an internal solution that contained only 0.1 mM EGTA, the current through Ca-activated chloride channels was no more than 1–2 μA/μF at the voltages where action potentials *c* and *d* in Fig. 2 *C* diverged (Hui and Chen, 1994). This is an order of magnitude smaller than the 15–20 μA/μF current that is required to explain the difference in the action potentials. Consequently, the affected current is probably carried by Ca-activated potassium channels, which, at least in myocytes from guinea pig urinary bladder, can be activated by Ca rapidly, within milliseconds (Markwardt and Isenberg, 1992). These results support the suggestion of Blatz and Magleby (1987) that Ca-activated potassium channels help stabilize and repolarize the transverse tubular membrane after an action potential.

### *Comparison of the Effect of High Affinity Ca Buffers and SR Ca Depletion on the Value of $f_1$ Elicited by an Action Potential*

In fibers equilibrated with 20 mM EGTA and partially depleted of SR Ca, a single action potential is able to release a large fraction of the SR Ca content, with values of $f_1$ as large as 0.5 (Fig. 4 *B*). The increase in $f_1$ with decreasing $[Ca_{SR}]_R$ is associated with a prolongation of the action potential (Fig. 3 *B*) and a slowing of the turn-off of SR Ca release (Fig. 4 *D*). Since a substantial increase in $f_1$ was also observed in voltage-clamp experiments (Fig. 6 *B*), the prolongation of the action potential cannot explain all of the increase in $f_1$ that accompanies a reduction in $[Ca_{SR}]_R$.

In previous studies with action potential stimulation of fibers equilibrated with 20 mM EGTA and 1.76 mM Ca, the value of $[Ca_{SR}]_R$ was 1,391–4,367 μM; $f_1$ varied between 0.13 and 0.17 and had a mean value of 0.144 (Pape et al., 1995). Although direct measurement of $[Ca_{SR}]_R$, and consequently of $f_1$, is only possible in fibers with a large myoplasmic concentration of an extrinsic Ca buffer such as EGTA or fura-2 to complex the Ca released from the SR, there is reason to believe that $f_1$ is larger with 20 mM than with 0–0.1 mM EGTA. In fibers stimulated by an action potential, the estimated amount of SR Ca release is increased by as much as twofold by the introduction of 0.5–1 mM fura-2 into the myoplasm (Baylor and Hollingworth, 1988; Hollingworth et al., 1992; Pape et al., 1993), which is expected to reduce myoplasmic free [Ca] to approximately the same extent as 20 mM EGTA (see above). In voltage-clamped fibers, the estimated peak rate of SR Ca release is increased by as much as twofold by 0.5–1 mM fura-2 (Jong et al., 1993) or by as much as threefold by 20 mM EGTA (Jong et al., 1995*a*). This ability of 0.5–1 mM fura-2 or 20 mM EGTA to increase SR Ca release is probably caused by a decrease in Ca inactivation of Ca release associated with the reduction in myoplasmic Δ[Ca] produced by the Ca buffer. Although the reduction in Δ[Ca] could be caused by a reduction in either $\Delta[Ca]_{ps}$ or $\Delta[Ca]_{os}$ (Eq. 4), the analysis in APPENDIX A suggests that 0.5–1 mM fura-2 or 20 mM EGTA reduces $\Delta[Ca]_{os}$ more than $\Delta[Ca]_{ps}$.

The amount of Ca inactivation that is able to develop in the presence of 0.5–1 mM fura-2 or 20 mM EGTA does not appear to be reduced substantially by 6 mM fura-2. In fibers with $[Ca_{SR}]_R$ = 1,306–2,852 μM, the value of $f_1$ elicited by an action potential was constant at about 0.13 for values of [fura-2] between 2 and 4 mM. Moreover, the value of $f_1$, as well as that of the peak fractional rate of release, decreased about twofold when [fura-2] was increased from 4 to 6 mM (Fig. 9 in Jong et al., 1995*a*). As the value of [fura-2] was increased from 2 to 4 to 6 mM, the turn-off of SR Ca release remained rapid and showed little or none of the slowing effect that was routinely observed when the value of $[Ca_{SR}]_R$ was decreased to values <1,000 μM.

Another measure of Ca inactivation is provided by the ratio $f_2/f_1$. $f_2$, the fraction of SR Ca content that is released by the second action potential in a train, is less than $f_1$, probably because Ca inactivation develops with the first stimulation and is only partially removed before the second stimulation. With action potentials 20 ms apart, the value of $f_2/f_1$ was 0.57 with 20 mM EGTA and 0.64 with 2–6 mM fura-2 (Fig. 10 *A* in Jong et al., 1995*a*); if Ca inactivation of Ca release had been eliminated by fura-2, the value of $f_2/f_1$ should have been unity.

The general conclusion from these results is that in fibers with $[Ca_{SR}]_R \geq 1{,}300$ μM, high affinity Ca buffers (20 mM EGTA or ≤6 mM fura-2) are able to increase the value of $f_1$ by a modest amount but are unable either to increase the value of $f_1$ above 0.17 or to slow the turn-off of SR Ca release. On the other hand, as shown in this article, the latter effects are routinely observed in fibers equilibrated with 20 mM EGTA when the value of $[Ca_{SR}]_R$ is reduced below 1,000 μM. If these effects are mediated by a Ca receptor located at a distance $r_{CaR}$ from the mouth of an SR Ca channel, the value of $r_{CaR}$ is expected to be small. For example, the

value of 0.21 for $f_1$ with $[Ca_{SR}]_R$ = 900 μM (Fig. 4 *B*) suggests that the value of $\Delta[Ca]$ at $r_{CaR}$ is smaller with $[Ca_{SR}]_R$ = 900 μM and 20 mM EGTA in the myoplasm than with $[Ca_{SR}]_R \cong$ 2,000 μM and 6 mM fura-2 in the myoplasm. With Eq. 2 and the assumption that $\phi_{point}$ is proportional to $[Ca_{SR}]_R$, this means that $900\exp(-r_{CaR}/78) < 2{,}000\exp(-r_{CaR}/27)$ or, with rearrangement, $\exp(-r_{CaR}/27)/\exp(-r_{CaR}/78) > 900/2{,}000 = 0.45$; 27 and 78 nm are the values of $\lambda_{Ca}$ for 6 mM fura-2 and 20 mM EGTA plus 0.44 mM Ca, respectively (Eq. 4). From this it follows that $r_{CaR}$ is < 33 nm. If contributions from $\Delta[Ca]_{os}$ (Eq. 4) are taken into account, the upper limit for $r_{CaR}$ is expected to be even smaller. For example, according to APPENDIX A, if $\phi_{point} \leq 1.5 \times 10^6$ ions $s^{-1}$, $r_{CaR}$ is ≤ 22 nm. Such close proximity to the mouth of the channel would be consistent with a regulatory Ca receptor or receptors located on the SR Ca channel (including the foot structure) and/or its voltage sensor.

Some of the assumptions used in this analysis may not hold exactly. In particular, the diffusion of Ca from an SR Ca channel may be more complicated than that assumed in Eq. 1 or 2; EGTA may not be uniformly distributed in the myoplasmic space that surrounds a channel; and more than one Ca receptor, each located at a different distance from the mouth of a channel, may be involved in the regulation of the processes that determine $f_1$. Nonetheless, the inequality $r_{CaR} \leq 22$ nm suggests that at least some action of Ca on an SR Ca channel or its voltage sensor, which acts to decrease Ca release, is regulated by a Ca receptor that is close to the mouth of the channel itself. It is not known whether the Ca receptor (or receptors) responsible for this effect also participates in the increase in SR Ca release that is produced by the introduction of 0.5–1 mM fura-2 or 20 mM EGTA into the myoplasm (see above). Such participation is possible since this amount of Ca buffering is able to substantially decrease $\Delta[Ca]_{os}$ and, as a consequence, $\Delta[Ca]$ near the mouth of an SR Ca channel (APPENDIX A).

### *Effect of SR Ca Depletion on the OFF Kinetics of $Q_{cm}$ and the Decay Kinetics of $d\Delta[Ca_T]/dt$*

Additional information about the factors that cause the increase in $f_1$ with partial SR Ca depletion can be obtained from voltage-clamp experiments. Partial SR Ca depletion slows the OFF kinetics of $Q_{cm}$ and the decay kinetics of $d\Delta[Ca_T]/dt$ after a brief depolarization, with a more marked effect on $d\Delta[Ca_T]/dt$ than on $Q_{cm}$ (Figs. 7–9). There is little or no effect on the ON kinetics of either signal.

With the smallest values of $[Ca_{SR}]_R$ studied, 140–300 μM, $Q_{cm}$ and $d\Delta[Ca_T]/dt$ returned to baseline with time courses that were similar within the noise of the $d\Delta[Ca_T]/dt$ signal (traces *c* in Fig. 9 *A* and associated text); with 1–2-min recovery periods, the mean values of $\tau_{Qcm}$ and $\tau_{d\Delta[CaT]/dt}$ were 17.7 and 16.2 ms, respectively. Under these conditions, the value of $\tau_{Qcm}$ was use-dependent; it decreased when the recovery period between trials was increased to 5–10 min (compare *open symbols* and *filled circles* in Fig. 8 *D*).

The general similarity between the values of $\tau_{Qcm}$ and $\tau_{d\Delta[CaT]/dt}$ with $[Ca_{SR}]_R$ = 140–300 μM is illustrated by a plot of the values of $\tau_{Qcm}/\tau_{d\Delta[CaT]/dt}$, which are about 1 with some scatter (Fig. 9, *B* and *C*). Under these conditions, at late times after a repolarization, the rate constant that underlies the return of charge to its resting state may be the same as the rate constant for the closing of SR Ca channels. If charge can be described by a sequential model with $n + 1$ states $x_0, x_1, \ldots, x_{n-1}, x_n$, and the SR Ca channel is closed for states $0, 1, \ldots, n-1$ and open only for state $n$ (see Jong et al., 1995*b*), closure of the SR Ca channel would be associated with the transition of charge from $x_n$ to $x_{n-1}$. During repolarization to the holding potential (−90 mV), the forward rate constants from $x_i$ to $x_{i+1}$, denoted by $k_{i,i+1}$ with $0 \leq i \leq n-1$, can probably be neglected so that the rate constant for channel closure would be given simply by the backward rate constant from $x_n$ to $x_{n-1}$, denoted by $k_{n,n-1}$. If the value of $k_{n,n-1}$ were sufficiently small compared with the values of the other reverse rate constants $k_{i,i-1}$, with $1 \leq i \leq n-1$, $k_{n,n-1}$ would also be the apparent rate constant for the return of charge to its resting state during the final stages of repolarization.

With $[Ca_{SR}]_R$ = 1,000–1,200 μM, the OFF kinetics of $Q_{cm}$ and the decay kinetics of $d\Delta[Ca_T]/dt$ were more rapid than those observed with $[Ca_{SR}]_R$ = 140–300 μM (Figs. 7 *D*, 8 *D*, and 9 *A*). The mean value of $\tau_{Qcm}$ was 10.0 ms (compared with 17.7 ms) and the mean value of $\tau_{d\Delta[CaT]/dt}$ was 2.5 ms (compared with 16.2 ms); thus, with larger $[Ca_{SR}]_R$, a single rate constant no longer appears to describe both the closure of the SR Ca channels and the return of charge to its resting state. In terms of the sequential model for charge movement described in the preceding paragraph, it seems likely that the value of $k_{n,n-1}$ is increased by an increase in $[Ca_{SR}]_R$ from 140–300 to 1,000–1,200 μM and that the time course of OFF $Q_{cm}$ may no longer depend only on the value of $k_{n,n-1}$ but also on the values of other reverse rate constants. Without additional information, it is difficult to decide whether a decrease in $k_{n,n-1}$ can explain all of the changes in the OFF kinetics of $Q_{cm}$ that occur when the value of $[Ca_{SR}]_R$ is decreased from 1,000–1,200 to 140–300 μM. It is also difficult to know which rate constants participate in the use dependence of $\tau_{Qcm}$ that is observed with $[Ca_{SR}]_R$ = 140–300 μM.

The OFF kinetics of $Q_{cm}$ is expected to underlie the time course of the removal of voltage-dependent activation of SR Ca release after repolarization from a brief depolarization. Since Ca inactivation of Ca release may

also contribute to the turn-off of $d\Delta[Ca_T]/dt$, it is of interest to consider the relative importance of these two processes when the value of $[Ca_{SR}]_R$ is decreased from 1,000–1,200 to 140–300 μM in fibers equilibrated with 20 mM EGTA. Several observations, taken together, are consistent with the idea that the strength of Ca inactivation decreases with decreasing values of $[Ca_{SR}]_R$ in this range. First, Ca inactivation of Ca release appears to contribute to the turn-off of SR Ca release after action potential stimulation under normal conditions without fura-2 or EGTA in the myoplasm (preceding section). Second, although Ca inactivation appears to be reduced by 0.5–1 mM fura-2 or 20 mM EGTA, it is by no means removed. In cut fibers equilibrated with 20 mM EGTA and studied with two stimulations separated by a variable period of recovery, either an action potential or a 10–15-ms prepulse to −20 mV appeared to inactivate 90% of the ability of the SR to release Ca immediately after the first period of release ($[Ca_{SR}]_R$ = 1,813–2,562 μM in the action potential experiments and 1,996–2,759 μM in the voltage-clamp experiments; Jong et al., 1995*a*). Third, since, with 20 mM EGTA, the Δ[Ca] signal at any myoplasmic location is expected to be proportional to $d\Delta[Ca_T]/dt$ (Pape et al., 1995), and the value of $d\Delta[Ca_T]/dt$ is approximately proportional to $[Ca_{SR}]$ (Figs. 4 *C*, 6 *C*, and 7 *B*), a decrease in $[Ca_{SR}]_R$ from 1,000–1,200 to 140–300 μM would be expected to reduce the local myoplasmic Δ[Ca] signal severalfold; this, in turn, would likely decrease the development of Ca inactivation. Fourth, a decrease in $[Ca_{SR}]_R$ from 1,000–1,200 to 140–300 μM increased $\tau_{d\Delta[CaT]/dt}$ by a factor of 6.47 but increased $\tau_{Qcm}$ by only a factor of 1.71 if the recovery period was 1–2 min or 1.47 if recovery was 10 min. Although these observations do not prove rigorously that Ca inactivation is diminished when the value of $[Ca_{SR}]_R$ is decreased from 1,000–1,200 to 140–300 μM in fibers equilibrated with 20 mM EGTA, they clearly show that the idea is reasonable.

In summary, if the value of $[Ca_{SR}]_R$ is increased from 140–300 to 1,000–1,200 μM, the turn-off of $d\Delta[Ca_T]/dt$ that occurs after an action potential or after repolarization from a brief depolarization is accelerated. This appears to be caused, at least in part, by an acceleration of the OFF kinetics of $Q_{cm}$, at least if the recovery period between trials is ≤10 min as used in the experiments reported here. Ca inactivation of Ca release may also play a role. Although it is difficult to assess the relative contributions of charge movement and Ca inactivation to the turn-off of $d\Delta[Ca_T]/dt$, the line of reasoning presented in the last two paragraphs of the preceding section suggests that at least some of the acceleration of the turn-off of SR Ca release through a particular SR Ca channel is regulated by a Ca receptor that is located ≤22 nm from the mouth of the channel. This receptor could act on the channel's voltage sensor to accelerate the OFF kinetics of $Q_{cm}$ and/or it could act on the channel to cause Ca inactivation of Ca release.

### *Effect of SR Ca Content on the Peak Value of $d\Delta[Ca_T]/dt$*

In the experiments described in this article, which used both action potential and voltage-clamp stimulation, the value of peak $d\Delta[Ca_T]/dt$ (in units of %/ms) was relatively constant when the value of $[Ca_{SR}]_R$ was varied between 140 and 1,200 μM (Figs. 4 *C*, 6 *C*, and 7 *B*). This observation may be relevant to the question of whether some SR Ca channels are gated open by Ca (Ca-induced Ca release; Ford and Podolsky, 1968; Endo et al., 1968; Endo, 1977), an idea that has received new attention with the electron microscope studies of Block et al. (1988) on muscle from toadfish swimbladder. Block et al. (1988) observed tetrads in the junctional tubular membrane, each of which is thought to consist of four dihydropyridine receptors, which function as the voltage sensors for SR Ca release (Ríos and Brum, 1987; Tanabe et al., 1988). Block et al. (1988) compared the spatial arrangement of these tetrads with that of the foot structures that span the region between the tubular and SR membranes (Franzini-Armstrong, 1975) and form the Ca channels in the SR membrane (Inui et al., 1987; Lai et al., 1988). The distance between tetrads along a row is twice that between foot structures, suggesting that only every other foot structure apposes a tetrad. This arrangement raises the possibility that the Ca channels in foot structures apposed to tetrads might be gated by voltage and that the Ca channels in alternate foot structures might be either silent or gated by a different mechanism (Block et al., 1988). Ríos and Pizarró (1988) expanded on this idea and speculated that the Ca channels in the nonapposed foot structures are gated by Ca itself. Under normal physiological conditions, this Ca would come from neighboring open Ca channels, which, immediately after depolarization, would be expected to be those gated by voltage.

In our experiments on fibers stimulated by brief pulses to −20 mV, $d\Delta[Ca_T]/dt$ (in units of %/ms) was decreased only slightly by reducing the value of $[Ca_{SR}]_R$ from 600–1,200 to 140–300 μM; the peak value of $d\Delta[Ca_T]/dt$ (in units of %/ms) with $[Ca_{SR}]_R$ = 140–300 μM was 0.861 (SEM, 0.016) times that with $[Ca_{SR}]_R$ = 600–1,200 μM (Fig. 7 *B* and associated text). The time course of ON $d\Delta[Ca_T]/dt$ (Fig. 7 *A*) and ON $Q_{cm}$ (Fig. 8 *A*) was little affected by these changes in $[Ca_{SR}]_R$. The simplest interpretation of the relative constancy of the time course of ON $d\Delta[Ca_T]/dt$ and its peak value (in units of %/ms) under these conditions is that the Ca flux through an open SR Ca channel is approximately proportional to the value of $[Ca_{SR}]_R$, and that the number of open SR Ca channels at the time of peak

changes little when $[Ca_{SR}]_R$ is decreased from 600–1,200 to 140–300 μM. Thus, if Ca-gated channels participate in SR Ca release when $[Ca_{SR}]_R$ = 600–1,200 μM, it seems likely that most of them also participate when $[Ca_{SR}]_R$ = 140–300 μM. If so, any model of SR Ca release (for example see Stern et al., 1997) must be able to explain how, in the presence of 20 mM EGTA, Ca gating is able to occur with $[Ca_{SR}]_R$ = 140–300 μM and the associated small rates of single-channel Ca flux but, with [EGTA] ≤ 0.1 mM, not spread regeneratively along the Z line when the value of $[Ca_{SR}]_R$ is almost certainly an order of magnitude larger (for example, in the local activation experiments of Huxley and Taylor [1958] and in the Ca spark experiments of Klein et al. [1996]).

## APPENDIX A

Eqs. 1 and 2 predict the steady-state increase in free [Ca] ($\Delta[Ca]_{ps}$) that develops near the mouth of an open SR Ca channel that behaves as a point source in an infinite isotropic medium. In many situations of physiological interest, however, the value of [Ca] near a particular channel is increased substantially by Ca flux from neighboring channels ($\Delta[Ca]_{os}$). In this case, the total increase in free [Ca] ($\Delta$[Ca]) is given by the sum of $\Delta[Ca]_{ps}$ and $\Delta[Ca]_{os}$ (Eq. 4). The aim of this appendix is to estimate $\Delta[Ca]_{ps}$ and $\Delta[Ca]_{os}$, both in the absence of Ca buffers and in the presence of ATP, troponin, EGTA, or fura-2.

As it turns out, at distances ≤30 nm from the mouth of an SR Ca channel, the transient change in $\Delta[Ca]_{ps}$ is nearly complete within 0.1 ms after a change in Ca flux. Consequently, steady-state equations can be used to estimate $\Delta[Ca]_{ps}$. Steady-state equations can also be used to estimate the contributions of individual channels to $\Delta[Ca]_{os}$ in the presence of 20 mM EGTA or ≥0.5 mM fura-2. Without such Ca buffers, however, time-dependent solutions must be used for the estimation of $\Delta[Ca]_{os}$.

### *General Description of the Estimation of $\Delta[Ca]_{os}$*

In frog muscle, the transverse tubular system is located at the Z line and is arranged as a lattice surrounding individual myofibrils; the mean lattice spacing is 0.6–0.7 μm (Peachey, 1965). In electron micrographs, the tubules appear flattened and the membrane on each side is separated from the apposing membrane of the SR by two parallel rows of foot structures (Franzini-Armstrong, 1975; Block et al., 1988). The foot structures form the Ca release channels in the SR membrane (Inui et al., 1987; Lai et al., 1988). Half of the foot structures lie on each side of the transverse tubular system. From symmetry, we assume that the Ca that leaves a channel on one side of the plane of the Z line remains on that side and does not, on average, cross the plane to the other side. This restriction, while somewhat arbitrary, does not influence the general conclusions from these calculations. The diffusion of Ca from each individual channel is treated as that of Ca from a point source into a semi-infinite medium, which represents the myoplasm that extends from the appropriate side of the plane of the Z line to the end of the fiber. For this reason, any equations for $\Delta$[Ca] that have been derived for a point source of Ca immersed in an infinite medium must be modified for the calculation of $\Delta[Ca]_{os}$. This modification, which requires replacing the factor $\phi_{point}/4\pi$ with $\phi_{point}/2\pi$, must be done for the equations in the DISCUSSION of this paper, in APPENDIXES B and C of this paper, and in APPENDIXES B and C of Pape et al. (1995).

In the calculations described below,

$$\Delta[Ca]_{os} = \sum_i \Delta[Ca]_i, \qquad (A1)$$

where $\Delta[Ca]_i$ represents the contribution of the $i^{th}$ Ca channel to $\Delta[Ca]_{os}$. The summation extends over all open Ca channels that lie on the specified side of the plane of the Z line, except the channel responsible for $\Delta[Ca]_{ps}$. The myoplasmic concentration of SR Ca channels or foot structures was taken to be 0.27 μM (Pape et al., 1995). With a sarcomere spacing of 3.6 μm, this concentration corresponds to a density of 585 SR Ca channels per $\mu m^2$ in the plane of the Z line, half of which lie on each side of the Z line. The initial choice of the value of $\phi_{point}$, $0.5 \times 10^6$ ions $s^{-1}$ (which corresponds to 0.16 pA), was selected so that the rate of Ca release with all channels open, 135 μM/ms, would be similar to the mean peak rate of release determined in our action potential experiments on fibers equilibrated with 20 mM EGTA plus 1.76 mM Ca, 143 μM/ms (Pape et al., 1995). The values of the parameters associated with the Ca buffers used in the calculations are given in Table I; $D_{Ca} = 3 \times 10^{-6}$ $cm^2$ $s^{-1}$.

Estimates were made with two different spatial arrangements of Ca channels, each suggested by a particular aspect of a muscle's structure. If the value of $\Delta[Ca]_{os}$ is influenced by Ca flux through channels that are located as far away as several myofibrils from the channel responsible for $\Delta[Ca]_{ps}$, the estimate of $\Delta[Ca]_{os}$ should be based on a two-dimensional arrangement of Ca channels in the plane of the Z line, such as the one illustrated in Fig. A1 *A*. On the other hand, if $\Delta[Ca]_{os}$ contains contributions from Ca channels that are only a short distance away, $\Delta[Ca]_{os}$ would depend mainly on Ca flux through the channels in the two parallel rows of foot structures that extend along one side of a short segment of tubule. In this case, $\Delta[Ca]_{os}$ should be estimated with a quasi–one-dimensional arrangement of Ca channels, such as that illustrated in Fig. A1 *B*.

TABLE I

*Parameters used for the calculations*

| 1 | 2 | 3 | 4 | 5 | 6 |
|---|---|---|---|---|---|
| Calcium buffer | $D_{buf}$ | $k_{1,buf}$ | $k_{-1,buf}$ | $K_{d,buf}$ | $[buf]_R$ |
| | $10^{-6}$ $cm^2 s^{-1}$ | $10^8 M^{-1} s^{-1}$ | $s^{-1}$ | $\mu M$ | $mM$ |
| EGTA | 1.7§ | 0.025§ | 1.485§ | 0.594 | 18.24 |
| ATP | 1.4‖ | 0.136‖ | 30,000‖ | 2,200 | 5.5 |
| troponin | 0 | 0.575* | 115* | 2 | 0.42§ |
| fura-2 | 0.54‡ | 0.7‡ | 30§ | 0.43 | 0.05-6 |

Column 1 gives the name of the Ca buffer. Column 2 gives the value of the diffusion coefficient in myoplasm. Columns 3 and 4 give the values of the apparent forward and backward rate constants for Ca complexation. Column 5 gives the values of the apparent dissociation constant, equal to the ratio of the values in columns 4 and 3. Column 6 gives the resting concentrations that were used for the calculations. The values in columns 4 and 5 for EGTA are estimated for pH = 6.9. The value in column 6 for troponin gives the concentration of Ca-regulatory sites on troponin (expressed in terms of myoplasmic concentration in the I-band) for a sarcomere length of 3.6 μm, with the assumption that all the troponin lies on the thin filaments, which have a length of 2.05 μm (Page and Huxley, 1963); the value of 0.42 mM for the concentration in the I-band corresponds to a spatially averaged myoplasmic concentration of (2.05/3.6)0.42 = 0.24 mM, as estimated by Baylor et al. (1983). Values of other parameters are $D_{Ca} = 3 \times 10^{-6}$ $cm^2$ $s^{-1}$ (Pape et al., 1995), and, unless noted otherwise, $\phi_{point} = 0.5 \times 10^6$ ions $s^{-1}$ (which corresponds to 0.16 pA). In the equations in Appendix C, $\alpha_{ATP} = K_{d,ATP}^{-1}$).

*Baylor et al. (1983), ‡Pape et al. (1993), §Pape et al. (1995), ‖Baylor and Hollingworth (1998).

### *$\Delta[Ca]_{ps}$ and $\Delta[Ca]_{os}$ Calculated with SR Ca Channels Arranged in Concentric Rings (Fig. A1 A) in the Absence of Ca Buffers and with 20 mM EGTA*

The simplest example of $\Delta[Ca]_{ps}$ and $\Delta[Ca]_{os}$ is that without intrinsic Ca buffers; a more complete analysis with the main intrinsic Ca buffers in muscle will be considered in the following section. The calculations in this section use the hypothetical arrangement of Ca channels illustrated in Fig. A1 *A*. The filled circle indicates the location of the channel used to calculate $\Delta[Ca]_{ps}$. The open circles, arranged on concentric rings around the filled circle (only the first two rings are shown in the figure), indicate the locations of the channels used to calculate $\Delta[Ca]_{os}$. The radii of the rings are integer multiples of $l$, and the number of channels on each ring is eight times that integer; the channels are equally spaced on each ring. This symmetrical arrangement gives a uniform density of channels in the following sense: inside any circle of radius $(n + 0.5)l$, where $n = 0, 1, 2, \ldots$, with the origin at the filled circle, the density of channels is constant, equal to one channel per $\pi l^2/4$. In the calculations described in Figs. A2 and A3, the value of $l$ was set to 66 nm to give a density of 585/2 channels per $\mu m^2$. (See above. The factor 2 is used because only half the channels in a Z line are assumed to contribute Ca to the myoplasm on a particular side of the plane of the Z line.)

Fig. A2 *A* shows the steady-state value of $\Delta[Ca]_{ps}$ plotted as a function of $r$, the distance from the mouth of the channel. The details of the calculations for this and subsequent figures are given in the figure legends. The curve labeled "No Buffer" assumes the absence of any freely diffusible Ca buffer (Eq. 1). With the value of $D_{Ca}$ used for these calculations ($3 \times 10^{-6}$ $cm^2$ $s^{-1}$) and with $r \leq 30$ nm, $\Delta[Ca]_{ps}$ reaches >90% of its steady level within 0.1 ms after a step change in Ca flux (from calculations with Eq. C20 with $[B_i]_R = 0$ and $D_{Ca,app} = D_{Ca}$). Consequently, the steady-state relation between $\Delta[Ca]_{ps}$ and $r$ provides a good approximation of $\Delta[Ca]_{ps}$ during an SR Ca release transient.

The curve labeled "EGTA" was calculated for the case of Ca in the presence of 18.24 mM EGTA (Eq. 2), the concentration that was used in our internal solution that contained 20 mM total EGTA plus 1.76 mM Ca. This steady-state relation can also be used to estimate $\Delta[Ca]_{ps}$ during an SR Ca release transient since the steady state is reached within 0.1 ms after a change in Ca flux (Appendix C in Pape et al., 1995). Since the right-hand side of Eq. 2 is equal to $\exp(-r/\lambda_{Ca})$ times the right-hand side of Eq. 1, the two curves in Fig. A2 *A* are similar for small values of $r$ and diverge at larger values.

In the absence of Ca buffers, the steady-state value of $\Delta[Ca]_{os}$ that is obtained from Eq. A1 is not finite for either of the (infinite) spatial arrangements of channels illustrated in Fig. A1. In this situation, the time-dependent solution of the diffusion equation, Eq. C20 (with $[B_i]_R = 0$ and $D_{Ca,app} = D_{Ca}$), can be used to estimate each individual channel contribution ($\Delta[Ca]_i$) to $\Delta[Ca]_{os}$

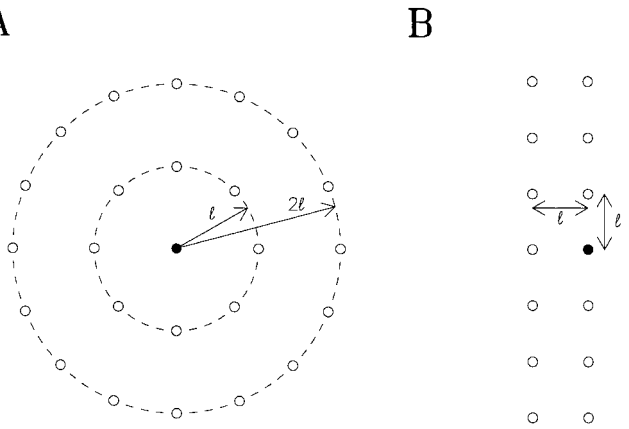


FIGURE A1. Two hypothetical arrangements of SR Ca channels in the plane of the Z line, one that is two dimensional (*A*) and another that is quasi–one dimensional (*B*). The filled and open circles indicate the channels used for the estimation of $\Delta[Ca]_{ps}$ and $\Delta[Ca]_{os}$, respectively. The concentric rings in *A* and the two rows in *B* are assumed to extend indefinitely. In A, $l = 66$ nm, which corresponds to 585/2 Ca release channels per $\mu m^2$; in B, $l = 30$ nm, which is approximately equal to the distance between feet as visualized with the electron microscope (Franzini-Armstrong, 1975; Block et al., 1988). Additional information is given in the text.

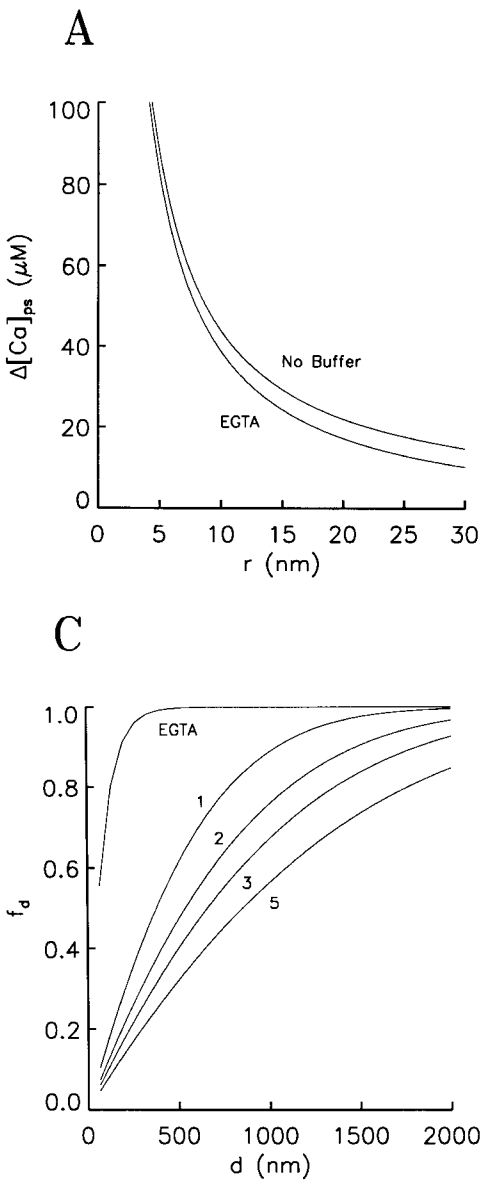


FIGURE A2. $\Delta[Ca]_{ps}$ and $\Delta[Ca]_{os}$ without Ca buffers (*No Buffer*) and with 18.24 mM EGTA (*EGTA*). (*A*) Steady-state estimates of $\Delta[Ca]_{ps}$, plotted as a function of $r$. The "No Buffer" and "EGTA" curves were calculated from Eqs. 1 and 2, respectively, with $\phi_{point}/2\pi$ instead of $\phi_{point}/4\pi$ on the right-hand sides. (*B*) $\Delta[Ca]_{os}$ at $r = 0$ calculated at different times after a step change in Ca flux from 0 to $\phi_{point}$ through the channels that surround the $\Delta[Ca]_{ps}$ channel. The continuous curves were calculated with the arrangement of Ca channels shown in Fig. A1 *A*. The dotted curves were calculated with a uniform density of Ca flux in the plane of the Z line. The continuous No Buffer curve was calculated from Eq. A1 with each $\Delta[Ca]_i$ calculated from Eq. C20 (with $[B_i]_R = 0$, $D_{Ca,app} = D_{Ca}$, and $\phi_{point}/2\pi$ instead of $\phi_{point}/4\pi$ on the right-hand side). The continuous EGTA curve was obtained in a similar way except that $\Delta[Ca]_i$ was calculated from Eqs. C17 and C18 (with $[B_i]_R = 0$, $D_{Ca,app} = D_{Ca}$, $\tau_{Ca,app} = \tau_{Ca}$, $\lambda_{Ca,app} = \lambda_{Ca}$, and $\phi_{point}/2\pi$ instead of $\phi_{point}/4\pi$ on the right-hand side of Eq. C17). The two dotted curves show approximations of $\Delta[Ca]_{os}$ ($\Delta[Ca]_{x=0}$) calculated with $\phi_{plane} = \phi_{point}/(\pi l^2/4)$. The dotted No Buffer curve was calculated from Eq. C36 with $c = 1$. The dotted EGTA curve was calculated from Eq. C31 with $c = 1$ and $\tau_{Ca,app} = \tau_{Ca}$. (*C*) Spatial dependence of $f_d$ at different times. The curves labeled with numbers show $f_d$ calculated without Ca buffers at different times (indicated in ms) after a step change in Ca flux, from the calculations in *B*. The curve labeled EGTA was calculated in a similar way except that $\Delta[Ca]_i$ in Eq. A1 was calculated from Eq. 2 (with $\phi_{point}/2\pi$ instead of $\phi_{point}/4\pi$ on the right-hand side). Each curve is plotted against $d$, beginning with $d = l$. The values of the parameters are given in Table I. Additional information is given in the text.

in Eq. A1. For this purpose, $r$ in Eq. C20 represents the distance from the mouth of the channel to the point of reference for $\Delta[Ca]_{os}$, and $\phi_{point}/4\pi$ on the right-hand side of Eq. C20 is replaced with $\phi_{point}/2\pi$.

The continuous curve labeled "No Buffer" in Fig. A2 *B* shows the value of $\Delta[Ca]_{os}$ during the first 10 ms after a step change in Ca flux from zero to $\phi_{point}$ through all of the neighboring sites (Fig. A1 *A*). Although this calculation was performed at $r = 0$ nm (corresponding to the mouth of the channel responsible for $\Delta[Ca]_{ps}$), closely similar curves of $\Delta[Ca]_{os}$ vs. $t$ were obtained at other nearby locations on the line that originates at the mouth of the $\Delta[Ca]_{ps}$ channel and extends perpendicularly from the plane of the Z line. In this context, $r$ represents the distance from the mouth of the $\Delta[Ca]_{ps}$ channel to the point of reference. For $0.1 \leq t \leq 10$ ms, the value of $\Delta[Ca]_{os}$ at $r = 30$ nm is only 7–8 μM less than the value at $r = 0$ nm. Part of the reason for the small variation in $\Delta[Ca]_{os}$ with $r$ arises from considerations of symmetry, which require that $\partial\Delta[Ca]_{os}/\partial r = 0$ at $r = 0$.

The dotted curve slightly above the "No Buffer" curve shows the value of $\Delta[Ca]_{x=0}$ calculated from Eq. C36 for a step of uniform Ca flux in the plane of the Z line, with a density $\phi_{plane} = \phi_{point}/(\pi l^2/4)$; the factor $\pi l^2/4$ is equal to the area per channel for the arrangement of channels illustrated in Fig. A1 *A*. From 0.1 to 10 ms, the dotted curve lies 25.8–26.7 μM above the continuous curve. The close similarity of the two curves shows that, in the absence of Ca buffers, $\Delta[Ca]_{x=0}$ calculated with Eq. C36 provides a good approximation of $\Delta[Ca]_{os}$ at $r = 0$.

The continuous curve labeled "EGTA" in Fig. A2 *B* shows $\Delta[Ca]_{os}$ at $r = 0$ nm with 18.24 mM EGTA and no

other Ca buffers (Eq. C17). As expected from the value of 22 μs for $\tau_{Ca}$ (Pape et al., 1995), $\Delta[Ca]_{os}$ had almost reached its final level of 42.6 μM by 0.1 ms, when the first point was plotted.

The dotted curve labeled "EGTA" shows the steady-state level of $\Delta[Ca]_{x=0}$, calculated for a uniform flux of Ca in the plane of the Z line in the presence of 18.24 mM EGTA (Eq. C31). The value of $\phi_{plane}$ was the same as that used for the "No Buffer" dotted curve. The steady level of $\Delta[Ca]_{os}$ is 65.6 μM. The absolute difference between the final values of $\Delta[Ca]_{r=0}$ and $\Delta[Ca]_{os}$ with EGTA, 23 μM, is similar to that without Ca buffers, 26–27 μM (see above), although the relative difference is more pronounced.

The curves in Fig. A2 *C* show the range of distances over which $\Delta[Ca]_i$ contributes to $\Delta[Ca]_{os}$ in Eq. A1. The abscissa is $d$ and the ordinate is $f_d$, the fractional value of $\Delta[Ca]_{os}$ that is contributed by channels that are located within a distance $d$ from the channel used to calculate $\Delta[Ca]_{ps}$ (indicated by the *filled circle* in Fig. A1 *A*); $r = 0$ nm. The curves marked by numbers were calculated without Ca buffers, at the times indicated (in ms). The curves become progressively broader with time because Ca ions are able to diffuse farther from their sources to contribute to $\Delta[Ca]_{os}$. At $t = 3$ ms, which is the approximate duration of SR Ca release after an action potential in fibers equilibrated with 20 mM EGTA and 1.76 mM Ca (Pape et al., 1995), $f_d = 0.50$ at 660 nm (denoted by $d_{0.5}$). This value of $d_{0.5}$ is roughly equal to the mean lattice spacing of the myofibrils (see above). Thus, the value of $\Delta[Ca]_{os}$ is determined by Ca ions that leave sites arranged along the perimeter of several myofibrils. On the other hand, with 18.24 mM EGTA, the value of $f_d$ was 0.56 with the first ring of sites at $d = 66$ nm (Fig. A1 *A*) and was 0.92 after inclusion of the third ring of sites at $d = 198$ nm. In this case, the value of $\Delta[Ca]_{os}$ is determined primarily by Ca ions that leave sites along a short segment at the perimeter of a single myofibril, as illustrated by the arrangement of sites in Fig. A1 *B* (see below).

In the estimates of $\Delta[Ca]_{os}$ described thus far, Eq. A1 was used with either Eq. C20 or C17, and the principle of superposition was implicitly assumed to hold. This is clearly the case in the absence of any Ca buffers. It is also expected to apply to fibers equilibrated with 20 mM EGTA because the fractional change in concentration of Ca-free buffer is expected to be small during the period of SR Ca release elicited by an action potential or a brief voltage pulse (Pape et al., 1995).

This section shows that steady-state equations can be used to estimate $\Delta[Ca]_{ps}$ without Ca buffers and with 18.24 mM EGTA. Steady-state equations can also be used to estimate the individual contributions of $\Delta[Ca]_i$ to $\Delta[Ca]_{os}$ with 18.24 mM EGTA. On the other hand, in the absence of Ca buffers, transient equations must be used for $\Delta[Ca]_{os}$. $\Delta[Ca]_{os}$ can make substantial contributions to $\Delta[Ca]$, especially in the absence of Ca buffers, when the value of $d_{0.5}$ is large. Without Ca buffers, the value of $\Delta[Ca]_{os}$ calculated with the arrangement of Ca channels in Fig. A1 *A* is very similar to that given by the analytical solution for a uniform Ca flux with $\phi_{plane} = \phi_{point}/(\pi l^2/4)$ (Eq. C36). These same general features apply with 5.5 mM ATP, as shown in the following section.

### *Effect of ATP and Troponin on $\Delta[Ca]_{ps}$ and $\Delta[Ca]_{os}$ Calculated with SR Ca Channels Arranged in Concentric Rings (Fig. A1 A)*

The principles that were used to estimate $\Delta[Ca]_{ps}$ and $\Delta[Ca]_{os}$ in Fig. A2 can also be applied to a situation that resembles muscle in which mobile and immobile intrinsic Ca buffers are present.

Freely diffusible intrinsic Ca buffers will be considered first. According to Baylor and Hollingworth (1998), most of this kind of buffering power in muscle is due to ATP. ATP acts as a rapidly equilibrating, low affinity Ca buffer with an apparent forward rate constant for Ca complexation of $0.136 \times 10^8$ $M^{-1}s^{-1}$, a backward rate constant of 30,000 $s^{-1}$, and an apparent dissociation constant of 2.2 mM (Table I); the effects of Mg and K complexation by ATP have been included in the estimation of these parameters. The total concentration of ATP used for the calculations here, 5.5 mM, is the same as that used in our internal end-pool solutions.

The continuous curves in Fig. A3 *A* show steady-state $\Delta[Ca]_{ps}$ plotted as a function of $r$. Curve *a* shows $\Delta[Ca]_{ps}$ without Ca buffers, replotted from the "No Buffer" curve in Fig. A2 *A*. Curve *b* was calculated with 5.5 mM ATP and the values of parameters in Table I, from the relation

$$\Delta[Ca]_{ps} = \frac{\phi_{point}}{2\pi D_{Ca} r} \cdot \left\{ \exp(-r/\lambda) + \frac{\lambda^2}{\lambda_{ATP}^2} \cdot [1 - \exp(-r/\lambda)] \right\}, \quad \text{(A2)}$$

in which

$$\lambda_{Ca} = \sqrt{\frac{D_{Ca}}{k_{1,ATP}[ATP]_R}}, \quad \text{(A3)}$$

$$\lambda_{ATP} = \sqrt{\frac{D_{ATP}}{k_{1,ATP}[Ca]_R + k_{-1,ATP}}}, \quad \text{(A4)}$$

and

$$1/\lambda^2 = 1/\lambda_{Ca}^2 + 1/\lambda_{ATP}^2 \quad \text{(A5)}$$

(with the parameters in Table I, $\lambda_{Ca} = 63.2$ nm, $\lambda_{ATP} = 68.3$ nm, and $\lambda = 46.4$ nm). The dotted curve shows the negative change in [ATP] associated with curve *b*,

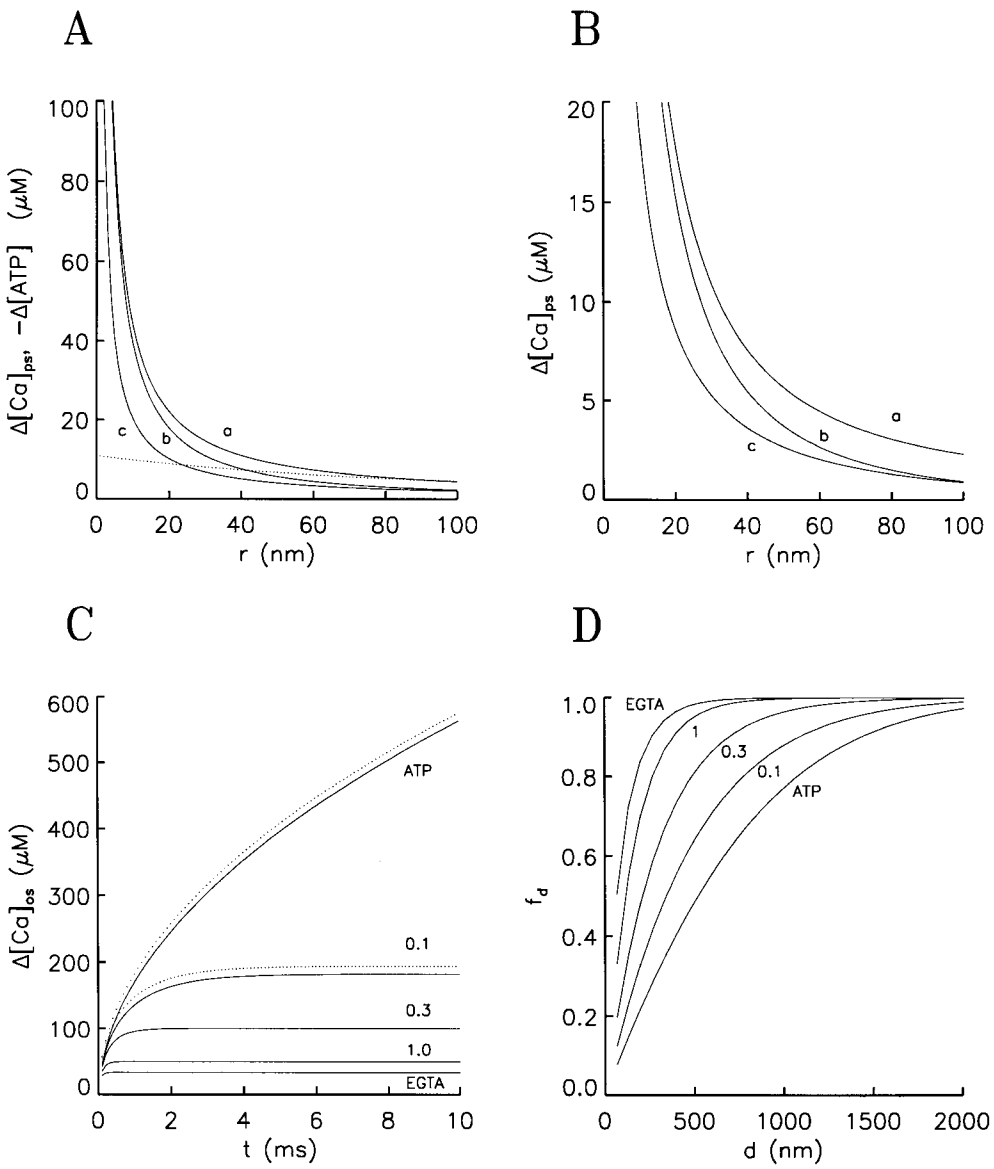


FIGURE A3. Effect of 5.5 mM ATP, 18.24 mM EGTA, and troponin on $\Delta[Ca]_{ps}$ and $\Delta[Ca]_{os}$. (*A*) Steady-state estimates of $\Delta[Ca]_{ps}$ and $-\Delta[ATP]$, plotted as a function of *r*. Curve *a* was calculated without Ca buffers (redrawn from the "No Buffer" curve in Fig. A2 *A*). Curve *b* was calculated with ATP from Eq. A2; the dotted curve shows the associated $-\Delta[ATP]$, calculated from Eq. A6. Curve *c* was also calculated with ATP, but with the approximation of Eq. C19 (with $\phi_{point}/2\pi$ instead of $\phi_{point}/4\pi$ on the right-hand side). (*B*) Format similar to *A*. Curve *a* was calculated with ATP (redrawn from curve *b* in *A*). Curve *b* was calculated with ATP plus EGTA, with the exact solution described in APPENDIX B (Eqs. B10, B11, B19, B29, and B32 with $\phi_{point}/2\pi$ instead of $\phi_{point}/4\pi$ on the right-hand sides). Curve *c* was also calculated with ATP and EGTA, but with the approximation of Eq. C16 (with $\phi_{point}/2\pi$ instead of $\phi_{point}/4\pi$ on the right-hand side). (*C*) $\Delta[Ca]_{os}$ at $r = 0$ calculated at different times after a step change in Ca flux from 0 to $\phi_{point}$ through the surrounding channels. The continuous curves were calculated with the arrangement of Ca channels shown in Fig. A1 *A*; the dotted curves were calculated with a uniform density of Ca flux in the plane of the Z line. $[ATP]_R = 5.5$ mM was used for all curves. The continuous curve labeled "ATP" was calculated with no other Ca buffers from Eq. A1 with each $\Delta[Ca]_i$ calculated from Eq. C20 (with $\phi_{point}/2\pi$ instead of $\phi_{point}/4\pi$ on the right-hand side). The continuous curve labeled "EGTA" (with EGTA and ATP) was calculated from Eq. A1 with each $\Delta[Ca]_i$ calculated from Eqs. C17 and C18 (with $\phi_{point}/2\pi$ instead of $\phi_{point}/4\pi$ on the right-hand side of Eq. C17). The continuous curves labeled "0.1," "0.3," and "1" were calculated in a manner similar to that used for the continuous EGTA curve except that Ca-regulatory sites on troponin were used instead of EGTA, with $[Trop]_R = 0.1$, 0.3, and 1 times 0.42 mM, respectively. The dotted curves show $\Delta[Ca]_{x=0}$. The dotted curve labeled ATP was calculated with Eq. C36 with $c = 0.36$. The dotted curve labeled "0.1" was calculated from Eq. C31 with 0.1 times 0.42 mM Ca-regulatory sites on troponin. (*D*) $f_d$ plotted as a function of *d*. The curves labeled ATP and 0.1–1 were obtained from the calculations in *C* at $t = 3$ ms. The curve labeled EGTA is steady state, with $\Delta[Ca]_i$ in Eq. A1 calculated from Eqs. B10, B11, B19, B29, and B32 (with $\phi_{point}/2\pi$ instead of $\phi_{point}/4\pi$ on the right-hand sides). The values of the parameters are given in Table I. Additional information is given in the text.

$$-\Delta[ATP] = \frac{\phi_{point}}{2\pi D_{ATP} r} \cdot [1 - \exp(-r/\lambda)] \cdot \left[1 - \frac{\lambda^2}{\lambda_{ATP}^2}\right]. \quad \text{(A6)}$$

Eqs. A2–A6 are similar to equations derived for EGTA in Appendix B in Pape et al. (1995).

Curve *c* in Fig. A3 *A* was also calculated with 5.5 mM ATP but with the simplifying assumptions that (*a*) the value of Δ[CaATP] is directly proportional to Δ[Ca] and (*b*) the equilibration of Ca with ATP is instantaneous. Assumption *a* follows from the relatively large value of $K_{d,ATP}$, 2.2 mM, and the relative constancy of [ATP]. The maximal change of 10.8 μM for $-\Delta[ATP]$ (*dotted curve* in Fig. A3 *A*) corresponds to only 0.2% of

the value of $[ATP]_R$, 5.5 mM. Assumption *b* follows approximately from the large value of $k_{1,ATP}$, 30,000 $s^{-1}$, which sets a lower limit for the apparent rate constant of Ca equilibration with ATP. APPENDIX C gives equations for $\Delta[Ca]$ that have been derived with these assumptions and with the assumption that the diffusion coefficient of the Ca buffer (in this case, ATP) is the same with and without Ca. Curve *c* was calculated from Eq. C19 with $\alpha_{ATP}$, the proportionality constant that relates $\Delta[CaATP]$ to $[ATP]_R\Delta[Ca]$, equal to $K_{d,ATP}^{-1}$ (Eq. C4).

Curve *b*, which gives the exact solution for $\Delta[Ca]_{ps}$, is similar to curve *a* for small values of *r*. This is expected because, when Ca is near the mouth of the channel, little time has elapsed since it left the channel and had a chance to become complexed by ATP. At larger values of *r*, more time has elapsed for Ca to diffuse from its source and equilibrate with ATP. Consequently, curve *b* becomes similar to *c*, which was calculated with the assumption that the concentrations of Ca and ATP were in equilibrium.

Eq. C20 gives transient solutions at different values of *r* that are associated with the steady-state curves *a* and *c*. Within 0.1 ms after a step change in Ca flux, $\Delta[Ca]_{ps}$ at $r \leq 30$ nm reaches >90% of its steady level in *a* (with $D_{Ca,app} = D_{Ca} = 3 \times 10^{-6}$ $cm^2s^{-1}$; see text discussion of the "No Buffer" curve in Fig. A2 *A*) and >87% of its steady level in *c* (with $D_{Ca,app} = 1.86 \times 10^{-6}$ $cm^2s^{-1}$). Although an exact transient solution is not available for the conditions used to calculate curve *b*, it seems likely that such a solution would be bracketed by the transient solutions for *a* and *c* and that, consequently, at $r \leq$ 30 nm, it would reach >87% of the steady level within 0.1 ms. Thus, during SR Ca release, the steady-state curve *b* is expected to provide a good approximation of $\Delta[Ca]_{ps}$ at the small values of *r* that are usually of interest (typically ≤30 nm).

On the other hand, the channels that contribute to $\Delta[Ca]_{os}$ are located sufficiently far from the $\Delta[Ca]_{ps}$ channel that the assumptions used for curve *c* are expected to apply reasonably well. Consequently, Eq. C20 can be used to estimate the transient solutions of $\Delta[Ca]_i$ that are used to calculate $\Delta[Ca]_{os}$ from Eq. A1. The continuous curve labeled "ATP" in Fig. A3 *C* shows $\Delta[Ca]_{os}$ at $r = 0$ nm calculated in this manner. The neighboring dotted curve shows $\Delta[Ca]_{x=0}$, calculated for a uniform Ca flux in the plane of the Z line; from 0.1 to 10 ms, the dotted curve lies 11.8–12.4 μM above the continuous curve. Similar to the comparison of the continuous and dotted "No Buffer" curves in Fig. A2 *B*, $\Delta[Ca]_{x=0}$ in Fig. A3 *C* provides a good approximation of $\Delta[Ca]_{os}$ at $r = 0$. The $\Delta[Ca]_{x=0}$ curves in Figs. A2 *B* and A3 *C* were both calculated from Eq. C36 and differ only by the value of the scaling factor *c*. According to Eq. C37, $c = 1$ without buffer (Fig. A2 *B*) and $c = 0.36$ with 5.5 mM ATP (Fig. A3 *C*). Thus, to a good approximation, the effect of 5.5 mM ATP on $\Delta[Ca]_{os}$ is to reduce its value according to the factor 0.36.

Fig. A3 *B* shows the effect of 18.24 mM EGTA on the steady-state $\Delta[Ca]_{ps}$ vs. *r* relation with 5.5 mM ATP. Curve *a* was calculated with ATP alone, redrawn from curve *b* in Fig. A3 *A*. Curve *b* was calculated with ATP and EGTA from the exact solution derived in APPENDIX B. Curve *c* was also calculated with ATP and EGTA but with the same simplifying assumptions that were used for curve *c* in Fig. A3 *A*, namely that the value of $\Delta[CaATP]$ is directly and instantaneously proportional to $\Delta[Ca]$ (Eq. C16). The transient solution with these assumptions, given by Eqs. C17 and C18, shows that, at $r \leq 30$ nm, $\Delta[Ca]_{ps}$ reaches >99% of its steady-state within 0.1 ms. Thus, for the same reasons used above for ATP alone, $\Delta[Ca]_{ps}$ with ATP and EGTA can be estimated from the steady-state solution (APPENDIX B) and the individual $\Delta[Ca]_i$ used to estimate $\Delta[Ca]_{os}$ can be calculated from the approximate transient solution, Eqs. C17 and C18.

The continuous curve labeled "EGTA" in Fig. A3 *C* shows $\Delta[Ca]_{os}$ at $r = 0$ nm for 5.5 mM ATP and 18.24 mM EGTA, calculated from Eq. A1 with $\Delta[Ca]_i$ calculated from Eqs. C17 and C18. Similar to the EGTA curve in Fig. A2 *B*, the final level is reached rapidly, within 0.2 ms. The final value, 33.5 μM, is similar to the exact steady-state value, 35.5 μM, that is obtained from Eq. A1 when $\Delta[Ca]_i$ is calculated from the equations in APPENDIX B. This similarity validates the use of (the approximate) Eqs. C17 and C18. The corresponding $\Delta[Ca]_{x=0}$ curve (not shown), calculated with Eq. C31, lies above the continuous curve by the amount 11.2 μM (similar to the difference between the continuous and dotted ATP curves).

The continuous curves labeled 0.1, 0.3, and 1.0 in Fig. A3 *C* show $\Delta[Ca]_{os}$ calculated for different concentrations of troponin, under the hypothetical condition that the concentration of sites available for Ca complexation does not change with time. With this restriction, $\Delta[Ca]_{os}$ can be evaluated from Eq. A1 with the individual $\Delta[Ca]_i$ calculated from Eqs. C17 and C18 with $k_{1,Trop} = 0.575 \times 10^8 M^{-1}s^{-1}$ and $[Trop]_R = 0.1$, 0.3, and $1.0 \times 0.42$ mM, respectively (Table I). The final values of the curves are 182.2, 100.3, and 49.9 μM, respectively. As the value of $[Trop]_R$ is increased, the time course becomes more rapid, and the final level becomes smaller. The $\Delta[Ca]_{x=0}$ curves lie 11.4–12.1 μM above the corresponding continuous curves; only the dotted 0.1 curve is shown.

Fig. A3 *D* shows $f_d$ plotted as a function of *d*, for the curves in Fig. A3 *C*. The curves labeled "ATP" and 0.1–1 were calculated at $t = 3$ ms. The curve labeled EGTA was calculated for steady-state conditions. The value of $d_{0.5}$ is 527 nm with ATP and 66 nm with ATP and EGTA; the values for troponin are intermediate.

In the calculations with 5.5 mM ATP illustrated in Fig. A3, all the $\Delta[Ca]_{ps}$ vs. $r$ relations lie on or between curves *a* and *b* in Fig. A3 *B*. The difference between these curves is small, <3.1 μM. Thus, the decreases in $\Delta[Ca]_{os}$ produced by 18.24 mM EGTA shown in Fig. A3 *C* are much larger than the associated decreases in $\Delta[Ca]_{ps}$. The significance of these results is considered in the final section of this appendix.

### *$\Delta[Ca]_{os}$ Calculated with SR Ca Channels Arranged in Two Parallel Rows (Fig. A1 B)*

With the arrangement of SR Ca channels illustrated in Fig. A1 *A*, and with 5.5 mM ATP plus either 18.24 mM EGTA or ≥0.5 mM fura-2 in the myoplasm, $f_d \geq 0.46$ with the first ring of sites (see Fig. A3 *D* for EGTA). In this situation, a more reliable estimate of $\Delta[Ca]_{os}$ is obtained with the arrangement of SR Ca channels in Fig. A1 *B*, with two rows of Ca channels on either side of a transverse tubule, similar to the two rows of feet observed by Franzini-Armstrong (1975) and Block et al. (1988). The spacing between channels in each row and the distance between rows is assumed to be the same, denoted by *l*, with $l \cong 30$ nm (Franzini-Armstrong, 1975; Block et al., 1988). Although only 14 channels are shown in Fig. A1 *B*, the rows are assumed to extend indefinitely in both directions. The filled and open circles indicate the locations of the channels used to calculate $\Delta[Ca]_{ps}$ and $\Delta[Ca]_{os}$, respectively.

The two curves labeled EGTA in Fig. A4 *A* show steady-state $\Delta[Ca]_{ps}$ with 18.24 mM EGTA, with (*continuous*) and without (*dotted*) 5.5 mM ATP, plotted as a function of *r*. The curves were redrawn from curve *b* in Fig. A3 *B* and the EGTA curve in Fig. A2 *A*, respectively. The curves labeled "fura-2" are similar except that 6 mM fura-2 was used instead of EGTA. With either EGTA or fura-2, the continuous and dotted curves are similar. This indicates that ATP has little effect on $\Delta[Ca]_{ps}$ in the presence of 18.24 mM EGTA or 6 mM fura-2 and, by inference, in the presence of ≥0.65 mM fura-2. The curve labeled "No Buffer" is plotted for comparison; it shows steady-state $\Delta[Ca]_{ps}$ in the absence of any Ca buffer and is redrawn from Fig. A2 *A*. All $\Delta[Ca]_{ps}$ curves considered in this article lie on or between the "No Buffer" and the continuous 6 mM fura-2 curve in Fig. A4 *A*.

Fig. A4 *B* shows $\Delta[Ca]_{os}$ at $r = 0$, with (*continuous*) and without (*dotted*) 5.5 mM ATP, plotted as a function of $[fura\text{-}2]_R$. These curves were calculated from Eq. A1; the steady-state relation was used for each $\Delta[Ca]_i$, an approximation that is reasonable with 18.24 mM EGTA (see above) and, for similar reasons, with ≥0.5 mM fura-2. If the concentration of a high affinity Ca buffer (with a small rate constant for Ca dissociation) is much larger than the amount of Ca released from the SR, the ability of the buffer to reduce free [Ca] near release sites is determined primarily by the product of its concentration and the forward rate constant for Ca com-

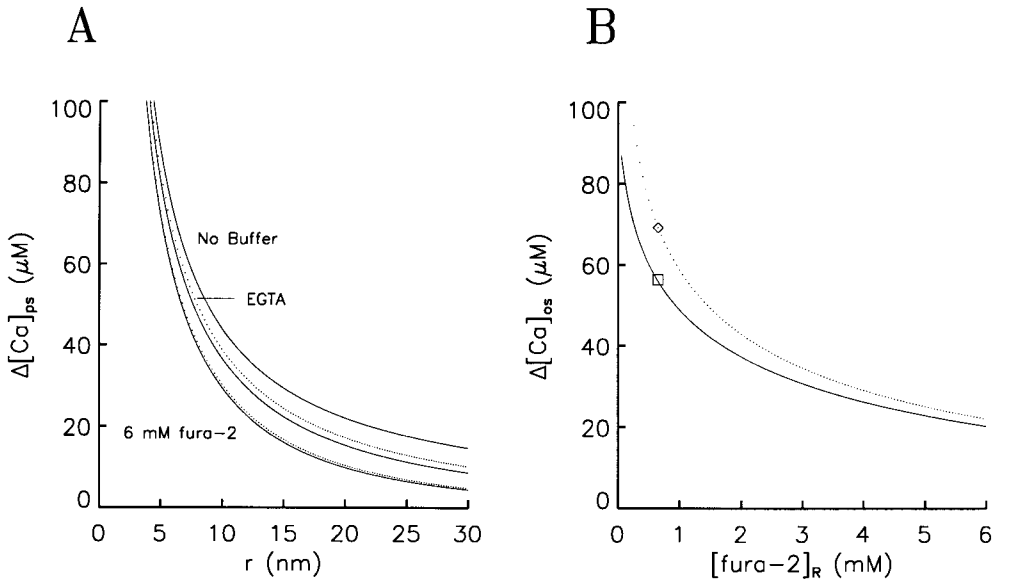


FIGURE A4. Steady-state $\Delta[Ca]_{ps}$ and $\Delta[Ca]_{os}$ calculated with 18.24 mM EGTA or fura-2, with and without 5.5 mM ATP, with the arrangement of Ca channels shown in Fig. A1 *B*. (*A*) Steady-state $\Delta[Ca]_{ps}$ plotted as a function of *r*. The continuous curve labeled "No Buffer" was redrawn from Fig. A2 *A*. The two dotted curves were calculated from Eq. 2 (with $\phi_{point}/2\pi$ instead of $\phi_{point}/4\pi$ on the right-hand side) with 18.24 mM EGTA or 6 mM fura-2 (as indicated), without ATP. The other two continuous curves are similar except that ATP was present; they were calculated from Eqs. B10, B11, B19, B29, and B32 (with $\phi_{point}/2\pi$ instead of $\phi_{point}/4\pi$ on the right-hand sides). (*B*) The dotted curve shows $\Delta[Ca]_{os}$ at $r = 0$ without ATP plotted as a function of $[fura\text{-}2]_R$; it was calculated from Eq. A1 with each $\Delta[Ca]_i$ calculated from Eq. 2 (with $\phi_{point}/2\pi$ instead of $\phi_{point}/4\pi$ on the right-hand side). The continuous curve was calculated with ATP from Eq. A1 with each $\Delta[Ca]_i$ calculated from Eqs. B10, B11, B19, B29, and B32 (with $\phi_{point}/2\pi$ instead of $\phi_{point}/4\pi$ on the right-hand sides). The diamond and square were calculated without and with ATP, respectively, for 18.24 mM EGTA and are plotted with the abscissa equal to 0.65 mM (for $[fura\text{-}2]_R$). The values of parameters are given in Table I. Additional information is given in the text.

plexation (Appendix B in Pape et al., 1995). The forward rate constant for fura-2 is 28 times that for EGTA, so that 18.24 mM EGTA is expected to be equivalent to 0.65 mM fura-2 in its ability to reduce free [Ca] and, consequently, $\Delta[Ca]_{os}$ (Jong et al., 1995*a*). The diamond and square symbols were calculated with 18.24 mM EGTA, without and with ATP, respectively, and plotted with their abscissa values equal to 0.65 mM; $\Delta[Ca]_{os}$ = 69.3 and 56.3 μM, respectively. As expected, the symbols lie very near the corresponding fura-2 curves.

*Application to Experimental Results*

The calculations described above can be applied to two experimental results (see DISCUSSION): (*a*) The addition of 0.5–1.0 mM fura-2 or 20 mM EGTA to myoplasm appears to increase action potential–stimulated SR Ca release by as much as twofold and to increase the peak rate of SR Ca release under voltage-clamp by two to threefold. (*b*) Action potential–stimulated $f_1$ is increased when the value of $[Ca_{SR}]_R$ is decreased in a manner that indicates that the value of Δ[Ca] at $r_{CaR}$ (the location of a putative regulatory Ca receptor) appears to be smaller with $[Ca_{SR}]_R$ = 900 μM and 20 mM EGTA in the myoplasm than with $[Ca_{SR}]_R \cong$ 2,000 μM and 6 mM fura-2 in the myoplasm. These two experimental results will be considered in terms of a decrease in Δ[Ca] produced by an increase in [EGTA] from 0 to 18.24 mM (*a*) and by a change in Ca buffers from 18.24 mM EGTA to 6 mM fura-2 (*b*). The intrinsic Ca buffers used in this analysis are ATP and the Ca-regulatory sites on troponin, the main mobile and immobile myoplasmic Ca buffers, respectively.

*Result a.* This result is consistent with the idea that Δ[Ca] and, as a result, Ca inactivation of Ca release are reduced when the value of [EGTA] is increased from 0 to 18.24 mM. Since $\Delta[Ca]_{ps}$ is reduced by <3.1 μM by 18.24 mM EGTA in the presence of 5.5 mM ATP (Fig. A3 *B*), any substantial decrease in Δ[Ca] would require a decrease in $\Delta[Ca]_{os}$. The two-dimensional arrangement of Ca channels in Fig. A1 *A* was used to analyze the effect of EGTA on $\Delta[Ca]_{os}$ because the value of $d_{0.5}$ is large without EGTA, 527 nm with 5.5 mM ATP and 660 nm without ATP, $t$ = 3 ms (Figs. A3 *D* and A2 *C*, respectively).

According to Fig. A3 *C*, at $t$ = 3 ms (the approximate duration of SR Ca release elicited by an action potential in fibers equilibrated with 20 mM EGTA plus 1.76 mM Ca), $\Delta[Ca]_{os}$ is 303 μM if 5.5 mM ATP is the only Ca buffer present. With the addition of Ca-regulatory sites on troponin, $\Delta[Ca]_{os}$ is expected to be reduced during a transient but to be unchanged in the steady state when Ca complexation by the immobile sites is in equilibrium with free [Ca]. Although the transient reduction in $\Delta[Ca]_{os}$ is difficult to evaluate analytically, it can be viewed qualitatively with the help of the curves labeled "0.1"–"1.0" in Fig. A3 *C*. After an action potential, when SR Ca release just begins, the curve labeled "1.0" is expected to apply. (The number refers to the fraction of sites that are unoccupied by Ca.) As Ca sites become occupied, the value of $\Delta[Ca]_{os}$ is expected to progressively increase until a peak fractional occupancy of ~0.9 is achieved (Hirota et al., 1989). The curves labeled 0.1–1.0 provide a rough idea of how this increase might take place: $\Delta[Ca]_{os}$ moves from the 1.0 curve to the 0.1 curve through a series of intermediate states, including the 0.3 curve. At $t$ = 3 ms, $\Delta[Ca]_{os}$ = 49.9, 100.2, and 174.0 μM on the curves labeled 1.0, 0.3, and 0.1, respectively. Although this description of events is qualitative, it seems reasonable to expect the value of $\Delta[Ca]_{os}$ to eventually lie near the 0.1 curve at $t$ = 3 ms with a value of ~174 μM.

If 18.24 mM EGTA is introduced, the development of steady-state conditions after a change in release is rapid, <0.1 ms, so that steady-state equations can be used. This gives $\Delta[Ca]_{os}$ = 35.5 μM for the arrangement of Ca channels in Fig. A1 *A* and 56.3 μM for the arrangement in Fig. A1 *B*, which is probably more reliable. This large reduction in $\Delta[Ca]_{os}$, from 174 to 56.3 μM, provides a plausible basis for result *a*. Moreover, for values of $r$ more than a few nanometers, the values of $\Delta[Ca]_{os}$ are larger than those of $\Delta[Ca]_{ps}$. At $r$ = 5 nm, for example, $\Delta[Ca]_{ps}$ = 80.3–83.2 μM (values from curves *a* and *b*, respectively, in Fig. A3 *B*). Without EGTA, $\Delta[Ca] = \Delta[Ca]_{ps} + \Delta[Ca]_{os}$ = 80–83 + 174 = 254–257 μM and, with EGTA, Δ[Ca] = 80 + 56 = 136 μM. In this case, 18.24 mM EGTA reduces $\Delta[Ca]_{os}$ 118 μM, and this reduction is mainly responsible for the almost twofold reduction in Δ[Ca], from 254–257 to 136 μM. As the value of $r$ is increased above 5 nm, the relative contribution of $\Delta[Ca]_{os}$ to Δ[Ca] becomes progressively larger. (The binding of Ca by troponin was not included in the estimate of $\Delta[Ca]_{os}$ with EGTA because, for reasons that are not entirely clear, troponin appears to bind little if any Ca released by an action potential in fibers equilibrated with 20 mM EGTA plus 1.76 mM Ca; pages 293–294 in Pape et al., 1995.)

*Result b.* This result can be used to estimate an upper limit for $r_{CaR}$, the distance of a putative regulatory Ca receptor from the mouth of an SR Ca channel. Steady-state equations are used to calculate $\Delta[Ca]_{ps}$ and $\Delta[Ca]_{os}$ with the arrangement of SR Ca channels in Fig. A1 *B* for $\Delta[Ca]_{os}$ (Fig. A4).

The continuous curves in Fig. A5 show Δ[Ca] (= $\Delta[Ca]_{ps} + \Delta[Ca]_{os}$) calculated with 5.5 mM ATP and either 18.24 mM EGTA or 6 mM fura-2, as indicated, plotted as a function of $r$. The upper limit for $r_{CaR}$ is given by the value of $r$ that satisfies the condition that Δ[Ca] with fura-2 is equal to 0.45 times Δ[Ca] with EGTA. The value 0.45 comes from the condition that

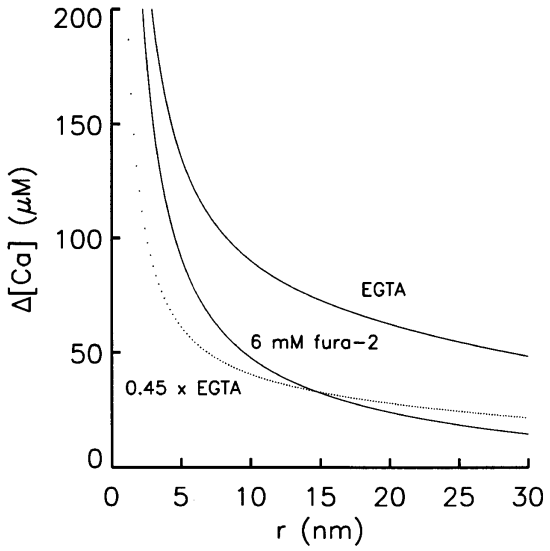


FIGURE A5. $\Delta[Ca]$ ($= \Delta[Ca]_{ps} + \Delta[Ca]_{os}$) calculated with 18.24 mM EGTA or 6 mM fura-2 (as indicated), with 5.5 mM ATP, plotted as a function of $r$. The parameters and equations are the same as those used in Fig. A4 *A* (for $\Delta[Ca]_{ps}$) and A4 *B* ($\Delta[Ca]_{os}$). The curve labeled "0.45 x EGTA" is the EGTA curve scaled by the factor 0.45.

$\Delta[Ca]$ at $r_{CaR}$ is smaller with $[Ca_{SR}]_R$ = 900 μM and 20 mM EGTA in the myoplasm than with $[Ca_{SR}]_R$ = 2,000 μM and 6 mM fura-2 in the myoplasm and from the assumption that $\phi_{point}$ is proportional to $[Ca_{SR}]_R$ (see DISCUSSION). The dotted curve shows the EGTA curve scaled by the factor 0.45. This curve intersects the fura-2 curve at $r$ = 14.7 nm, which gives the inequality $r_{CaR} \leq$ 14.7 nm. At the intersection, $\Delta[Ca]$ = 33.2 μM ($\Delta[Ca]_{ps}$ = 16.6 μM, $\Delta[Ca]_{os}$ = 16.6 μM with fura-2; $\Delta[Ca]_{ps}$ = 10.3 μM, $\Delta[Ca]_{os}$ = 22.9 μM with 18.24 mM EGTA and the scaling factor 0.45). At $r$ = 5 nm (the value of $r$ used for calculations above in *a*), $\Delta[Ca]$ = 91.7 μM ($\Delta[Ca]_{ps}$ = 72.0 μM, $\Delta[Ca]_{os}$ = 19.7 μM) with 6 mM fura-2.

The value of the upper limit of $r_{CaR}$ depends on the value used for $\phi_{point}$. In the calculations illustrated in Figs. A2–A5, $\phi_{point} = 0.5 \times 10^6$ ions $s^{-1}$, which corresponds to a single channel current of 0.16 pA. This value of $\phi_{point}$ represents a lower limit since it was obtained from the peak rate of SR Ca release after an action potential on the assumption that all of the SR Ca channels were open. If some channels were closed, perhaps because they had not been activated by the voltage sensor or because they had been turned off by Ca inactivation, the value of $\phi_{point}$ would be larger.

Mejia-Alvarez et al. (1998) carried out experiments on single canine cardiac ryanodine receptor channels incorporated into planar lipid bilayers. From their results, they estimate that, under normal physiological conditions, the single channel current is <0.5 pA, corresponding to $\phi_{point} \leq 1.5 \times 10^6$ ions $s^{-1}$. Although an increase in the value of $\phi_{point}$ would increase the value of $\Delta[Ca]_{ps}$, the value of $\Delta[Ca]_{os}$, on average, should be unchanged because the spatially averaged rate of SR Ca release is unchanged; thus, any increase in $\phi_{point}$ used for the determination of $\Delta[Ca]_{os}$ must be offset by a decrease in mean open probability so that the product of $\phi_{point}$ times mean open probability remains constant. Calculations similar to those in Fig. A5 give the inequality $r_{CaR} \leq 21.6$ nm for $\phi_{point} = 1.5 \times 10^6$ ions $s^{-1}$. Thus, with the simplifying assumptions used for these calculations, it seems reasonable to conclude that $r_{CaR} \leq 22$ nm.

## APPENDIX B

Appendix B in Pape et al. (1995) describes the steady-state changes in concentrations of free Ca, Ca-free EGTA, and Ca-complexed EGTA that are expected to develop in the myoplasm near an open SR Ca channel in a fiber equilibrated with EGTA. Although the equations were developed for EGTA, they apply to any Ca buffer that binds Ca with a 1:1 stoichiometry.

This appendix extends the theory to include any finite number of Ca buffers and, in particular, EGTA and ATP. The SR Ca channel is approximated by a point source of Ca immersed in an infinite isotropic medium, as was done in Appendix B in Pape et al. (1995). An important assumption in the derivations in Appendix B in Pape et al. (1995) and those given below is that the concentration of each Ca-free buffer decreases by only a relatively small amount, even at the Ca source.

Consider $N$ species of buffers. $[B_i]$ and $[CaB_i]$ represent, respectively, the concentration of Ca-free and Ca-complexed buffer, $i$ = 1, 2, .., $N$. $D_i$ represents the diffusion coefficient of the buffer, which is assumed to be independent of the state of Ca complexation; $k_i$ and $k_{-i}$ represent the forward and backward rate constants for Ca complexation, respectively.

The steady-state differential equation for the diffusion and complexation of Ca by the buffers, in spherical coordinates without angular dependence, is given by

$$D_{Ca}\{d^2[Ca]/dr^2 + (2/r)\,d[Ca]/dr\} - \sum_{i=1}^{N}\{k_i[Ca][B_i] - k_{-i}[CaB_i]\} = 0. \quad \text{(B1)}$$

For each species of Ca buffer, there are two equations,

$$D_i\{d^2[B_i]/dr^2 + (2/r)\,d[B_i]/dr\} - \{k_i[Ca][B_i] - k_{-i}[CaB_i]\} = 0 \quad \text{(B2)}$$

and

$$D_i\{d^2[\mathrm{CaB}_i]/dr^2 + (2/r)\,d[\mathrm{CaB}_i]/dr\}$$

$$+ \{k_i[\mathrm{Ca}][\mathrm{B}_i] - k_{-i}[\mathrm{CaB}_i]\} = 0,\quad i = 1, 2, .., N. \quad \text{(B3)}$$

The concentrations of free Ca and the Ca-free buffers can each be expressed as a change with respect to the resting concentration, denoted by the subscript R,

$$\Delta[\mathrm{Ca}] = [\mathrm{Ca}] - [\mathrm{Ca}]_R \quad \text{(B4)}$$

and

$$\Delta[\mathrm{B}_i] = [\mathrm{B}_i] - [\mathrm{B}_i]_R,\quad i = 1, 2, .., N. \quad \text{(B5)}$$

Addition of Eqs. B2 and B3 shows that, in the absence of any sources or sinks for buffer, $[B_i] + [CaB_i]$ is constant and, consequently, $\Delta[CaB_i] = -\Delta[B_i]$.

If $|\Delta[B_i]| << [B_i]_R$, Eqs. B4 and B5 can be combined with B1 and B2 to give

$$D_{\mathrm{Ca}}\{d^2\Delta[\mathrm{Ca}]/dr^2 + (2/r)\,d\Delta[\mathrm{Ca}]/dr\} =$$

$$\sum_{i=1}^{N} k_i[\mathrm{B}_i]_R\Delta[\mathrm{Ca}] + \sum_{i=1}^{N}\{k_i[\mathrm{Ca}]_R + k_{-i}\}\cdot\Delta[\mathrm{B}_i] \quad \text{(B6)}$$

and

$$D_i\{d^2\Delta[\mathrm{B}_i]/dr^2 + (2/r)\,d\Delta[\mathrm{B}_i]/dr\} =$$

$$k_i[\mathrm{B}_i]_R\Delta[\mathrm{Ca}] + \{k_i[\mathrm{Ca}]_R + k_{-i}\}\cdot\Delta[\mathrm{B}_i],$$

$$i = 1, 2, .., N. \quad \text{(B7)}$$

At any value of $r$, the combined flux of Ca and $CaB_i$ must equal that of the source, $\phi_{\mathrm{point}}$. Consequently, remembering that $\Delta[CaB_i] = -\Delta[B_i]$,

$$\phi_{\mathrm{point}} = -4\pi r^2\{D_{\mathrm{Ca}}d\Delta[\mathrm{Ca}]/dr - \sum_{i=1}^{N} D_i d\Delta[\mathrm{B}_i]/dr\}. \quad \text{(B8)}$$

Multiplication by $dr/(4\pi r^2)$ and integration from $r$ to $\infty$ gives

$$\frac{\phi_{\mathrm{point}}}{4\pi r} = D_{\mathrm{Ca}}\Delta[\mathrm{Ca}] - \sum_{i=1}^{N} D_i\Delta[\mathrm{B}_i]. \quad \text{(B9)}$$

At this stage, it is convenient to introduce the variable $y_i$ defined as follows,

$$y_0 = \Delta[\mathrm{Ca}]\,r \quad \text{(B10)}$$

and

$$y_i = \Delta[\mathrm{B}_i]\,r,\quad i = 1, 2, .., N. \quad \text{(B11)}$$

Substitution into Eqs. B6 and B7 gives

$$D_{\mathrm{Ca}}y_0'' = \sum_{i=1}^{N} k_i[\mathrm{B}_i]_R y_0 + \sum_{i=1}^{N}\{k_i[\mathrm{Ca}]_R + k_{-i}\}\cdot y_i \quad \text{(B12)}$$

and

$$D_i y_i'' = k_i[\mathrm{B}_i]_R y_0 + \{k_i[\mathrm{Ca}]_R + k_{-i}\}y_i,\quad i = 1, 2, .., N, \quad \text{(B13)}$$

where $y_i''$ denotes $d^2y/dr^2$. Eqs. B12 and B13 can be rearranged to give

$$y_0'' = y_0\sum_{i=1}^{N} a_i + \sum_{i=1}^{N} b_i c_i y_i \quad \text{(B14)}$$

and

$$y_i'' = y_0(a_i/c_i) + b_i y_i,\quad i = 1, 2, .., N, \quad \text{(B15)}$$

where

$$a_i = k_i[\mathrm{B}_i]_R/D_{\mathrm{Ca}}, \quad \text{(B16)}$$

$$b_i = (k_i[\mathrm{Ca}]_R + k_{-i})/D_i, \quad \text{(B17)}$$

and

$$c_i = D_i/D_{\mathrm{Ca}}. \quad \text{(B18)}$$

Eq. B9, with Eqs. B10 and B11, can be rewritten,

$$y_0 = \frac{\phi_{\mathrm{point}}}{4\pi D_{\mathrm{Ca}}} + \sum_{i=1}^{N} c_i y_i. \quad \text{(B19)}$$

Eq. B14 and the $N$ equations represented by Eq. B15 are not independent. $N$ independent equations can be obtained by combining Eq. B19 with Eq. B15 to give

$$y_i'' = (a_i/c_i)\left(\frac{\phi_{\mathrm{point}}}{4\pi D_{\mathrm{Ca}}} + \sum_{i=1}^{N} c_i y_i\right) + b_i y_i,\quad i = 1, 2, .., N. \quad \text{(B20)}$$

Eq. B20 can be written in matrix notation:

$$\boldsymbol{Y}'' = \mathbf{M}\boldsymbol{Y} + \frac{\phi_{\mathrm{point}}}{4\pi D_{\mathrm{Ca}}}\boldsymbol{F}. \quad \text{(B21)}$$

$\boldsymbol{Y}$ is a column vector with $N$ elements $y_i$, $i = 1, 2, .., N$; $\mathbf{M}$ is an $N \times N$ matrix with the diagonal elements given by $m_{ii} = a_i + b_i$ and the off diagonal elements given by $m_{ij} = a_i c_j/c_i$; $\boldsymbol{F}$ is a column vector with $N$ elements given by $f_i = a_i/c_i$. With

$$\mathbf{Z} = \boldsymbol{Y} + \frac{\phi_{\mathrm{point}}}{4\pi D_{\mathrm{Ca}}}\mathbf{M}^{-1}\boldsymbol{F}, \quad \text{(B22)}$$

where $\mathbf{M}^{-1}$ is the inverse of $\mathbf{M}$, Eq. B21 becomes

$$\boldsymbol{Z}'' = \mathbf{M}\boldsymbol{Z}. \quad \text{(B23)}$$

**M**, in general, is nonsingular and can be diagonalized by a similarity transformation to give

$$\mathbf{D} = \mathbf{G}^{-1}\mathbf{M}\mathbf{G}. \tag{B24}$$

**D** is a diagonal matrix of the eigenvalues ($d_{ii}$) of **M**, and **G** is a matrix whose columns are the components of the unit eigenvectors of **M**. Since

$$\mathbf{M} = \mathbf{G}\mathbf{D}\mathbf{G}^{-1}, \tag{B25}$$

Eqs. B23 and B25 can be combined to give

$$\begin{aligned}\mathbf{G}^{-1}\mathbf{Z}'' &= \mathbf{G}^{-1}\mathbf{G}\mathbf{D}\mathbf{G}^{-1}\mathbf{Z} \\ &= \mathbf{D}\mathbf{G}^{-1}\mathbf{Z}.\end{aligned} \tag{B26}$$

Since $\mathbf{G}^{-1}\mathbf{Z}'' = (\mathbf{G}^{-1}\mathbf{Z})''$, and the solutions of Eq. B26 must be finite at large values of $r$, $\mathbf{G}^{-1}\mathbf{Z}$ has the general solution

$$\mathbf{G}^{-1}\mathbf{Z} = \mathbf{H}\boldsymbol{E}, \tag{B27}$$

where **H** is an $N \times N$ diagonal matrix with elements $h_{ii}$ and $\boldsymbol{E}$ is a column vector with elements $e_i = \exp(-r\sqrt{d_{ii}})$. Premultiplying both sides by **G** gives

$$\boldsymbol{Z} = \mathbf{G}\mathbf{H}\boldsymbol{E}, \tag{B28}$$

which, when combined with Eq. B22, gives

$$\boldsymbol{Y} = \mathbf{G}\mathbf{H}\boldsymbol{E} - \frac{\phi_{\text{point}}}{4\pi D_{\text{Ca}}}\mathbf{M}^{-1}\boldsymbol{F}. \tag{B29}$$

Since the flux of $B_i$ is zero at $r = 0$ ($i = 1, 2, .., N$), the value of $\Delta[B_i]$ must be finite everywhere (see, for example, the dotted curve in Fig. A3 *A*). Consequently, according to Eq. B11 and the definition of $\boldsymbol{Y}$,

$$y_i(r = 0) = 0, \quad i = 1, 2, .., N, \tag{B30}$$

$$\boldsymbol{Y}(r = 0) = 0, \tag{B31}$$

and Eq. B29 (with Eq. B25) can be rearranged to give

$$\mathbf{H}\boldsymbol{E}(r = 0) = \frac{\phi_{\text{point}}}{4\pi D_{\text{Ca}}}\mathbf{D}^{-1}\mathbf{G}^{-1}\boldsymbol{F}, \tag{B32}$$

from which the values of $h_{ii}$ can be determined. The $y_i$'s can be evaluated from Eq. B29 and $y_0$ can be obtained from Eq. B19. Division of the $y_i$'s by $r$ gives $\Delta$[Ca] and $\Delta[B_i]$ (Eqs. B10 and B11).

The functional form of $\Delta$[Ca] and of each $\Delta[B_i]$ consists of the sum of $N$ terms of the form [constant $\times$ $\exp(-r\sqrt{d_{ii}})/r$] plus a term of the form [constant/$r$]. The [constant $\times$ $\exp(-r\sqrt{d_{ii}})/r$] terms can be summed over infinite distributions of Ca sources such as those illustrated in Fig. A1, *A* and *B*, to give finite contributions to $\Delta[Ca]_{os}$. On the other hand, a similar summation of the [constant/$r$] term is not finite.

## APPENDIX C

Junge and McLaughlin (1987) and Irving et al. (1990), each with different assumptions, derived a partial differential equation for the apparent diffusion of a substance such as protons or Ca ions in the presence of mobile and immobile rapidly equilibrating buffers. For Ca buffers, an important limitation of these derivations is the assumption that the concentration of Ca-complexed buffer is directly proportional to free [Ca] at all times, an assumption that requires instantaneous equilibration of Ca and buffer. This requirement holds reasonably well for many low affinity Ca buffers, such as ATP (for $r \geq 60$ nm, Fig. A3 *A*), but clearly doesn't hold for high affinity buffers such as EGTA that have a small rate constant for Ca dissociation.

This appendix extends the analyses of Junge and McLaughlin (1987) and Irving et al. (1990) in two ways: first, to include mobile high affinity Ca buffers such as EGTA from which Ca dissociates slowly (at least compared with the duration of SR Ca release) and second, to give the time course of free [Ca] that is expected to develop after a step change in Ca flux (*a*) near an open SR Ca channel, which is approximated by a point source of Ca immersed in an infinite isotropic medium and (*b*) near a planar source of Ca that can diffuse into a semi-infinite medium. As was the case with the analyses of Junge and McLaughlin (1987) and Irving et al. (1990), the equations given below can be applied to the diffusion of other substances such as protons that are buffered inside cells.

According to Junge and McLaughlin (1987) and Irving et al. (1990), the partial differential equation that describes the diffusion of Ca in an isotropic medium in the presence of mobile and immobile rapidly equilibrating buffers is

$$\begin{aligned}\partial[\text{Ca}]/\partial t + \sum_{i=0}^{N}\partial[\text{CaB}_i]/\partial t = \\ D_{\text{Ca}}\nabla^2[\text{Ca}] + \sum_{i=1}^{N} D_i\nabla^2[\text{CaB}_i].\end{aligned} \tag{C1}$$

$N$ denotes the number of species of mobile Ca buffers, each with a resting concentration $[B_i]_R$ and diffusion coefficient $D_i$, which is assumed to be independent of the state of Ca complexation, $i = 1, 2, .., N$; $[B_0]_R$ denotes the concentration of fixed or immobile Ca buffers. If [Ca] and $[CaB_i]$ are expressed as changes with respect to their resting values, as was done in APPENDIX B, Eq. C1 becomes

$$\begin{aligned}\partial\Delta[\text{Ca}]/\partial t + \sum_{i=0}^{N}\partial\Delta[\text{CaB}_i]/\partial t = \\ D_{\text{Ca}}\nabla^2\Delta[\text{Ca}] + \sum_{i=1}^{N} D_i\nabla^2\Delta[\text{CaB}_i].\end{aligned} \tag{C2}$$

According to APPENDIXES B and C in Pape et al. (1995), if a large concentration of a high affinity, slowly

dissociating Ca buffer (such as EGTA) is used in the solution, any changes in buffer concentration are expected to be negligibly small, so that the buffer behaves as a sink that removes Ca at the rate $k_{on}[\mathrm{Buf}]_R\Delta[\mathrm{Ca}]$. $[\mathrm{Buf}]_R$ denotes the resting concentration of Ca-free buffer and $k_{on}$ denotes the forward rate constant for Ca complexation. Thus, if a high affinity, slowly dissociating Ca buffer is added to the solution of mobile and immobile rapidly equilibrating Ca buffers, Eq. C2 becomes

$$\partial\Delta[\mathrm{Ca}]/\partial t + \sum_{i=0}^{N}\partial\Delta[\mathrm{CaB}_i]/\partial t = D_{\mathrm{Ca}}\nabla^2\Delta[\mathrm{Ca}] + \sum_{i=1}^{N}D_i\nabla^2\Delta[\mathrm{CaB}_i] - k_{on}[\mathrm{Buf}]_R\Delta[\mathrm{Ca}]. \quad \text{(C3)}$$

If $\Delta[\mathrm{CaB}_i]$ is sufficiently small, it is expected to be proportional to $\Delta[\mathrm{Ca}]$. The proportionality constant ($\alpha_i$) can be defined by

$$\Delta[\mathrm{CaB}_i] = \alpha_i[\mathrm{B}_i]_R\Delta[\mathrm{Ca}], \quad i = 0, 1, .., N. \quad \text{(C4)}$$

If the stoichiometry of Ca binding is 1:1 and $[\mathrm{Ca}]_R$ is much smaller than the dissociation constant of the buffer ($K_{d,i}$), $\alpha_i \cong K_{d,i}^{-1}$.

Replacement of $\Delta[\mathrm{CaB}_i]$ in Eq. C3 by the right-hand side of Eq. C4 gives

$$\partial\Delta[\mathrm{Ca}]/\partial t = D_{\mathrm{Ca,app}}\nabla^2\Delta[\mathrm{Ca}] - \tau_{\mathrm{Ca,app}}^{-1}\Delta[\mathrm{Ca}]. \quad \text{(C5)}$$

The apparent diffusion coefficient of Ca ($D_{\mathrm{Ca,app}}$) is given by

$$D_{\mathrm{Ca,app}} = D_{\mathrm{Ca}}\frac{1 + \sum_{i=1}^{N}\alpha_i[\mathrm{B}_i]_R D_i/D_{\mathrm{Ca}}}{1 + \sum_{i=0}^{N}\alpha_i[\mathrm{B}_i]_R}, \quad \text{(C6)}$$

and the apparent time constant for Ca complexation by the high affinity Ca buffer ($\tau_{\mathrm{Ca,app}}$) is given by

$$\tau_{\mathrm{Ca,app}} = \tau_{\mathrm{Ca}}\left(1 + \sum_{i=0}^{N}\alpha_i[\mathrm{B}_i]_R\right), \quad \text{(C7)}$$

where

$$\tau_{\mathrm{Ca}} = (k_{on}[\mathrm{Buf}]_R)^{-1}. \quad \text{(C8)}$$

The characteristic distance associated with Ca diffusion ($\lambda_{\mathrm{Ca,app}}$) is given by

$$\lambda_{\mathrm{Ca,app}} = \sqrt{\tau_{\mathrm{Ca,app}}D_{\mathrm{Ca,app}}} \quad \text{(C9)}$$

$$= \lambda_{\mathrm{Ca}}\sqrt{1 + \sum_{i=1}^{N}\alpha_i[\mathrm{B}_i]_R D_i/D_{\mathrm{Ca}}}, \quad \text{(C10)}$$

where

$$\lambda_{\mathrm{Ca}} = \sqrt{\frac{D_{\mathrm{Ca}}}{k_{on}[\mathrm{Buf}]_R}}. \quad \text{(C11)}$$

In the absence of rapidly equilibrating Ca buffers, $D_{\mathrm{Ca,app}} = D_{\mathrm{Ca}}$, $\tau_{\mathrm{Ca,app}} = \tau_{\mathrm{Ca}}$, and $\lambda_{\mathrm{Ca,app}} = \lambda_{\mathrm{Ca}}$. Since the diffusion coefficient of Ca buffers is smaller than that of free Ca, Eq. C6 shows that rapidly equilibrating Ca buffers, both mobile and immobile, decrease the value of $D_{\mathrm{Ca,app}}$. In addition, rapidly equilibrating Ca buffers, both mobile and immobile, increase the time required for the high affinity Ca buffer to complex Ca (Eq. C7). Rapidly equilibrating mobile Ca buffers increase the distance that Ca is able to diffuse before capture by the high affinity Ca buffer (Eq. C10).

*Δ[Ca] Near a Point Source of Ca Flux*

In spherical coordinates without angular dependence, Eq. C5 can be written

$$\partial\Delta[\mathrm{Ca}]/\partial t = D_{\mathrm{Ca,app}}\{\partial^2\Delta[\mathrm{Ca}]/\partial r^2 + (2/r)\,\partial\Delta[\mathrm{Ca}]/\partial r\} - \tau_{\mathrm{Ca,app}}^{-1}\Delta[\mathrm{Ca}], \quad \text{(C12)}$$

where $r$ is the distance from the point source of Ca flux. Eq. C12 is similar to Eq. C3 in Pape et al. (1995).

The steady-state solution of Eq. C12 for an infinite medium is given by

$$\Delta[\mathrm{Ca}] = \frac{A}{r}\exp(-r/\lambda_{\mathrm{Ca,app}}) \quad \text{(C13)}$$

(Neher, 1986; Stern, 1992; Pape et al., 1995). The value of the coefficient $A$ is determined by the boundary condition at the Ca source,

$$\phi_{\mathrm{point}} = -\lim_{r\to 0} 4\pi r^2\left\{D_{\mathrm{Ca}}\partial\Delta[\mathrm{Ca}]/\partial r + \sum_{i=1}^{N}D_i\partial\Delta[\mathrm{CaB}_i]/\partial r\right\} \quad \text{(C14)}$$

$$= 4\pi A\left\{D_{\mathrm{Ca}} + \sum_{i=1}^{N}\alpha_i[\mathrm{B}_i]_R D_i\right\}. \quad \text{(C15)}$$

Eqs. C13 and C15 give the desired steady-state solution,

$$\Delta[\mathrm{Ca}] = \frac{\phi_{\mathrm{point}}}{4\pi D_{\mathrm{Ca}} r\left\{1 + \sum_{i=1}^{N}\alpha_i[\mathrm{B}_i]_R D_i/D_{\mathrm{Ca}}\right\}}\exp(-r/\lambda_{\mathrm{Ca,app}}). \quad \text{(C16)}$$

After a step change in $\phi_{\mathrm{point}}$, the transient solution of Eq. C12 is given by the product of the steady-state solu-

tion (right-hand side of Eq. C16) and $F(r,t)$ (which equals unity as $t \rightarrow \infty$),

$$\Delta[\mathrm{Ca}] = \frac{\phi_{\mathrm{point}}}{4\pi D_{\mathrm{Ca}} r \left\{1 + \sum_{i=1}^{N} \alpha_i [\mathrm{B}_i]_{\mathrm{R}} D_i / D_{\mathrm{Ca}}\right\}} \cdot \exp(-r/\lambda_{\mathrm{Ca,app}}) F(r,t), \quad \text{(C17)}$$

where

$$F(r,t) = 0.5\left[\mathrm{erfc}\left(\frac{r}{\sqrt{4D_{\mathrm{Ca,app}}t}} - \sqrt{t/\tau_{\mathrm{Ca,app}}}\right) + \exp(2r/\lambda_{\mathrm{Ca,app}}) \cdot \mathrm{erfc}\left(\frac{r}{\sqrt{4D_{\mathrm{Ca,app}}t}} + \sqrt{t/\tau_{\mathrm{Ca,app}}}\right)\right] \quad \text{(C18)}$$

(Appendix C in Pape et al., 1995).

In the special case in which $[\mathrm{Buf}]_{\mathrm{R}} = 0$, the values of $\lambda_{\mathrm{Ca,app}}$ and $\tau_{\mathrm{Ca,app}} \rightarrow \infty$ and Eqs. C16 and C17 are replaced by

$$\Delta[\mathrm{Ca}] = \frac{\phi_{\mathrm{point}}}{4\pi D_{\mathrm{Ca}} r \left\{1 + \sum_{i=1}^{N} \alpha_i [\mathrm{B}_i]_{\mathrm{R}} D_i / D_{\mathrm{Ca}}\right\}} \quad \text{(C19)}$$

and

$$\Delta[\mathrm{Ca}] = \frac{\phi_{\mathrm{point}}}{4\pi D_{\mathrm{Ca}} r \left\{1 + \sum_{i=1}^{N} \alpha_i [\mathrm{B}_i]_{\mathrm{R}} D_i / D_{\mathrm{Ca}}\right\}} \cdot \mathrm{erfc}\left(\frac{r}{\sqrt{4D_{\mathrm{Ca,app}}t}}\right), \quad \text{(C20)}$$

respectively (see section 10.4 in Carslaw and Jaeger, 1959).

*Δ[Ca] Near a Planar Source of Ca Flux*

The one-dimensional form of Eq. C5,

$$\partial\Delta[\mathrm{Ca}]/\partial t = D_{\mathrm{Ca,app}}\partial^2\Delta[\mathrm{Ca}]/\partial x^2 - \tau_{\mathrm{Ca,app}}^{-1}\Delta[\mathrm{Ca}], \quad \text{(C21)}$$

is solved with the boundary condition that Ca enters the semi-infinite medium at $x = 0$.

The Laplace transform of Eq. C21 with the initial condition $\Delta[\mathrm{Ca}] = 0$ at $t = 0$ is given by

$$p\overline{\Delta[\mathrm{Ca}]} = D_{\mathrm{Ca,app}} d^2\overline{\Delta[\mathrm{Ca}]}/dx^2 - \tau_{\mathrm{Ca,app}}^{-1}\overline{\Delta[\mathrm{Ca}]}, \quad \text{(C22)}$$

where $\overline{\Delta[\mathrm{Ca}]}$ is the Laplace transform of $\Delta[\mathrm{Ca}]$ and $p$ represents the transform variable. The general solution that is finite at large values of $x$ is given by

$$\overline{\Delta[\mathrm{Ca}]} = A \exp\left(-x\sqrt{(p + \tau_{\mathrm{Ca,app}}^{-1})/D_{\mathrm{Ca,app}}}\right), \quad \text{(C23)}$$

where the value of $A$ is determined from the boundary condition that the Ca flux at $x = 0$ undergoes a step change from 0 to $\phi_{\mathrm{plane}}$ at $t = 0$. This gives

$$\phi_{\mathrm{plane}}/p = -\lim_{x \rightarrow 0}\left\{D_{\mathrm{Ca}} d\overline{\Delta[\mathrm{Ca}]}/dx + \sum_{i=1}^{N} D_i d\overline{\Delta[\mathrm{CaB}_i]}\, dx\right\} \quad \text{(C24)}$$

$$= A\left\{D_{\mathrm{Ca}} + \sum_{i=1}^{N} \alpha_i [\mathrm{B}_i]_{\mathrm{R}} D_i\right\} \cdot \sqrt{(p + \tau_{\mathrm{Ca,app}}^{-1})/D_{\mathrm{Ca,app}}} \quad \text{(C25)}$$

$$= A\left\{1 + \sum_{i=0}^{N} \alpha_i [\mathrm{B}_i]_{\mathrm{R}}\right\} D_{\mathrm{Ca,app}} \cdot \sqrt{(p + \tau_{\mathrm{Ca,app}}^{-1})/D_{\mathrm{Ca,app}}}. \quad \text{(C26)}$$

Consequently,

$$\overline{\Delta[\mathrm{Ca}]} = \frac{\phi_{\mathrm{plane}} \exp\left(-x\sqrt{(p + \tau_{\mathrm{Ca,app}}^{-1})/D_{\mathrm{Ca,app}}}\right)}{p\left\{1 + \sum_{i=0}^{N} \alpha_i [\mathrm{B}_i]_{\mathrm{R}}\right\}\sqrt{(p + \tau_{\mathrm{Ca,app}}^{-1})\, D_{\mathrm{Ca,app}}}}. \quad \text{(C27)}$$

For the purposes of this paper, it is sufficient to consider the value of $\overline{\Delta[\mathrm{Ca}]}$ and its inverse Laplace transform at $x = 0$. If $[\mathrm{Buf}]_{\mathrm{R}} > 0$ and, consequently, $\tau_{\mathrm{Ca,app}}$ is finite,

$$\overline{\Delta[\mathrm{Ca}]}_{x=0} = \frac{\phi_{\mathrm{plane}}}{p\left\{1 + \sum_{i=0}^{N} \alpha_i [\mathrm{B}_i]_{\mathrm{R}}\right\}\sqrt{(p + \tau_{\mathrm{Ca,app}}^{-1})\, D_{\mathrm{Ca,app}}}}. \quad \text{(C28)}$$

The inverse transform is given by

$$\Delta[\mathrm{Ca}]_{x=0} = \frac{\phi_{\mathrm{plane}} \mathrm{erf}\left(\sqrt{t/\tau_{\mathrm{Ca,app}}}\right)}{\left\{1 + \sum_{i=0}^{N} \alpha_i [\mathrm{B}_i]_{\mathrm{R}}\right\}\sqrt{\tau_{\mathrm{Ca,app}}^{-1} D_{\mathrm{Ca,app}}}} \quad \text{(C29)}$$

$$= \frac{\phi_{\mathrm{plane}} \tau_{\mathrm{Ca,app}}}{\left\{1 + \sum_{i=0}^{N} \alpha_i [\mathrm{B}_i]_{\mathrm{R}}\right\}\lambda_{\mathrm{Ca,app}}} \cdot \mathrm{erf}\left(\sqrt{t/\tau_{\mathrm{Ca,app}}}\right) \quad \text{(C30)}$$

$$= c\frac{\phi_{\mathrm{plane}} \tau_{\mathrm{Ca}}}{\lambda_{\mathrm{Ca}}} \cdot \mathrm{erf}\left(\sqrt{t/\tau_{\mathrm{Ca,app}}}\right), \quad \text{(C31)}$$

where

$$c = \frac{1}{\sqrt{1 + \sum_{i=1}^{N} \alpha_i [\mathrm{B}_i]_{\mathrm{R}} D_i / D_{\mathrm{Ca}}}}. \quad \text{(C32)}$$

The steady-state solution is given by

$$\Delta[\mathrm{Ca}]_{x=0} = c \cdot \frac{\phi_{\mathrm{plane}}\tau_{\mathrm{Ca}}}{\lambda_{\mathrm{Ca}}}. \quad \text{(C33)}$$

On the other hand, if $[\mathrm{Buf}]_R = 0$ and $\tau_{\mathrm{Ca,app}}^{-1} = 0$,

$$\overline{\Delta[\mathrm{Ca}]}_{x=0} = \frac{\phi_{\mathrm{plane}}}{p\left\{1 + \sum_{i=0}^{N} \alpha_i [\mathrm{B}_i]_R\right\}\sqrt{pD_{\mathrm{Ca,app}}}}, \quad \text{(C34)}$$

and the inverse transform is

$$\Delta[\mathrm{Ca}]_{x=0} = \frac{\phi_{\mathrm{plane}}}{1 + \sum_{i=0}^{N} \alpha_i [\mathrm{B}_i]_R}\sqrt{\frac{4t}{\pi D_{\mathrm{Ca,app}}}} \quad \text{(C35)}$$

$$= c \cdot \phi_{\mathrm{plane}}\sqrt{\frac{4t}{\pi D_{\mathrm{Ca}}}}, \quad \text{(C36)}$$

where

$$c = \frac{1}{\sqrt{1 + \sum_{i=1}^{N} \alpha_i [\mathrm{B}_i]_R D_i/D_{\mathrm{Ca}}}\sqrt{1 + \sum_{i=0}^{N} \alpha_i [\mathrm{B}_i]_R}}. \quad \text{(C37)}$$

In this case, $\Delta[\mathrm{Ca}]_{x=0} \to \infty$ as $t \to \infty$, indicating that there is no steady-state solution. The value of $c$ is unity in the absence of rapidly equilibrating Ca buffers and is 0.36 with 5.5 mM [ATP].

We thank the staff of the Biomedical Instrumentation Laboratory of the Yale Department of Cellular and Molecular Physiology for help with the design and construction of equipment. We also thank Drs. Steve Baylor and Stephen Hollingworth for many helpful discussions and for critically reading the manuscript.

This work was supported by the U.S. Public Health Service grant AM-37643.

*Original version received 21 January 1998 and accepted version received 15 July 1998.*

*Note added in proof.* After the submission of the final manuscript for this article, the authors became aware of an article that describes a theoretical analysis of Ca diffusion in the presence of mobile Ca buffers that is similar to some of the theoretical results in our APPENDIXES A–C (Naraghi, M., and E. Neher. 1997. Linearized buffered $Ca^{2+}$ diffusion in microdomains and its implications for calculation of $[Ca^{2+}]$ at the mouth of a calcium channel. *J. Neurosi.* 17:6961–6973).

## REFERENCES

Baylor, S.M., W.K. Chandler, and M.W. Marshall. 1983. Sarcoplasmic reticulum calcium release in frog skeletal muscle fibres estimated from arsenazo III calcium transients. *J. Physiol. (Camb.).* 344:625–666.

Baylor, S.M., and S. Hollingworth. 1988. Fura-2 calcium transients in frog skeletal muscle fibres. *J. Physiol. (Camb.).* 403:151–192.

Baylor, S.M., and S. Hollingworth. 1998. Model of sarcomeric $Ca^{2+}$ movements, including ATP $Ca^{2+}$ binding and diffusion, during activation of frog skeletal muscle. *J. Gen. Physiol.* 112:297–316.

Blatz, A.L., and K.L. Magleby. 1987. Calcium-activated potassium channels. *Trends Neurosci.* 10:463–467.

Block, B.A., T. Imagawa, K.P. Campbell, and C. Franzini-Armstrong. 1988. Structural evidence for direct interaction between the molecular components of the transverse tubule/sarcoplasmic reticulum junction in skeletal muscle. *J. Cell Biol.* 107:2587–2600.

Carslaw, H.S., and J.C. Jaeger. 1959. Conduction of Heat in Solids. 2nd edition. Oxford University Press, London, UK.

Chandler, W.K., and C.S. Hui. 1990. Membrane capacitance in frog cut twitch fibers mounted in a double Vaseline-gap chamber. *J. Gen. Physiol.* 96:225–256.

Chandler, W.K., R.F. Rakowski, and M.F. Schneider. 1976. Effects of glycerol treatment and maintained depolarization on charge movement in skeletal muscle. *J. Physiol. (Camb.).* 254:285–316.

Csernoch, L., V. Jacquemond, and M.F. Schneider. 1993. Microinjection of strong calcium buffers suppresses the peak of calcium release during depolarization in frog skeletal muscle fibers. *J. Gen. Physiol.* 101:297–333.

Endo, M. 1977. Calcium release from the sarcoplasmic reticulum. *Physiol. Rev.* 57:71–108.

Endo, M., M. Tanaka, and S. Ebashi. 1968. Release of calcium from sarcoplasmic reticulum in skinned fibers of the frog. *Proc. Intl. Congr. Physiol. Sci.* 7:126.

Ford, L.E., and R.J. Podolsky. 1968. Force development and calcium movements in skinned muscle fibers. *Fed. Proc.* 27:375.

Franzini-Armstrong, C. 1975. Membrane particles and transmission at the triad. *Fed. Proce.* 34:1382–1389.

Grynkiewicz, G., M. Poenie, and R.Y. Tsien. 1985. A new generation of Ca indicators with greatly improved fluorescence properties. *J. Biol. Chem.* 260:3440–3450.

Hirota, A., W.K. Chandler, P.L. Southwick, and A.S. Waggoner. 1989. Calcium signals recorded from two new purpurate indicators inside frog cut twitch fibers. *J. Gen. Physiol.* 94:597–631.

Hodgkin, A.L., and A.F. Huxley. 1952. A quantitative description of membrane current and its application to conduction and excitation in nerve. *J. Physiol. (Camb.).* 117:500–544.

Hollingworth, S., A.B. Harkins, N. Kurebayashi, M. Konishi, and S.M. Baylor. 1992. Excitation–contraction coupling in intact frog skeletal muscle fibers injected with mmolar concentrations of fura-2. *Biophys. J.* 63:224–234.

Hui, C.S., and W.K. Chandler. 1990. Intramembranous charge movement in frog cut twitch fibers mounted in a double Vaseline-gap chamber. *J. Gen. Physiol.* 96:257–297.

Hui, C.S., and W.K. Chandler. 1991. $Q_\beta$ and $Q_\gamma$ components of intramembranous charge movement in frog cut twitch fibers. *J. Gen. Physiol.* 98:429–464.

Hui, C.S., and W. Chen. 1994. Origin of delayed outward ionic current in charge movement traces from skeletal muscle. *J. Physiol. (Camb.).* 479:109–125.

Huxley, A.F., and R.E. Taylor. 1958. Local activation of striated muscle fibres. *J. Physiol. (Camb.).* 144:426–441.

Inui, M., A. Saito, and S. Fleischer. 1987. Purification of the ryanodine receptor and identity with feet structures of junctional terminal cisternae of sarcoplasmic reticulum from fast skeletal muscle. *J. Biol. Chem.* 262:1740–1747.

Irving, M., J. Maylie, N.L. Sizto, and W.K. Chandler. 1987. Passive electrical and intrinsic optical properties of cut frog twitch fibers. *J. Gen. Physiol.* 89:1–40.

Irving, M., J. Maylie, N.L. Sizto, and W.K. Chandler. 1990. Intracellular diffusion in the presence of mobile buffers—application to proton movement in muscle. *Biophys. J.* 57:717–721.

Jacquemond, V., L. Csernoch, M.G. Klein, and M.F. Schneider. 1991. Voltage-gated and calcium-gated calcium release during depolarization of skeletal muscle fibers. *Biophys. J.* 60:867–873.

Jong, D.-S., P.C. Pape, S.M. Baylor, and W.K. Chandler. 1995*a*. Calcium inactivation of calcium release in frog cut muscle fibers that contain millimolar EGTA of fura-2. *J. Gen. Physiol.* 106:337–388.

Jong, D.-S., P.C. Pape, and W.K. Chandler. 1995*b*. Effect of sarcoplasmic reticulum calcium depletion on intramembranous charge movement in frog cut muscle fibers. *J. Gen. Physiol.* 106: 659–704.

Jong, D.-S., P.C. Pape, W.K. Chandler, and S.M. Baylor. 1993. Reduction of calcium inactivation of sarcoplasmic reticulum calcium release in voltage-clamped cut twitch fibers with fura-2. *J. Gen. Physiol.* 102:333–370.

Junge, W., and S. McLaughlin. 1987. The role of fixed and mobile buffers in the kinetics of proton movement. *Biochim. Biophys. Acta.* 890:1–5.

Klein, M.G., H. Cheng, L.F. Santana, Y.-H. Jiang, W.J. Lederer, and M.F. Schneider. 1996. Two mechanisms of quantized calcium release in skeletal muscle. *Nature.* 379:455–458.

Lai, F.A., H.P. Erickson, E. Rousseau, Q.-Y. Liu, and G. Meissner. 1988. Purification and reconstruction of the calcium release channel from skeletal muscle. *Nature.* 331:315–319.

Markwardt, F., and G. Isenberg. 1992. Gating of maxi $K^+$ channels studied by $Ca^{2+}$ concentration jumps in excised inside-out multichannel patches (myocytes from guinea pig urinary bladder). *J. Gen. Physiol.* 99:841–862.

Mejia-Alvarez, R., C. Kettlun, E. Rios, M. Stern, and M. Fill. 1998. Unitary calcium currents through cardiac ryanodine receptors under physiological conditions. *Biophys. J.* 74:*A*58.

Neher, E. 1986. Concentration profiles of intracellular calcium in the presence of a diffusible chelator. *In* Calcium Electrogenesis and Neuronal Functioning. U. Heinemann, M. Klee, E. Neher, and W. Singer, editors. Springer-Verlag, Berlin, Germany. 80–96.

Page, S., and H.E. Huxley. 1963. Filament lengths in striated muscle. *J. Cell Biol.* 19:369–390.

Pallotta, B.S., K.L. Magleby, and J.N. Barrett. 1981. Single channel recordings of $Ca^{2+}$ activated $K^+$ currents in rat muscle cell culture. *Nature.* 293:471–474.

Pape, P.C., D.-S. Jong, and W.K. Chandler. 1995. Calcium release and its voltage dependence in frog cut muscle fibers equilibrated with 20 mM EGTA. *J. Gen. Physiol.* 106:259–336.

Pape, P.C., D.-S. Jong, W.K. Chandler, and S.M. Baylor. 1993. Effect of fura-2 on action-potential-stimulated calcium release in cut twitch fibers from frog muscle. *J. Gen. Physiol.* 102:295–332.

Peachey, L.D. 1965. The sarcoplasmic reticulum and transverse tubules of the frog's sartorius. *J. Cell Biol.* 25:209–231.

Ríos, E., and G. Brum. 1987. Involvement of dihydropyridine receptors in excitation-contraction coupling in skeletal muscle. *Nature.* 325:717–720.

Ríos, E., and G. Pizarró. 1988. Voltage sensors and calcium channels of excitation-contraction coupling. *News Physiol. Sci.* 3:223–227.

Schneider, M.F., and B.J. Simon. 1988. Inactivation of calcium release from the sarcoplasmic reticulum in frog skeletal muscle. *J. Physiol. (Camb.).* 405:727–745.

Simon, B.J., and D.A. Hill. 1992. Charge movement and SR calcium release in frog skeletal muscle can be related by a Hodgkin-Huxley model with four gating particles. *Biophys. J.* 61:1109–1116.

Simon, B.J., M.G. Klein, and M.F. Schneider. 1991. Calcium dependence of inactivation of calcium release from the sarcoplasmic reticulum in skeletal muscle fibers. *J. Gen. Physiol.* 97:437–471.

Simon, B.J., M.F. Schneider, and G. Szücs. 1985. Inactivation of sarcoplasmic reticulum calcium release in frog skeletal muscle is mediated by calcium. *J. Gen. Physiol.* 86:36*a*.

Stern, M.D. 1992. Buffering of calcium in the vicinity of a channel pore. *Cell Calcium.* 13:183–192.

Stern, M.D., G. Pizarro, and E. Ríos. 1997. Local control model of excitation-contraction coupling in skeletal muscle. *J. Gen. Physiol.* 110:415–440.

Tanabe, T., K.G. Beam, J.A. Powell, and S. Numa. 1988. Restoration of excitation-contraction coupling and slow calcium current in dysgenic muscle by dihydropyridine receptor complementary DNA. *Nature.* 336:134–139.